CHARACTERIZATION OF STRENGTH AND DEFORMATION PROPERTIES OF ROCK MATERIAL FOR DESIGN OF DRILLED SHAFTS UNDER LATERAL LOAD

by

Thomas Cawley Timpson

A thesis submitted to the faculty of
The University of Utah
in partial fulfillment of the requirements for the degree of

Master of Science

Department of Civil and Environmental Engineering

The University of Utah

December 2011

The University of Utah Graduate School

STATEMENT OF THESIS APPROVAL

The thesis of **Thomas Cawley Timpson**

has been approved by the following supervisory committee members:

Evert Lawton	, Chair	**5/12/11** Date Approved
Steven Bartlett	, Member	**5/12/11** Date Approved
Chris Pantelides	, Member	**5/12/11** Date Approved

and by **Paul Tikalsky**, Chair of the Department of **Civil and Environmental Engineering**

and by Charles A. Wight, Dean of The Graduate School.

ABSTRACT

One of the most challenging aspects of geotechnical engineering is the characterization of subsurface material. In practice, engineers often base recommendations both directly and indirectly on index properties and corresponding correlations and models. However, these models should be calibrated for site-specific conditions prior to being used as the basis for any substantial design.

This study includes details of a geotechnical case study. The objective of this study was to evaluate existing models used to estimate strength and deformation characteristics of intact rock and rock mass with respect to analyzing laterally loaded drilled shafts. Geological and geotechnical investigations were conducted for the given site. The field investigation employed sampling methods such as rock coring to obtain specimens that could be tested in the laboratory, as well as in-situ pressuremeter testing (PMT). Laboratory tests performed included uniaxial compression, point-load, Brazilian tension, rebound hardness, unit weight, and water content. The subsurface profile was shown to consist of alternating layers of claystone, limestone, and sandstone, overlain by a layer of clayey sand.

To develop a basis for evaluating existing models, the variability associated with strength and index properties was assessed. In addition, site-specific correlations were developed between uniaxial compressive strength (q_u) and the various index properties of the intact rock materials. The predictive capability of existing correlations to estimate q_u

based on index properties was examined. It was found that point-load index ($I_{s(50)}$) provided the best estimate of q_u among the index correlations studied. Additional rock mass correlations were evaluated on the basis of the strength and deformation characteristics derived from the PMT data. It was found that neither rock mass rating (RMR) nor geological strength index (GSI) produced reasonable estimates of rock mass deformation characteristics based on correlations examined.

The method used by the computer program *LPILE* to develop *p-y* curves for weak rock (Reese 1997) was evaluated in terms of how well the predicted *p-y* curves developed compared with those from PMT data. It was found that the *weak rock* model highly overestimated the stiffness of the rock mass for this particular site compared to stiffness estimated from the PMT results.

TABLE OF CONTENTS

LIST OF FIGURES

LIST OF TABLES

1 INTRODUCTION

One of the most challenging aspects of geotechnical engineering is the characterization of subsurface material with respect to strength and deformation parameters. In practice, geotechnical consultants often base recommendations both directly and indirectly on index properties and corresponding existing correlations. However, these correlations are typically based on site-specific conditions and minimal calibration data, and may not be applicable in every case. Subterranean material, especially rock, typically exhibits a high degree of variability in strength and behavior. This variability is due to factors such as geological history, depositional environment, material type, heterogeneity, and isotropy. With these factors in mind, existing correlations should be calibrated for site-specific conditions prior to being used as the basis for any substantial design recommendation. Furthermore, site-specific correlations should be developed if adequate information is available.

The present study is a site-specific case study (Lima Substation) conducted in the context of designing laterally loaded drilled shaft foundations in rock material. The overlying objective was to evaluate existing correlations and models used for estimating strength and deformation characteristics of rock material with respect to designing laterally loaded drilled shaft foundations. These correlations were evaluated in terms of how well they apply to the material at the site of investigation. This evaluation was

conducted on the basis of high quality field and laboratory data. Specifically, this study aims to complete the following objectives:

- Assess the variability of strength and index properties of the subsurface material at the given site of investigation.
- Develop site-specific correlations between strength and index properties of the intact rock at the site of investigation.
- Evaluate existing correlations used to estimate strength of intact rock based on index properties.
- Evaluate existing correlations used to estimate strength and deformation characteristics of rock mass based on strength of intact rock and characterization parameters of the rock mass.
- Evaluate the method used in the computer program *LPILE* (Reese 1997) to develop *p-y* curves in weak rock in terms of how well it applies to rock at the site of investigation.

To complete the above objectives, it was first necessary to research existing correlations and models presented in the literature. This literature review is presented in Chapter 2, which includes information regarding rock mass classification systems and how they are used in rock mechanics. In addition, existing correlations that apply to intact rock and rock mass are discussed. Furthermore, some analytical methods used to estimate the magnitude of geometrical deformations for laterally loaded shafts are presented. One analytical method is the *p-y* approach, in which the response of the foundation material is modeled as a series of nonlinear springs along the length of the

shaft. The method proposed by Reese (1997) for developing *p-y* curves in weak rock will be evaluated and discussed.

The details regarding the scope of work conducted during this study are presented in Chapters 3 through 5. The tasks conducted during this project include detailed geological and geotechnical field and laboratory investigations. The geological investigation employed research of existing geologic maps and data to obtain a general understanding of the subsurface material. The field investigation employed material sampling and in-situ field testing. Rock coring was the primary means of sampling while pressuremeter testing (PMT) was the primary in-situ test conducted. The laboratory investigation included standard strength and index property testing of the intact rock.

The field and laboratory data are reduced, evaluated, and presented in Chapter 6. The purpose of this chapter is to develop the basis for evaluating existing correlations and models. This basis first includes the high quality data obtained from PMT, from which reasonable estimates of deformation characteristics are obtained. In addition, the results of uniaxial compression (UAC) tests were taken as the best estimate for strength of intact rock core. Furthermore, site-specific correlations between strength and index properties of intact rock are developed, and the variability of the subsurface materials is assessed.

The predictive capability of existing correlations is examined in Chapter 7. Such correlations include those developed in the literature for the purposes of estimating strength of intact rock based on index properties. These correlations are evaluated based on the assumption that UAC testing results in the best estimate of strength. Additional correlations exist between strength of intact rock, characteristics of discontinuities, and the strength and deformation characteristics of rock mass. These correlations are

evaluated on the basis of the strength and deformation characteristics derived from the PMT data. Finally, recommendations are made for strength, index, and deformation characteristics of the intact rock and rock mass.

Some analytical methods used to estimate the magnitude of geometrical deformations for laterally loaded shafts are evaluated in Chapter 8. These methods include a simple analytical approach in which the shaft is assumed to be an elastic beam within a homogeneous, elastic continuum. Another method is the *p-y* approach, in which the response of the subsurface material is modeled as a series of discrete, nonlinear springs along the shaft length. This evaluation leads to questions regarding the method used by the computer program *LPILE* (Reese 1997) to develop *p-y* curves in weak rock. This model is examined in terms of how well the *p-y* curves developed compare with those developed using PMT data.

2 LITERATURE REVIEW

2.1 Overview

The focus of this study is to evaluate existing correlations and models used to estimate strength and deformation characteristics of rock in the context of designing laterally loaded drilled shaft foundations. There are two general procedures used to estimate these properties. The first is to incorporate a detailed geotechnical laboratory investigation in which both qualitative and quantitative data are gathered and used to characterize the rock mass. The second is to conduct a detailed field investigation in which in-situ testing such as pressuremeter testing (PMT) is performed.

Characterization of the rock mass is typically done using strength and deformation data of the intact rock in conjunction with rock mass classification systems. Strength of intact rock may be estimated directly through laboratory testing (e.g. uniaxial compression) or indirectly through index testing. Results of index testing may be used in conjunction with existing correlations to estimate strength (e.g. Bieniawski 1975 and Hassani et al. (1979). Examples of rock mass classification systems include rock mass rating (RMR, Bieniawski 1976) or geological strength index (GSI, Marinos and Hoek 2005). These parameters may be used to estimate strength and deformation characteristics of the rock mass. Laboratory results may also be used to develop load-displacement (*p*-*y*) curves (Reese 1997). These methods and relationships will be discussed in this section.

Reliable data representing the strength and behavior of a rock mass may be obtained from the results of in-situ testing. PMT is an example of in-situ testing, which was conducted during the field investigation for the current study (Section 4.4). The result of PMT may be used to estimate the deformation modulus of the rock mass (E_{rm}) and to develop *p-y* curves (Briaud 1992). These procedures will be discussed in this section, and the results will be used to evaluate the empirical method described above.

2.2 Rock Mass Classification Systems

In engineering rock foundations, it is necessary to assess the strength and deformation characteristics of the rock mass. Routine laboratory strength and index testing may be conducted to estimate the strength of the intact rock. However, the strength of the rock mass is highly influenced by discontinuities within the rock mass system. Therefore, the results of laboratory testing do not directly indicate the strength of the rock mass, and the characteristics of discontinuities must be considered. Accounting for the effects of discontinuities is often done through rock mass classification systems such as the rock mass rating (RMR) developed by Bieniawski (1976) and the geological strength index (GSI) developed by Marinos and Hoek (2000). These classification systems are used to produce index values that may be used in conjunction with empirical correlations to estimate the strength and deformation characteristics of the rock mass. The RMR and GSI classification systems are discussed in the following sections.

2.2.1 Rock Mass Rating (RMR)

The rock mass rating (RMR) system developed by Bieniawski (1976) is based on the strength of the intact rock core and the characteristics of the discontinuities within the

rock mass. The strength of the intact rock is typically determined from testing samples in uniaxial compression (UAC). The discontinuities are characterized by parameters such as rock quality designation (RQD), joint spacing, joint condition, and ground water conditions. RQD is expressed as a percentage, and is taken as the sum of the lengths of core pieces greater than 4 in. divided by the total length of the corresponding run. Bieniawski (1976) proposed an incremental rating system based on each of the above parameters, the criteria for which are shown in Table 2-1. After assigning a rating increment for each parameter, all increments are summed to produce a final value of RMR between 0 and 100%. With the final RMR value, the rock mass is assigned a geomechanics classification determined using the criteria shown in Table 2-2.

2.2.2 Geological Strength Index (GSI)

The geological strength index (GSI) was developed by Marinos and Hoek (2000) specifically to estimate rock mass properties using the Hoek-Brown strength criterion. As opposed to RMR, this system is not governed by RQD but is based on basic geological observations. The GSI is a number, or range of numbers, selected based on a qualitative assessment of the blockiness of the rock mass and the general condition of discontinuities within the rock mass. This number is selected using the chart developed by Marinos and Hoek (2005).

2.3 Existing Empirical Correlations

In practice, it is often desired to estimate the strength of material based on index properties that can be readily determined, rather than by conducting strength tests that demand considerably more time and more sophisticated equipment. Consequently,

Table 2-1. Rock Mass Rating (RMR) (modified from Goodman 1980)

	Parameter	Range of Values						
1	Uniaxial Compressive Strength of Intact Rock, q_u (ksi)	> 29.4	14.7 – 29.4	7.3 – 14.7	3.7 – 7.3	1.5 – 3.7	0.4 – 1.5	< 0.4
	Rating Increment	15	12	7	4	2	1	0
2	RQD (%)	91 – 100	76 – 90	51 – 75	25 – 50	< 25		
	Rating Increment	20	17	13	8	3		
3	Discontinuity Spacing (ft)	> 9.8	3.3 – 9.8	1.0 – 3.3	0.016 – 1.0	< 0.016		
	Rating Increment	30	25	20	10		5	
4	Discontinuity Condition	Very rough surfaces of limited extent; hard wall rock	Slightly rough surfaces; aperture less than 0.04 in.; hard wall rock	Slightly rough surfaces; aperture less than 0.04 in.; soft wall rock	Smooth surfaces, or gouge filling 0.04 - 0.20 in. thick, or aperture of 0.04 - 0.20 in.; joints extend more than several feet		Open joints filled with more than 0.20 in. of gouge, or open more than 0.20 in.; joints extend more than several feet	
	Rating Increment	25	20	12	6		0	
5	General groundwater condition	Completely dry	Moist	Water under moderate pressure			Severe water problems	
	Rating Increment	10	7	4			0	

Table 2-2. Geomechanics Classification of Rock Masses (after Goodman 1980)

Class	Description of Rock Mass	RMR (%)
I	Very good rock	81 -- 100
II	Good rock	61 -- 80
III	Fair rock	41 -- 60
IV	Poor rock	21 -- 40
V	Very poor rock	0 -- 20

several empirical correlations have been developed between index properties and strength and deformation characteristics of both intact rock and rock mass. In this study, these correlations will be applied to material at the site of investigation to evaluate their predictive capability in terms of estimating strength. Correlations presented in the literature that are applicable to the material at the given site are discussed in this section.

2.3.1 Strength versus Index Properties for Intact Rock

In rock mechanics, uniaxial compressive strength (q_u) is a common parameter used in design models. The literature includes several correlations between q_u and index properties of intact rock that are based on site-specific conditions such as rock type and core size. Index properties that are routinely used to estimate strength of intact rock include point-load index [$I_{s(50)}$], Brazilian tension (σ_t), rebound hardness (R_N), and unit weight (γ). Correlations found in the literature for each of these index tests are presented in Table 2-3.

Correlations between q_u and $I_{s(50)}$ generally take on the form $q_u = mI_{s(50)}$, where m ranges between about 20 and 29, although there are cases where the equation may include an intercept. An equation developed by Bieniawski (1975) is selected for this study

Table 2-3. Index Property Correlations

Index test	Equation	Source
Point Load	$q_u = 21\ I_{s(50)}$	Bieniawski (1975)
Brazilian Tension	$q_u = 10.5\ \sigma_t + 176.3$	Hassani et al. (1979)
Rebound Hardness	$q_u = 2.21\ e^{(0.07\ R_N)}$	Katz et al. (2000)
Unit Weight	$q_u = 0.0864\ e^{(0.291\ \gamma)}$	Smorodinov et al. (1970)

Note: γ in KN/m^3 q_u, σ_t, and $I_{s(50)}$ in psi

because it was obtained using NX core, the same type of core obtained for the current study (Section 4.3). Hassani et al. (1979) developed a correlation between q_u and σ_t based on about 1000 tests conducted on several rock types, including sandstone, of varying moisture conditions. Aydin and Basu (2005) presented a significant number of correlations between q_u and R_N – the equation shown in Table 2-3 (Katz et al. 2000) was based on testing for sandstone and limestone, which were found to be the two predominant rock types at the subject site of investigation (Section 6.2). Gunsallus and Kulhawy (1984) gave an overview of several correlations and their predictive capability in terms of estimating strength for general types of rock. They found correlations between q_u and $I_{s(50)}$ and σ_t resulted in the best predictive capabilities, and that significant variability is associated with the strength and index properties of intact rock.

2.3.2 Rock Mass Properties versus Intact Rock and Discontinuity Properties

The capacity of foundations in rock is governed by the strength of the rock mass as opposed to that of the intact rock. The strength properties of the rock mass are highly influenced by the presence of discontinuities such as joints, fractures, and bedding planes. These discontinuities introduce an additional element of variability into the equation.

Even with the most detailed geotechnical investigation, it is difficult to provide a comprehensive assessment of the strength and behavior of the rock mass. Correlations have therefore been developed to associate the properties of the rock mass to indicators such as RQD, RMR, and GSI. Equations used to estimate the deformation modulus of the rock mass (E_{rm}) are shown in Table 2-4. Equations relating E_{rm} to RMR an RQD are based on the elastic modulus of the intact rock ($E_r = E_{t50}$), which serves as an upper bound value. The equation relating E_{rm} to GSI is based on q_u.

The GSI can be used in conjunction with a series of equations to determine strength and deformation properties of a rock mass. These equations are based on a fundamental rock mass constant, m_i, which is determined according to Marinos and Hoek (2000). Eq. 2-1 through 2-9 presented below are based on the most recent Hoek-Brown failure criterion (Hoek et al. 2002). These equations can be used to determine the effective shear strength parameters and deformation modulus of the rock mass.

$$m_b = m_i \exp\left(\frac{GSI - 100}{28 - 14D}\right) \tag{2-1}$$

Table 2-4. Equations Used to Estimate Rock Mass Deformation Modulus

Independent Variable	Equation	Authors
RMR	$E_{rm,RMR} = \frac{E_{t50}}{100}\left[0.0028(RMR)^2 + 0.9e^{\left(\frac{RMR}{22.82}\right)}\right]$	Nicholson & Bieniawski (1990)
RQD	$E_{rm,RQD} = E_{t50}10^{0.0186RQD-1.91}$	Zhang & Einstein (2004)
GSI	$E_{rm,GSI} = \sqrt{\frac{q_u}{100}}10^{((GSI-10)/40)}$	Hoek et al. (2002)

$$s = \exp\left(\frac{GSI - 100}{9 - 3D}\right) \tag{2-2}$$

$$a = \frac{1}{2} + \frac{1}{6}\left(e^{-GSI/15} - e^{-20/3}\right) \tag{2-3}$$

$$\sigma'_{cm} = q_u \frac{\left[m_b + 4s - a\left(m_b - 8s\right)\right]\left(\frac{m_b}{4} + s\right)^{a-1}}{2\left(1+a\right)\left(2+a\right)} \tag{2-4}$$

$$\sigma'_{3\max} = 0.72\sigma'_{cm}\left(\frac{\sigma'_{cm}}{\gamma H}\right)^{-0.91} \tag{2-5}$$

$$\sigma_{3n} = \frac{\sigma'_{3\max}}{q_u} \tag{2-6}$$

$$\phi' = \sin^{-1}\left[\frac{6am_b\left(s + m_b\sigma'_{3n}\right)^{a-1}}{2\left(1+a\right)\left(2+a\right) + 6am_b\left(s + m_b\sigma'_{3n}\right)^{a-1}}\right] \tag{2-7}$$

$$c' = \frac{q_u\left[\left(1+2a\right)s + \left(1-a\right)m_b\sigma'_{3n}\right]\left(s + m_b\sigma'_{3n}\right)^{a-1}}{\left(1+a\right)\left(2+a\right)\sqrt{1 + \left(\frac{6am_b\left(s + m_b\sigma'_{3n}\right)^{a-1}}{\left(\left(1+a\right)\left(2+a\right)\right)}\right)}} \tag{2-8}$$

$$E_{rm}(GPa) = \left(1 - \frac{D}{2}\right)\sqrt{\frac{q_u}{100}}10^{\frac{GSI-10}{40}} \quad (2\text{-}9)$$

where:

m_b = material constant related to frictional properties of rock

s = rock mass constant

a = rock mass constant

σ'_{cm} = rock mass strength

σ'_{3max} = maximum confining stress

σ_{3n} = normalized maximum stress

ϕ' = effective friction angle of rock mass

c' = effective cohesion or rock mass

E_{rm} = rock mass deformation modulus

2.4 Pressuremeter (PMT) Data

Pressuremeter testing (PMT) was conducted for the present study, and is taken to be the most reliable source of data representing lateral load-deformation characteristics of the subsurface material at the site of investigation. The following sections detail how parameters such as rock mass deformation modulus (E_{rm}) and *p-y* curves may be derived from PMT data.

2.4.1 Initial Pressuremeter Modulus (E_o)

Results from a PMT can be used to determine the initial PMT modulus, E_o. This modulus can be used as an estimate of the rock mass deformation modulus (E_{rm}), as

opposed to that of intact rock (E_{t50}) (Goodman 1980). Because E_o is obtained from an in-situ test that closely simulates lateral loading of a drilled shaft, it is assumed to be the most reliable estimate of rock mass deformation for this study. It can therefore be used to evaluate empirical relationships typically used to estimate E_{rm} (Section 2.3.2), which will done in the current study (Section 7.3). The initial PMT modulus may be determined using the following equation from Briaud (1992) in conjunction with PMT data obtained in the field (Section 4.4).

$$E_o = (1+\nu)(p_2 - p_1)\frac{\left(1+\left(\frac{\Delta R}{R_o}\right)_{c2}\right)^2 + \left(1+\left(\frac{\Delta R}{R_o}\right)_{c1}\right)^2}{\left(1+\left(\frac{\Delta R}{R_o}\right)_{c2}\right)^2 - \left(1+\left(\frac{\Delta R}{R_o}\right)_{c1}\right)^2} \qquad (2\text{-}10)$$

where:

$(\Delta R/R_o)_{c1}$

and

$(\Delta R/R_o)_{c2}$ = radial strain of the borehole cavity at two points on the PMT loading curve corresponding to two pressure values p_{PMT1} and p_{PMT2}, respectively.

p_{PMT} = PMT pressure

2.4.2 Developing *p-y* Curves from PMT Data

The *p-y* method is a common method of analysis for laterally loaded piles, as will be discussed in more detail later in Sections 2.5.2 and 8.1. This method utilizes nonlinear

load-displacement (*p-y*) curves to model the soil-structure interaction and behavior under lateral loading. The most challenging aspect of the *p-y* method is developing the *p-y* curves, as they are typically nonlinear and depend on in-situ conditions and characteristics of the deep foundation elements. Correlations typically used in design to develop these curves are generally empirical, site-specific, and are based on minimal calibration data [as is the case for Reese (1997)]. Consequently, there is a high level of uncertainty when using these relationships in design. This section details the procedure for developing *p-y* curves based on PMT data. Results from PMT can be effectively used to develop *p-y* curves because the expansion of the pressuremeter probe within a soil cavity mimics, to some extent, the lateral deflection of a laterally loaded shaft (Briaud 1992). Consequently, *p-y* curves developed from PMT data in this study will subsequently be used to evaluate how well the existing empirical model proposed by Reese (1997) predicts the load-deflection response.

P-y curves may be developed point-by-point from PMT curves produced from PMT data (PMT data were obtained for the present study and is presented and discussed in Section 4.4). The method described by Briaud (1992) for making this transformation is detailed below. For demonstration purposes, this discussion utilizes PMT data from one test conducted during the present study [at 11.5 ft (Section 4.4) – *p-y* curves developed for each test location will be presented and discussed in Section 6.5.2]. In this case, the transformation is made assuming an 11-ft diameter shaft.

The first step in this process is to correct the PMT data for membrane and volume loss calibrations. The membrane correction accounts for the radial pressure the membrane experiences upon expansion. This value is subtracted from each raw data value, as it

detracts from the actual pressure within the probe to produce the net pressure on the soil cavity wall. The volume loss correction is due to the expansion of the system, including hydraulic tubing, fittings, etc. In addition, hydrostatic pressure due to the hydraulic fluid within the pressuremeter lines must be accounted for; the pressure transducer obtains readings at the ground surface as opposed to at the location of the probe. The method of applying the three corrections is described in more detail below.

The membrane calibration data are obtained by expanding the PMT probe to high levels of pressure under atmospheric air pressure; such data are shown plotted in Fig. 2-1. As can be seen in this figure, a polynomial best-fit trend line may be applied to the data, facilitating an expression of pressure versus volume expansion. Using this fourth-degree polynomial expression, a pressure correction can be determined for each data point of each test.

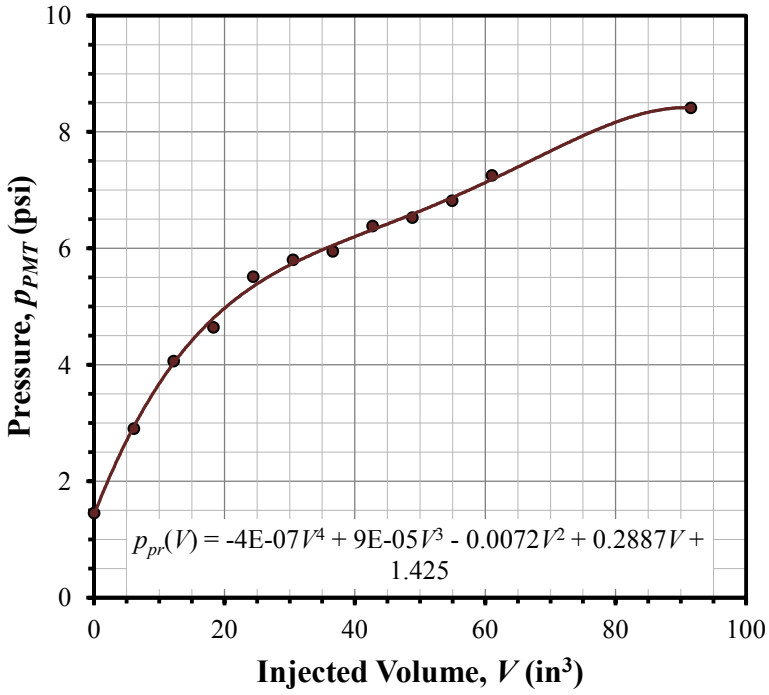

Fig. 2-1. Membrane correction curve

The volume loss calibration is determined in a similar fashion to that of pressure. The PMT probe is inserted into a stiff, steel sleeve with a tight fit. Hydraulic fluid is then pumped into the system and the volume expansion of the system is measured as a function of the pressure attained. Such data are shown plotted in Fig. 2-2. The volume loss correction is obtained by fitting a tangent line to the quasi-linear portion of the data, as shown by the dashed line in the figure. This tangent line is extended to the volume axis, the intersection of which marks the location of a transformed axis. The volume correction is taken as the difference between the tangent line and the transformed vertical axis, and therefore can be determined as a function of pressure using the linear relationship shown in Fig. 2-2.

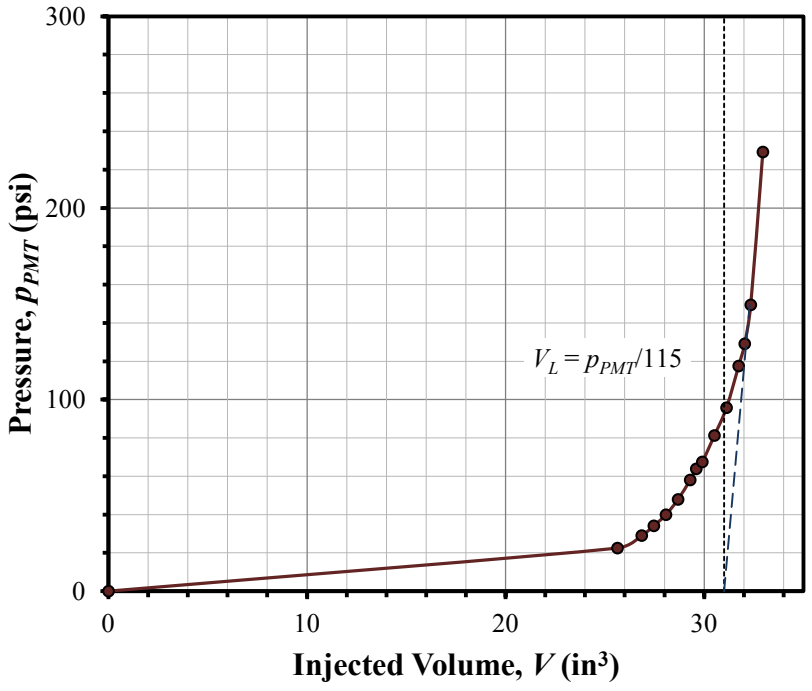

Fig. 2-2. Volume loss correction curve for soil PMT

The hydrostatic pressure is determined by multiplying the unit weight of the hydraulic fluid by the depth to the center of the probe during a particular test. For this study, the specific gravity of the hydraulic fluid was taken as 1.03 for the soil PMT and 0.97 for the rock PMT.

PMT curves for both raw and corrected data are shown in Fig. 2-3. The next step in developing the *p-y* curve is to perform an axis shift to an origin that represents the pressure and volume at which the PMT membrane contacts the cavity wall; the pressure at this point is taken to be the at-rest horizontal stress (Briaud 1992). This stress is taken at the maximum point of curvature on the loading curve, represented by point B in Fig. 2-3. Furthermore, a line is drawn through points D and E to represent the initial slope of

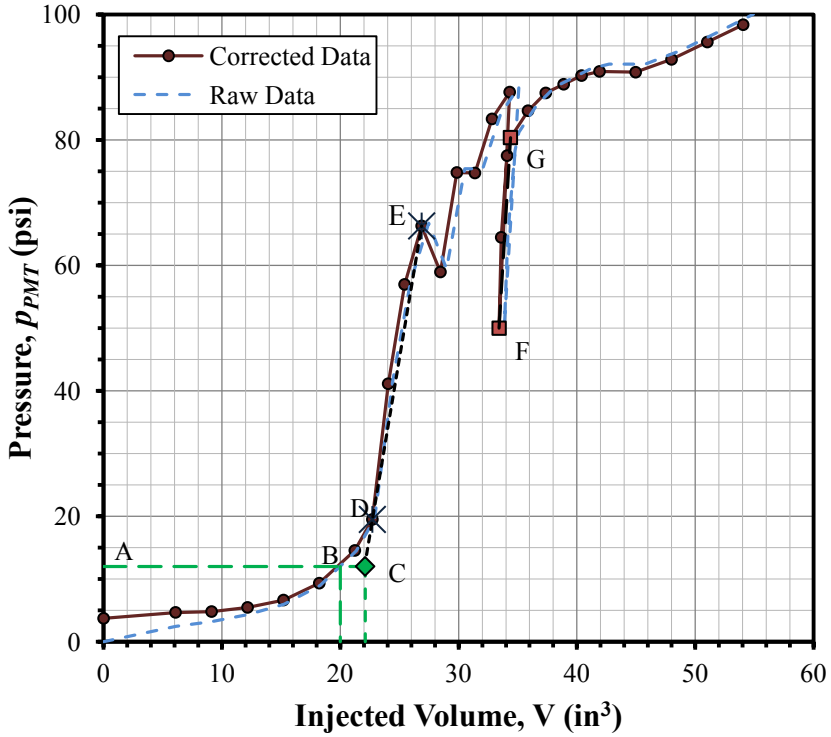

Fig. 2-3. Corrected and raw PMT curves at a depth of 11.5 ft

the loading curve. This line is extended until it intersects the horizontal line A-B. The intersection of these lines at point C is taken as the origin for the *p-y* curve, and represents the in-situ horizontal stress and the volume of the PMT probe upon contact with the cavity wall. With the volume at this point known, the diameter of the cavity can be back-calculated.

The transformed loading curve, including an axis shift and unit conversion, is shown in Fig. 2-4. The next step involves transforming each point on the new curve to correspond to a point on the *p-y* curve. The *p-y* curve is typically defined by the sum of two load-displacement curves – the *Q-y* and *F-y* curves, representing normal resistance and tangential shear resistance, respectively. The *Q-y* curve is developed point-by-point using the following equations:

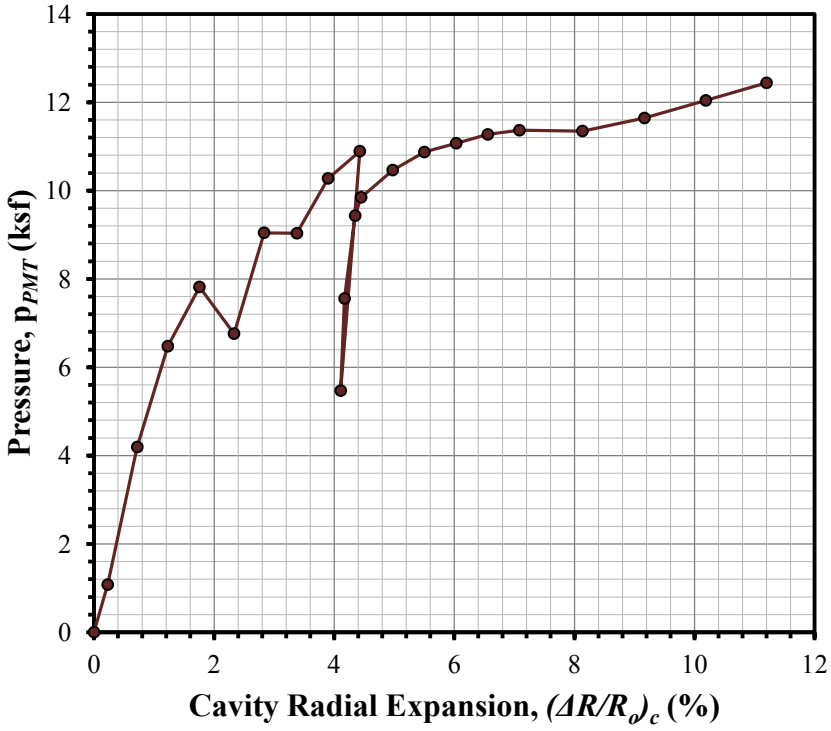

Fig. 2-4. PMT curve with axis shift and unit transformation

$$Q = \alpha p_{PMT} B_s SF \tag{2-11}$$

$$y = \frac{\Delta R_c}{R_c}\frac{B_s}{2} \tag{2-12}$$

$$\frac{\Delta R_c}{R_c} = \sqrt{\frac{V_o + v_c}{V_{oc}}} \tag{2-13}$$

$$D_{cr} = B_s \; if \; RR = \frac{1}{B_s}\sqrt[4]{\frac{EI}{p_L^*}} \le 6.33 \tag{2-14}$$

$$D_{cr} = \frac{3B_s}{4}(RR - 5) if \; RR > 6.33 \tag{2-15}$$

where:

y = lateral deflection at depth z

Q = normal resistance in force per unit length

p_{PMT} = PMT pressure

B_s = shaft diameter

SF = safety factor of $\pi/4$

$\Delta R_c/R_c$ = radial expansion of the cavity

V_o = initial volume of the probe

v_c = corrected volume reading

V_{oc} = volume of the probe upon contacting the cavity wall

D_{cr} = critical depth for the pile

EI = rigidity of the pile

p_L^* = net limit pressure

α = determined graphically as a function of z/D_{cr}

For this study, α was found to be 0.84, 0.97, and 1.0 for the PMTs at depths of 5.5, 11.5, and 16.5 ft, respectively. The shear-force-displacement curve is computed using the following equations from Briaud (1992):

$$F = \tau_{\max} B_s SF \tag{2-16}$$

$$y = \frac{\Delta R_c}{R_c}\frac{B_s}{2} \tag{2-17}$$

$$\tau_{\max} = X(1+X)\frac{\Delta p_{PMT}}{\Delta X} \tag{2-18}$$

$$X = \frac{\Delta V}{V_{or}} \tag{2-19}$$

where:

F = friction force per unit length

τ_{max} = maximum shear stress of the pile-soil interface

V_{or} = volume of the probe at the beginning of the reload curve

Δp_{PMT} = change in pressure corresponding to a change in volume, ΔV, along the reload curve.

Applying the above equations to the transformed PMT data results in *Q-y* and *F-y* curves similar to those shown in Fig. 2-5. Also shown in this figure is the final *p-y* curve, taken as the sum of the *Q-y* and *F-y* components. For this case, irregularities in the curves

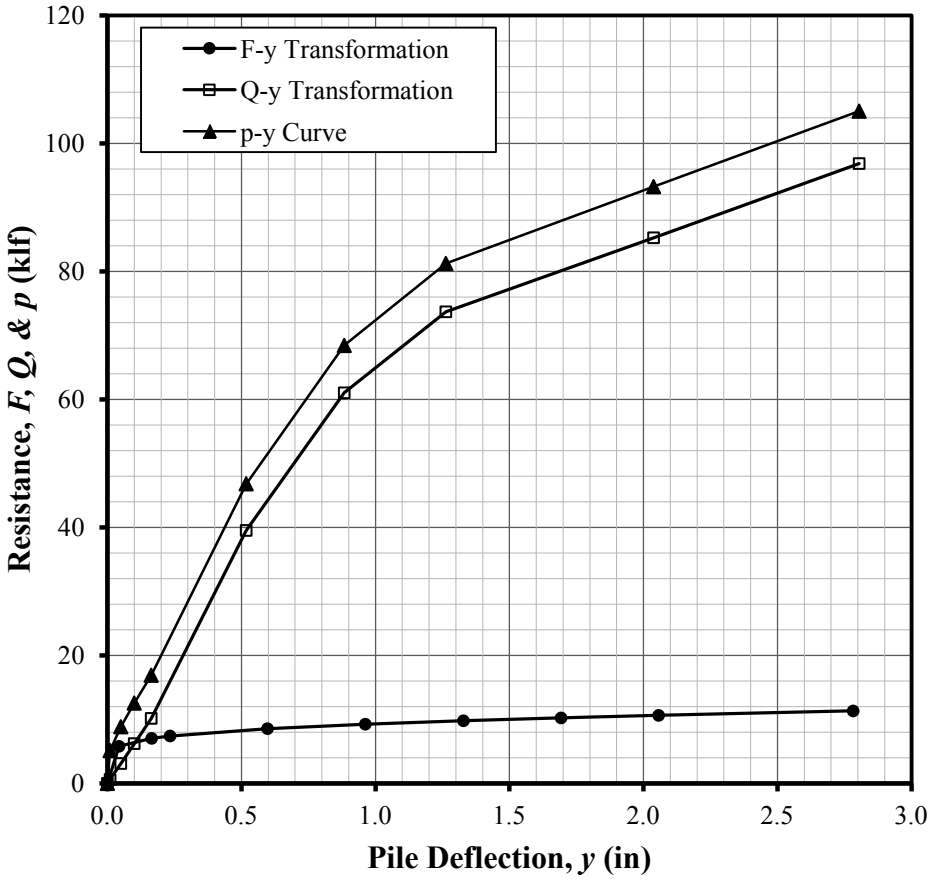

Fig. 2-5. *Q-y*, *F-y*, and *p-y* curves at 11.5 ft

were eliminated to produce a smoother curve. In addition, the curves were cut short at a deflection of about 3 in. because the data were limited in computing the *F-y* curve.

The above process of transforming PMT data to produce *p-y* curves may also be applied to rock PMT data. However, there are two differences in performing this transformation for the rock PMT data. The first is that the load values for the *Q-y* curve are multiplied by 0.5, as prescribed by Yang et al. (2010). The second is that the maximum tangential shear stress is taken to be that typically computed for vertical shaft resistance. This step is done as recommended by Zhang and Einstein (1998) using the following equation:

$$\tau_{\max} = \min\left(1.25\sqrt{\frac{q_u}{p_A}}, 0.05\frac{f_c'}{p_A}\right)p_A \quad (2\text{-}20)$$

where:

F = friction force per unit length

q_u = UAC strength of the intact rock

p_A = atmospheric pressure (14.696 psi)

f'_c = compressive strength of concrete (taken as 3000 psi)

τ_{max} = maximum shear stress of the pile-soil interface

All *p-y* curves are presented and discussed in Section 6.5.2.

2.5 Analytical Methods

Different methods of analysis have been developed to compute lateral deflections for laterally loaded drilled shafts embedded in rock material. One simple approach is to model the shaft as a vertical elastic beam within an elastic continuum. Closed form solutions for how this might be done for flexible and rigid shafts within a rock foundation have been given by Carter and Kulhawy (1992). Another, more complex method is to model the response of the foundation material as a series of discrete, linear springs along the length of the shaft, using the subgrade modulus as the spring constant. This method has been advanced to incorporate nonlinear springs through the use of *p-y* curves. "Interim" recommendations for computing *p-y* curves in weak rock have been proposed by Reese (1997). The proposed methods discussed above are presented in more detail in the following subsections.

2.5.1 Elastic Beam in Elastic Rock Continuum

The design of laterally loaded shafts is often governed by the magnitude of geometric deformations, as is the case in the current study. A simple approach to compute the deflection of the shaft head is to assume an elastic shaft embedded in a homogeneous, isotropic, linearly elastic continuum of soil or rock mass. This approach ignores the nonlinear response of the soil, but accounts for the continuous nature of the foundation response. In this approach, the deflections are computed through application of a series of closed form equations, which are available for rigid and flexible shafts socketed into rock (Carter and Kulhawy 1992). Methods such as the *p-y* method (discussed below) account for nonlinear effects, but they neglect the continuous nature of the soil and demand time and a numerical solution. The method given by Carter and Kulhawy (1992) for predicting the geometric deformations of a shaft embedded within a rock mass is discussed in detail below.

Different equations for estimating the magnitude of geometric deformations apply depending on whether the shaft socket is rigid or flexible. Thus, it is first necessary to determine whether the shaft is rigid, flexible, or intermediate, as can be done using the following equations:

Shaft is flexible if:

$$\frac{L_s}{B_s} \geq \left(\frac{E_e}{G^*} \right)^{2/7} \tag{2-21}$$

Shaft is rigid if:

$$if\ \frac{L_s}{B_s} \le 0.05\left(\frac{E_e}{G^*}\right)^{1/2} \tag{2-22}$$

Shaft is intermediate if:

$$0.05\left(\frac{E_e}{G^*}\right)^{1/2} < \frac{L_{sock}}{B_s} < \left(\frac{E_e}{G^*}\right)^{2/7} \tag{2-23}$$

where:

$$E_e = \frac{(EI)_s}{\frac{\pi B_s{}^4}{64}} \tag{2-24}$$

$$G_{rm}{}^* = G_{rm}\left(1+\frac{3v_{rm}}{4}\right) \tag{2-25}$$

$$G_{rm} = \frac{E_{rm}}{2(1+v_{rm})} \tag{2-26}$$

and:

$(EI)_s$ = bending stiffness of shaft

E_e = equivalent elastic modulus

$G_{rm}{}^*$ = equivalent shear modulus

G_{rm} = rock mass shear modulus

v_{rm} = rock mass Poisson's ratio

L_{sock} = depth of shaft embedment in rock

B_s = diameter of shaft

The equations for estimating deformations given below (Eq. 2-27 and 2-28) for the rigid and flexible cases were validated through extensive finite element analysis by Carter and Kulhawy (1992). When the shaft is classified as intermediate (Eq. 2-23), it was found that the actual deflection exceeded that computed using the given equations. It is therefore recommended by Carter and Kulhawy (1992) that, in the case the shaft is intermediate, the deformations be computed using each set of equations, and that the largest resulting value be multiplied by 1.25 to produce a reasonable estimate. These equations are valid for $1 < E_e/E_r < 10^6$ and $10 > L_s/B_s > 1$.

$$y_{flex} = 0.50\left(\frac{V_r}{G_{rm} * B_s}\right)\left(\frac{E_e}{G_{rm} *}\right)^{-1/7} + 1.08\left(\frac{M_r}{G_{rm} * B_s^{\,2}}\right)\left(\frac{E_e}{G_{rm} *}\right)^{-3/7}$$

$$\theta_{flex} = 1.08\left(\frac{V_r}{G_{rm} * B_s^{\,2}}\right)\left(\frac{E_e}{G_{rm} *}\right)^{-3/7} + 6.40\left(\frac{M_r}{G_{rm} * B_s^{\,3}}\right)\left(\frac{E_e}{G_{rm} *}\right)^{-5/7} \quad \text{flexible shafts (2-27)}$$

$$y_{rig} = 0.4\left(\frac{V_r}{G_{rm} * B_s}\right)\left(\frac{2L_s}{B_s}\right)^{-1/3} + 0.3\left(\frac{M_r}{G_{rm} * B_s^{\,2}}\right)\left(\frac{2L_s}{B_s}\right)^{-7/8}$$

$$\theta_{rig} = 0.3\left(\frac{V_r}{G_{rm} * B_s^{\,2}}\right)\left(\frac{2L_s}{B_s}\right)^{-7/8} + 0.8\left(\frac{M_r}{G_{rm} * B_s^{\,3}}\right)\left(\frac{2L_s}{B_s}\right)^{-5/3} \quad \text{rigid shafts} \qquad (2\text{-}28)$$

where:

V_r = lateral load at rock surface

M_r = bending moment at rock surface

For the rigid shaft case, the shaft rotates as a rigid body, so the depth to the pivot of rotation, or point of zero lateral deflection, can be computed using the following parametric equation.

$$z_r = B_s \frac{0.4\left(\frac{2L_s}{B_s}\right)^{-1/3} + 0.3\left(\frac{e_L}{B_s}\right)\left(\frac{2L_s}{B_s}\right)^{-7/8}}{0.3\left(\frac{2L_s}{B_s}\right)^{-7/8} + 0.8\left(\frac{e_L}{B_s}\right)\left(\frac{2L_s}{B_s}\right)^{-5/3}} \qquad \text{for rigid shafts} \qquad (2\text{-}29)$$

Carter and Kulhawy (1992) go into more detail regarding the case that bedrock is overlain by soil, as shown in Fig. 2-6. This case will not be discussed in detail here, but the method prescribed by Carter and Kulhawy (1992) is considered later in Section 8.5 in applying the above equations.

2.5.2 *p-y* Curves for Weak Rock

Development of *p-y* curves from PMT data was previously discussed in Section 2.4.2. However, it is rare that such quality in-situ data are obtained in typical practice, for which case empirical models have been developed. Reese (1997) proposed an interim approach for developing *p-y* curves for weak rock that employs data that may be readily obtained during a field and laboratory investigation. This model however, has been calibrated with minimal experimental data. Considering the lack of more supporting data

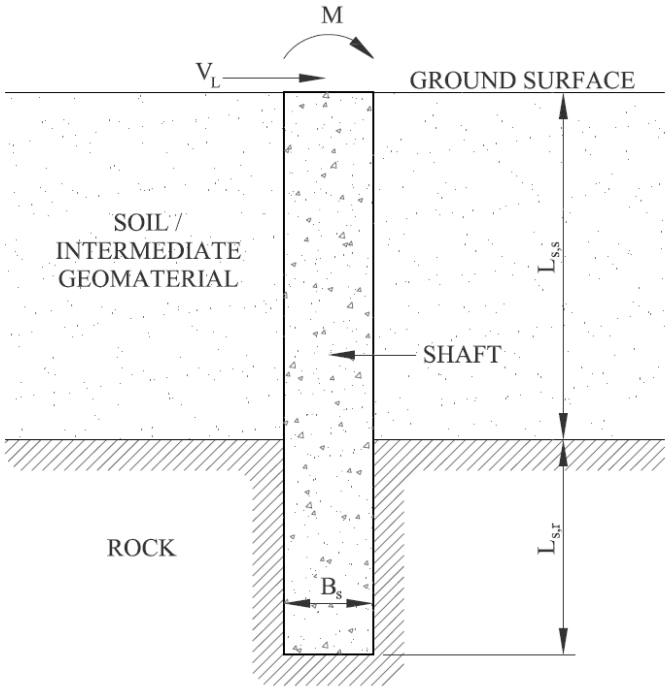

Fig. 2-6. Rock socketed shaft under lateral loading – overlying soil layer (modified from Carter and Kulhawy 1992)

and the variability of rock mass strength, the author cautions the designer in using this model. A brief overview of the *p-y* method and its employment in weak rock is discussed below.

In using the *p-y* method to analyze a laterally loaded shaft, the response of the soil is modeled as a series of discrete, nonlinear springs uniformly spaced along the length of the shaft, as indicated in Fig. 1 of Reese (1997). Modeling the response of the soil in this way is conducive to a solution using the finite difference method, but it neglects the continuous nature of the soil. In applying the *p-y* method, the response of a laterally loaded shaft in regard to rotation, displacement, bending moment, and shear is governed by the following nonlinear differential equation given by Reese (1997):

$$\frac{d^2}{dz^2}\left[(EI)_s \frac{d^2y}{dz^2}\right] + P_a \frac{d^2y}{dz^2} - p - W = 0 \qquad (2\text{-}30)$$

where:

$(EI)_s$ = bending stiffness of shaft

y = lateral deflection at depth z

z = depth along shaft

P_a = axial load on shaft

p = soil resistance per unit length along shaft

W = distributed load along shaft

For the *p-y* method, the nonlinear response of the soil (p in Eq. 2-30) is given by ky, where k is a nonlinear expression of the response as a function of y. In addition, for a reinforced concrete shaft, the rigidity of the shaft, $(EI)_s$, has been shown to be nonlinear (Reese 1997), as the stiffness is greatly reduced upon cracking of the concrete. The following discussion details the interim procedure for developing *p-y* curves for weak rock proposed by Reese (1997), which is the *weak rock* model used in the computer program *LPILE*.

A typical *p-y* curve for weak rock is shown in Fig. 4 of Reese (1997). The first step in developing the curve is to establish the defining parameters p_{ur} and K_{ir}. The ultimate soil resistance of the rock mass, p_{ur}, is given as a function of q_u by the following equation:

$$p_{ur} = \alpha_r q_u B_s \left(1 + 1.4 \frac{z_r}{B_s}\right) \qquad 0 \le z_r \le 3B_s \qquad (2\text{-}31)$$

$$p_{ur} = 5.2 \alpha_r q_u B_s \qquad z_r > 3B_s \qquad (2\text{-}32)$$

where:

p_{ur} = ultimate resistance per unit length along shaft

z_r = depth below rock surface along shaft

B_s = diameter of shaft

α_r = strength reduction factor assumed to be 1/3 for RQD of 100 and to increase linearly to 1 for RQD of 0.

The initial slope of the *p-y* curve is governed by the parameter K_{ir}, which is determined using the following equations from Reese (1997):

$$K_{ir} = k_{ir} E_{ir} \qquad (2\text{-}33)$$

$$k_{ir} = \left(100 + \frac{400 z_r}{3B_s}\right) \qquad 0 \le z_r \le 3B_s \qquad (2\text{-}34)$$

$$k_{ir} = 500 \qquad z_r > 3B_s \qquad (2\text{-}35)$$

where:

k_{ir} = dimensionless constant

E_{ir} = modulus of rock

In the case that PMT data are available, q_u may be taken as p_L* as the net limit resistance (with RQD = 0), and E_{ir} may be taken as the initial pressuremeter modulus.

Reese (1997) indicates p_{ur} and E_{ir} may also be determined from UAC strength of the intact rock. However, this assumption may be erroneous because the ultimate resistance of the rock mass is usually less than that of the intact rock due to the influence of discontinuities (Section 7.3). This method for developing *p-y* curves was calibrated through a case study using the results of two full-scale load tests. For the first case study (Islamorada), the strength properties of the intact rock were used. For the second case study (San Francisco), pressuremeter data was available and the corresponding modulus was consequently used. However, apparently the PMT were not taken to ultimate failure of the rock, so the net limit pressure (p_L*) could not be obtained. Accordingly, the ultimate resistance of the rock was inferred from the PMT modulus in conjunction with existing general correlations between E_{ir} and q_u (Reese 1997).

With p_{ur} and K_{ir} defined above, the complete *p-y* curve can be expressed in three segments using the following equations from Reese (1997, see Fig. 4).

$$p = K_{ir} y \qquad y \le y_A \tag{2-36}$$

$$p = \frac{p_{ur}}{2}\left(\frac{y}{y_{rm}}\right)^{0.25} \qquad y \ge y_A;\ p \le p_{ur} \tag{2-37}$$

$$p = p_{ur} \tag{2-38}$$

$$y_{rm} = k_{rm} B \tag{2-39}$$

$$y_A = \left[\frac{p_{ur}}{2(y_{rm})^{0.25} K_{ir}}\right]^{1.33} \tag{2-40}$$

where:

k_{rm} = constant ranging between 0.00005 to 0.0005 that represents the overall stiffness of the curve

Reese (1997) indicates that the above procedure outlined for developing *p-y* curves produces results that are in agreement with the available experimental data. However, the supporting data are minimal, and the author advises the designer to use them with caution, especially in the absence of detailed geotechnical data. Gabr et al. (2002) showed the above method overestimates the lateral stiffness of weathered rock within the piedmont region of Southeastern United States. The above method for developing *p-y* curves is used by *LPILE* for weak rock foundations, and will subsequently be used to evaluate the model in terms of the predicted *p-y* curves (Section 8.4) and how they compare with those developed directly from pressuremeter data.

2.6 Summary

Methods used for classification and characterization of engineering properties of rock mass were discussed in this section. These methods will be explored in more detail throughout this study in terms of their applicability to the material in a site-specific case.

3 GEOLOGICAL INVESTIGATION

3.1 Overview

The site of investigation for this study was at the proposed Lima Substation for PacifiCorp located in Wyoming near the western boundary of the Green River Basin, 4 miles southwest of Opal, Lincoln County, Wyoming on Wagon Wheel Road (Fig. 3-1). The coordinates for this site are 41°43'17.99"N and 110°21'59.17"W, which is found in Section 14 of Township 20 North and Range 115 West. The body of water located nearest to Lima Substation is Hams Fork, a perennial stream located about 4 miles north of the project. The ground surface at the project site is approximately 6715 ft above average sea level, and is situated on gently sloping terrain of approximately 2 to 3% to the southeast. The semi-arid environment supports desert shrubs and grass for livestock and native wildlife grazing. The only significant human development within 15 miles, except scattered ranch houses and unpaved roads, includes the towns Kemmerer and Opal, Wyoming. North and west of the project site are found State Highways 30 and 189, respectively; the Union Pacific Railroad parallels Highway 30. In addition, a natural gas pipeline is located about 0.5 miles to the west of the site. The geology of the site is discussed in this section in terms of rock formations and potential geologic hazards.

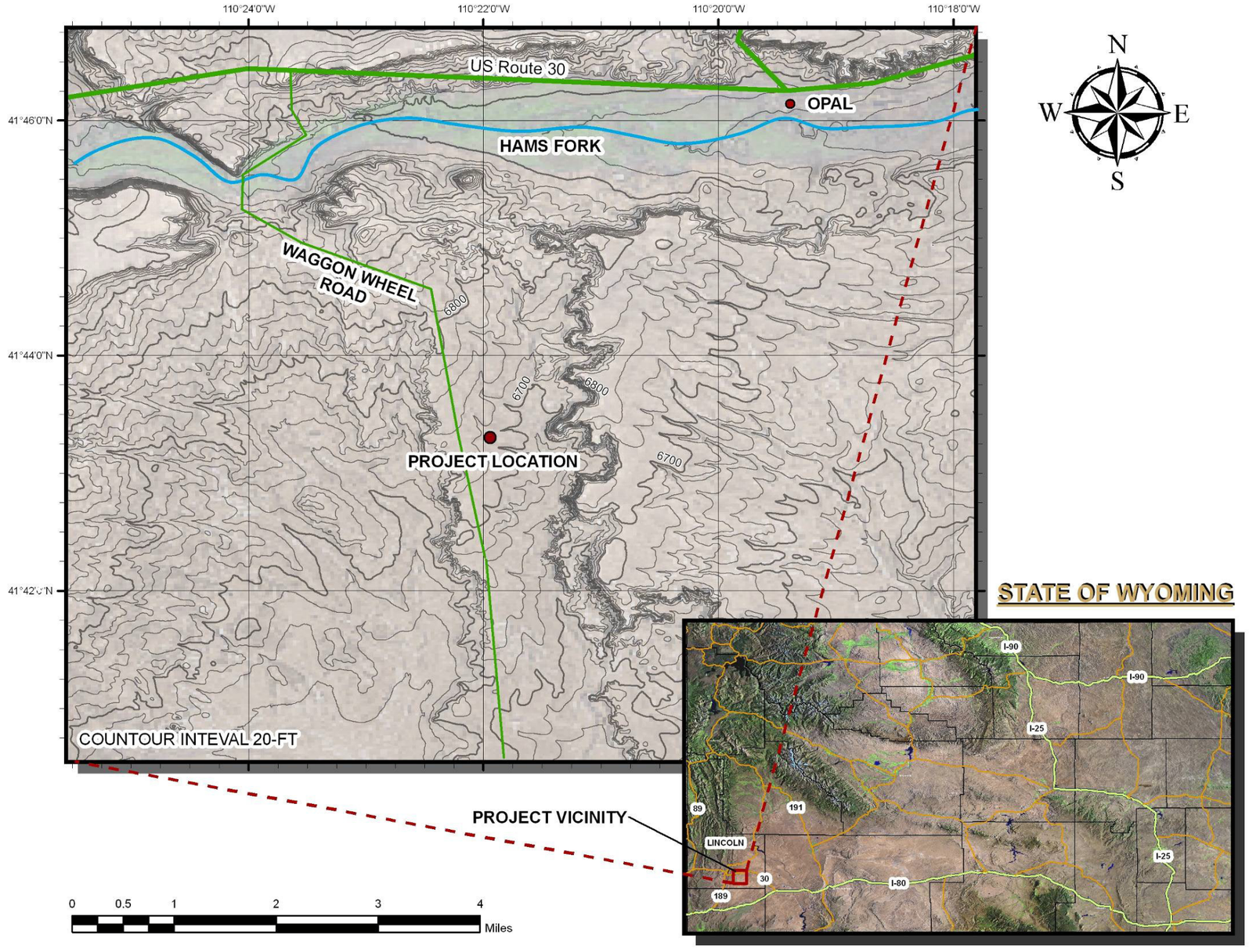

Fig. 3-1. Lima Substation location and topographic map (WSGS 2010, USGS 2010)

3.2 Regional and Local Geology

The site is located in the Green River Basin, which is one of four major structural units that together form an intermountain basin – the three others being the Washakie Basin, the Great Divide Basin, and the Rock Springs Uplift (Bradley 1964). The Green River Basin is delineated by the Wasatch Range to the west, the Wind River Range to the north, the Uinta Range to the south, and the Continental Divide of the Laramie Range to the east. As the largest of the structural units, the Green River Basin is approximately 60 miles wide (east to west) and 100 miles long (north to south). It is primarily defined by conspicuous, outward-facing escarpments of the Wasatch and Green River Formations; one exception being a 40-mile stretch to the south that is defined by a gradual, gravelly slope that approaches the north side of the Uinta Mountain Range. In a general sense, the basin floor is nearly flat with landscape characterized by badlands, buttes, and hills with several intermittent and perennial streams that are tributaries of the Green River.

The Green River Basin is composed of three primary formations of fluvial and lacustrine origin: Wasatch, Green River, and Bridger (Bradley 1964). Generally speaking, the Green River Formation is underlain by the Wasatch Formation and overlain by the Bridger Formation. These formations are attributed to the presence and fluctuations of Gosiute Lake that formed during the middle and lower Eocene Epoch. This fresh-water lake was formed by continual downwarping of the basin floor that also increased the potential for fluvial deposition of the Wasatch Formation. Gosiute Lake formed the lacustrine deposits that are manifest as several tongues within the Green River Formation. Lake fluctuations also caused interfingering of this formation with the Wasatch Formation. As the lake transgressed to its largest extent, it deposited the prominent Laney Shale Member of the Green River Formation. Eventually the rate of

sedimentation exceeded the rate of downwarping of the lake bed, which ultimately resulted in a lake full of sediments, breaking the water body into several smaller units. It was during the existence of these smaller lakes that the Bridger Formation was deposited.

Subsequent erosion has redefined the terrain, resulting in the exposure of each of the three major formations within a 2 mile radius of the site (Fig. 3-2). At the ground surface, there exists about 5 ft of light-brown, powdery fluvial residuum and topsoil. According to M'Gonigle and Dover (1992), the site is located in the lower Bridger A (Tba) unit that consists of light-gray and medium-gray to greenish-gray mudstone, claystone, siltstone, and sandstone; minor interbeds of light-gray and green tuff, tan to light-gray limestone and marlstone; and thin lignite and coal (Figs. 3-2 and 3-3). The Bridger A unit is estimated to be about 330 ft thick and contains three layers of light-gray limestone. In addition, this member is split by a 35-ft thick upper Laney Shale member (Tglu) of the Green River Formation (Fig. 3-3).

The Green River Formation is described as gray to tan limestone, gray to brown shale, and marlstone, oil shale, and tuff beds (M'Gonigle and Dover, 1992). A 375 ft thick lower Lane Shale member (Tgll) underlies the lower Bridger A unit (Tba) and overlies the upper member of the Wasatch Formation (Twu). As described by M'Gonigle and Dover (1992), the Wasatch Formation is composed of "red, brown, green, yellow, and gray sequences of mudstone, fluvial sandstone, siltstone, and claystone; subordinate diamictite, conglomerate, grit, marlstone, and pisolithic limestone." The upper member of this formation is about 165-ft thick, and includes "fine- to coarse-grained, locally conglomeratic sandstone."

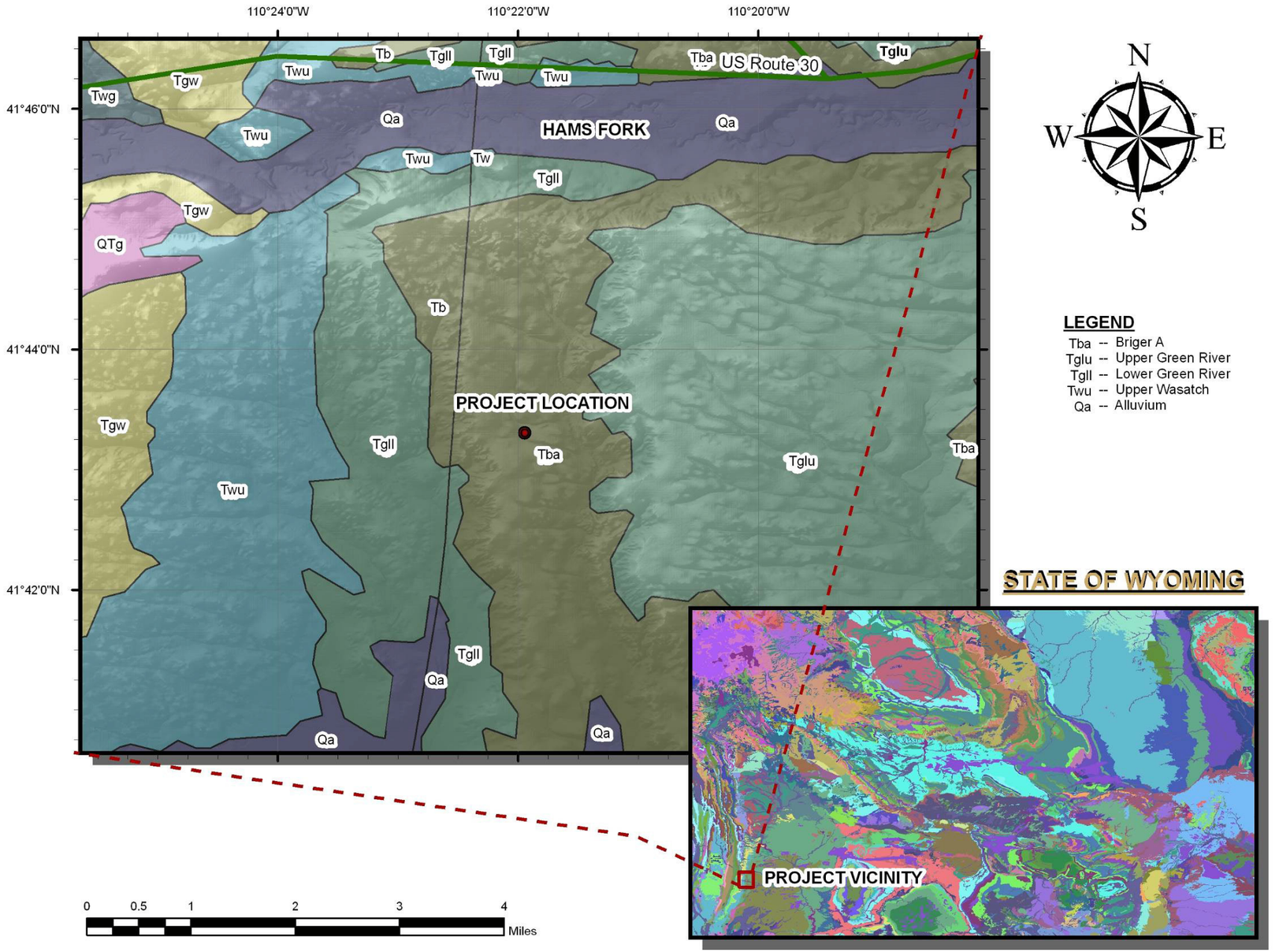

Fig. 3-2. Bedrock map for Lima Substation (WSGS 2010, USGS 2010)

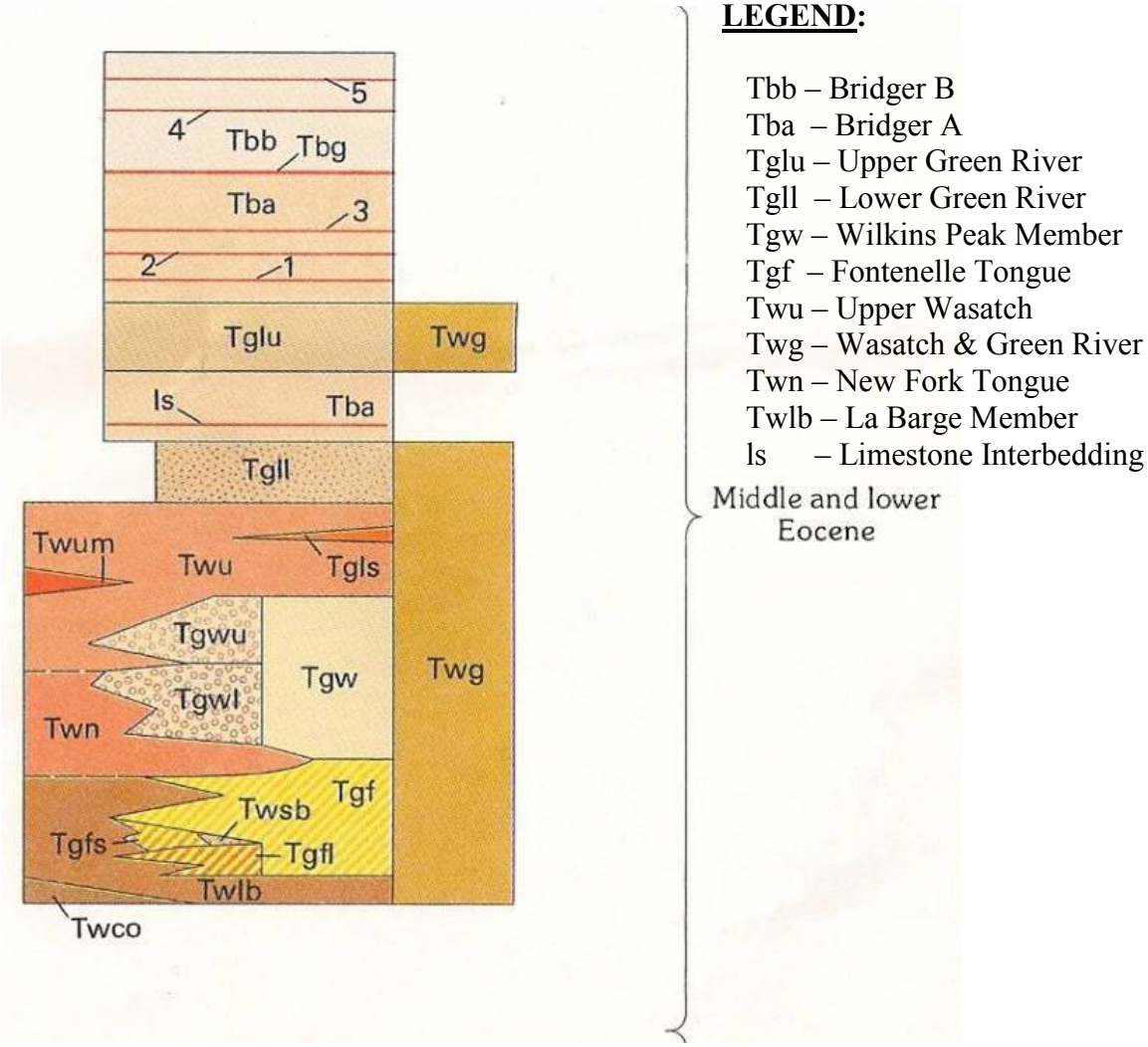

Fig. 3-3. Stratigraphic sequence at Lima Substation (M'Gonigle and Dover 1992)

It is possible that all three formations, previously described, may be encountered within 200 ft of the ground surface at Lima Substation. The upper Laney Shale Member (Tglu) is exposed approximately 1 mile to the east of the site in low-lying foothills. This geologic exposure suggests that the site is located within the lower portions of the A Member of the Bridger Formation (Tba), which is estimated to be about 65-ft thick at the project site and consists of minor limestone beds near its base (Fig. 3-3). The Bridger A Member is underlain by the lower Laney Shale Member (Tgll) of the Green River

Formation, which is exposed in a ravine located about 0.5 miles west of the site. Beneath the *Tgll* Member is the upper member of the Wasatch Formation (Twu), which is exposed in a shallow valley located approximately 1.5 miles to the west.

The geologic formations shown in Figs. 3-2 and 3-3 are composed largely of mudstone, sandstone, limestone, and shale with various degrees of weathering. Accordingly, a primary issue for this site is the rock quality in terms of amount of weathering, fracturing, and other imperfections. These issues will be addressed in more detail during the subsequent discussions regarding coring and geotechnical evaluations.

3.3 Geologic Conditions and Potential Hazards

3.3.1 Groundwater Conditions

There is nothing to suggest the presence of groundwater near the surface. PSI (2010) did indicate the possibility of perched groundwater between depths 40 and 45 ft below the surface.

3.3.2 Surficial Soils

Dickey and M'Gonigle (1992) indicate that Lima Substation is located within a zone that contains abundant swelling clays derived from weathered rock. Many of the surficial rock formations within southwestern Wyoming contain beds of weathered volcanic ash that form bentonite and severely expansive clays (Case 1986).

3.3.3 Earthquake Hazards

Wyoming is one of six states that FEMA has declared as a "high seismic-hazard state." There are several faults throughout its southwest region that are capable of

producing magnitude 7 (M7), or Modified Mercalli Intensity X (MMI X) earthquakes. The project site is located near the eastern bench of the Wyoming Overthrust Belt (Fig. 3-4). The thrusting that formed this belt began in the late Paleozoic and continued into the early Cenozoic era. However, some late Cenozoic activity still exists along the earlier fault zones and has been noted to be the source of several seismic events over the past century, the most severe of these being of M4.6, (MMI V) in September of 1985 (Case 1997). Of all seismic zones in the state, this belt poses the highest potential for producing damaging strong motion at the site.

However, there are no mapped faults within immediate vicinity of the Lima Substation site; therefore, there is no significant hazard from surface fault rupture. Based on the web-based 2008 USGS seismic hazards map developed for Wyoming, the expected peak ground acceleration (pga) at this site from nearby faults is about 0.09 to 0.10 *g,* with a 10% probability of exceedance in 50 years (Fig. 3-5). There is no liquefaction hazard at this site because this is essentially a weathered rock site (site class B) with relatively deep groundwater.

3.3.4 Flammable Gas

As previously mentioned, there exists a gas pipeline about 0.5 miles to the west of Lima Substation. However, there is no indication that flammable gas exists directly at the site.

3.3.5 Other Considerations

The corrosiveness of the local soil/ rock is unknown and these materials should be tested to determine the corrosiveness. In addition, high spring run-off from melting snow

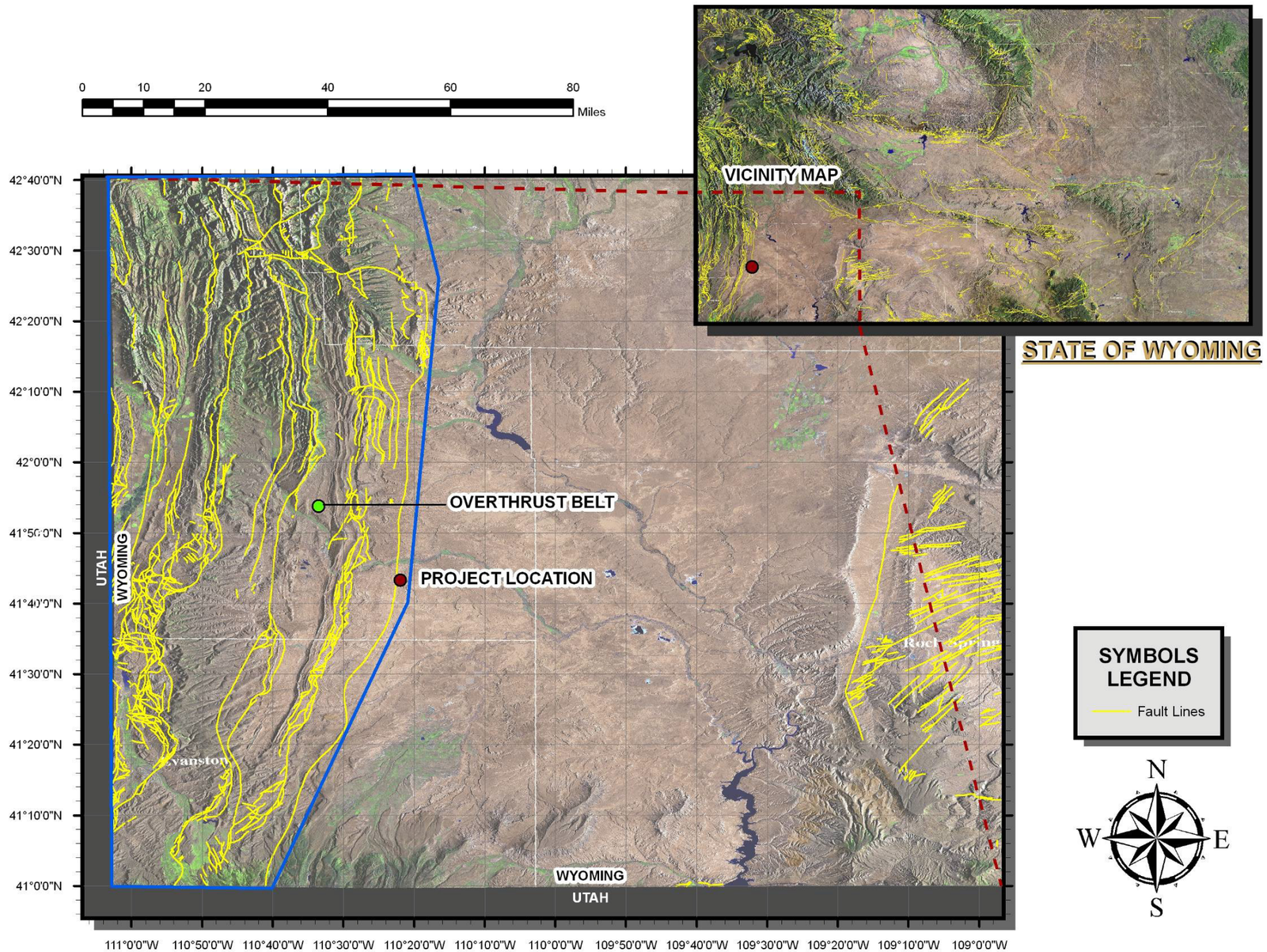

Fig. 3-4. Wyoming fault map (WSGS (2010), USGS (2010))

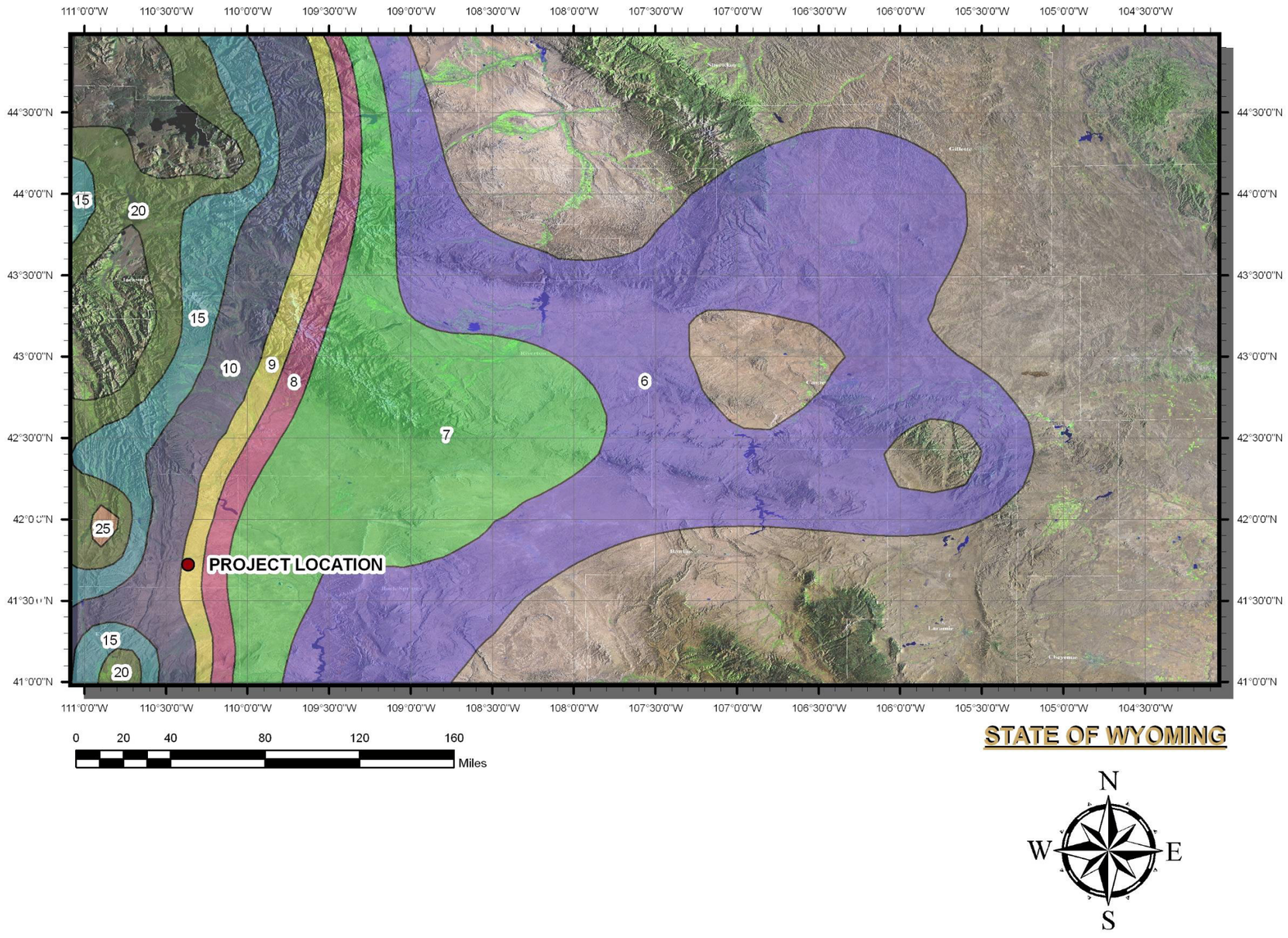

Fig. 3-5. Estimates of peak ground acceleration (pga, %g) with 10% probability of exceedance in 50 years for the state of Wyoming (USGS 2010)

and rainstorms could cause local surface erosion at this site. Proper surface drainage should be provided at this facility.

3.4 Summary

The local and regional geology of the site of investigation was described in this chapter in terms of geological formations and potential geologic hazards. It was determined that the site is likely located in the lower member of the Bridger A formation, which is largely composed of mudstone, sandstone, limestone, and shale. With various degrees of weathering, it was concluded that it will be necessary to account for the effect of discontinuities and the strength of the rock mass. It was concluded that significant geologic hazards are of little concern in regard to the current investigation.

4 FIELD INVESTIGATIONS

4.1 Overview

The subsurface investigation at Lima Substation employed generally accepted sampling methods and in-situ geotechnical testing to investigate the subsurface conditions. Accordingly, it was first necessary to gain a general idea of the expected types of geomaterials. The findings of the geological investigation described in Chapter 3 suggest the presence of an approximately 5 ft layer of light-brown, powdery fluvial residuum at the surface (Section 3.2). Below this to a depth of about 60 ft, alternating layers of mudstone, claystone, siltstone, sandstone, and limestone were indicated in the geological reports. Furthermore, results of prior subsurface investigations by PSI (2010) indicate the presence of very hard/dense subsurface geomaterials beyond a depth of about 20 ft. Considering the presence of these materials, it was concluded that rock coring would be the most appropriate sampling method at Lima Substation.

The initial plan was to conduct two site visits: the first to obtain core samples to a depth of about 60 ft, and a subsequent visit to conduct pressuremeter testing (PMT) to the same depth. However, at the time of PMT, the capacity of the PMT equipment used by In-Situ Tech. Inc. was limited to testing only the weaker geomaterial within the upper 17 ft of the profile. Consequently, arrangements were made to revisit the site to perform rock PMT within the layers of the stronger rock material. This later PMT was done by In-Situ Soil Testing. In all, five (5) boreholes were drilled at this site, as indicated in

Fig. 4-1. In this chapter, the purpose of each of these boreholes and the procedures followed throughout the field investigation are discussed, which include soil sampling, rock core sampling, and in-situ PMT.

4.2 Soil Sampling

The first drilling was done at the location of LS #1 (Fig. 4-1) on July 6–8, 2010. The goal was to obtain samples to a depth of about 60 ft. Sampling was accomplished using a CME 85 wire-line drill rig operated by Inberg-Miller Engineers (Fig. 4-2). A macro sampler was used to obtain a continuous, disturbed sample for the weaker, weathered material near the surface. This sampling was accomplished using a 1.68-in. inside diameter (ID) clear PVC tube liner within the macro sampler rod, which was driven using an SPT hammer. The blow counts were not recorded for this nonstandard sampler, but numerous N_{SPT}-values are available in the PSI (2010) report. The macro sampler was used until very hard material was reached at a depth of about 17.5 ft. Upon bringing the 5-ft long samples to the surface, the material was inspected and logged with respect to general soil type, particle size, texture, color, etc. (Figs. 4-3 and 4-4). After the field borehole log was prepared, the sample tubes were sealed at both ends with duct tape to preserve natural moisture and soil fabric conditions. Rock coring was used below a depth of 17.5 ft.

In an attempt to perform borehole shear tests (BST), a hole was hand-augured to a depth of about 5 ft and the soil was bagged for transportation to the laboratory. BST was abandoned, as material below 5 ft was too hard to hand-augur.

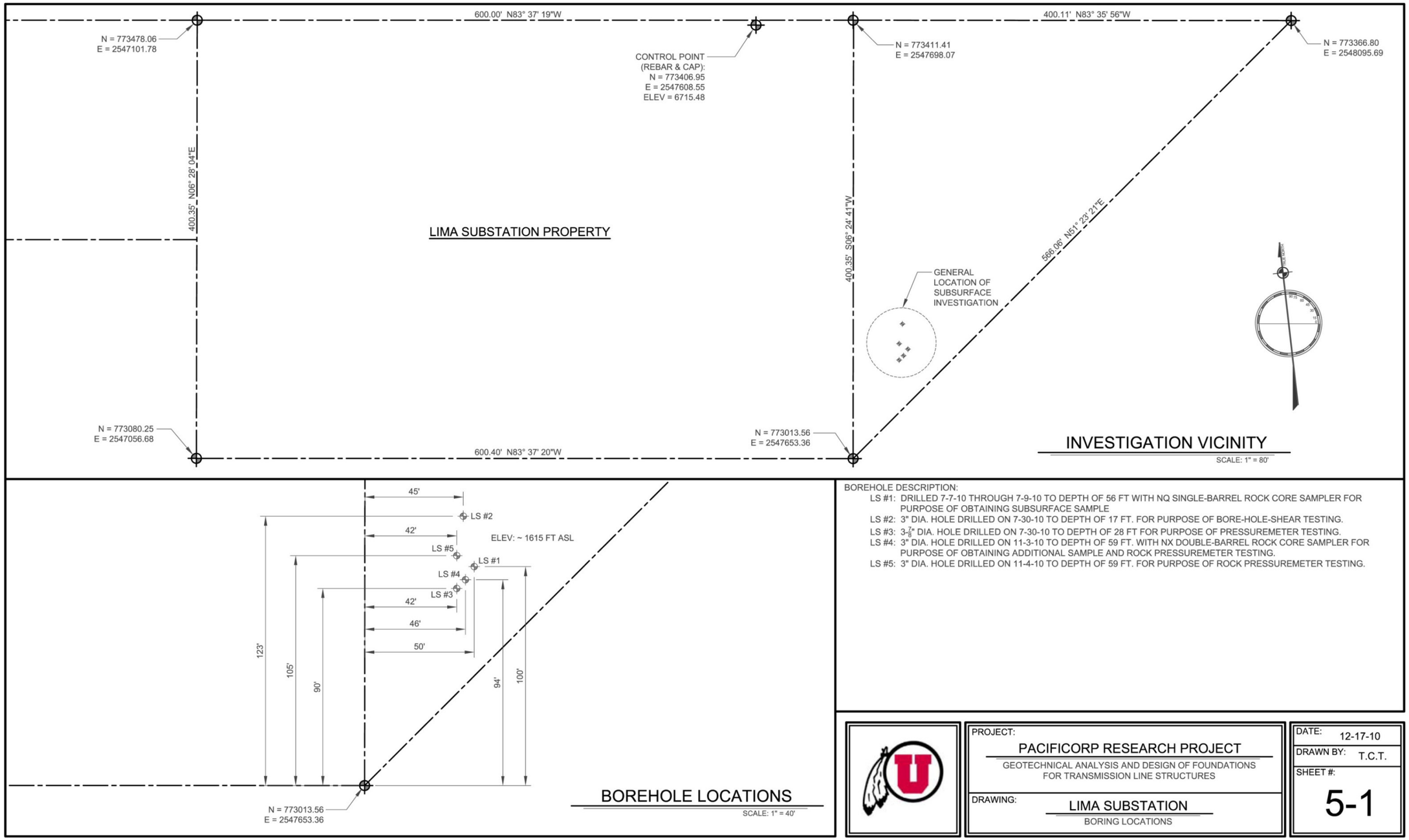

Fig. 4-1. Field investigation borehole / corehole locations

Fig. 4-2. CME 85 drill rig setup for LS #1 on July 7, 2010

THE UNIVERSITY OF UTAH

Project: LIMA SUBSTATION
Project Location: NEAR OPAL, WYOMING
Project Number:

Log of Boring LS #1
Sheet 1 of 2

Date(s) Drilled: 7/7/10 - 7/8/10	Logged By: THOMAS TIMPSON	Checked By:
Drilling Method: CORING	Drill Bit Size/Type:	Total Depth Drilled (feet): 56
Drill Rig Type: CME 85 - AIR ROTARY	Drilled By: INBERG-MILLER ENGINEERS	Hammer Weight/ Drop (lbs/in.):
Apparent Groundwater Depth: ___ ft ATD ___ ft after ___ hrs ___ ft after ___ hrs		Surface Elevation (feet): 6715
Comments:	Borehole Backfill:	Elevation Datum:

Depth, feet	Elevation, feet	ROCK CORE: Run No.	Box No.	Recovery, %	Frac. Freq.	R Q D, %	Fracture Drawing/ Number	Lithology	MATERIAL DESCRIPTION	Packer Tests	SOIL SAMPLES: Type	Number	Blows per foot	Drill Rate, feet/hour	FIELD NOTES/ LAB DATA
0	6715														
		1	OBTAINED USING MACRO SAMPLER CONTAINED IN PLAST TUBE (5-FT SECTIONS)	80	N/A	N/A	N/A	CLAYEY SAND (SC)	SAND, CLAY, MEDIUM DENSE, LIGHT BROWN TO WHITISH, FINE TO VERY FINE, CLAYEY SAND (SC) WITH GRAVEL, MOIST							
5	6710	2		90	N/A	N/A	N/A	LS	LIMESTONE, OLIVE GREEN, THINLY BEDDED, FINE GRAINED, MODERATELY TO HIGHLY WEATHERED (INFILL MAT.), WEAK, MOIST.						
10	6705	3		100	N/A	N/A	N/A	CS	CLAYSTONE, DARK GREENISH GRAY, THINLY BEDDED, FINE GRAINED, MODERATELY TO HIGHLY WEATHERED, WEAK, MOIST.						
15	6700	4		100	N/A	N/A	N/A								
		5	1	50	0	15	M	LIMESTONE	LIMESTONE, LIGHT GREENISH GRAY, THINLY BEDDED, VERY FINE GRAINED, FRESH TO MODERATELY WEATHERED, STRONG, DAMP, MECHANICL FRACTURING, NATRUAL FRACTURING.					4	
20	6695	6	1	80	0	30	M							4	
25	6690	7	1	10	0	10	M		LIMESTONE (6-1/2" INTACT SAMPLE), LIGHT GREENISH GRAY, THINLY BEDDED, FINE GRAINED, FRESH, STRONG, DAMP, MECHNICAL FRACT.					5	
30	6685														

Fig. 4-3. Boring/coring Log LS #1 for Lima Substation site – 0 to 30 ft

THE UNIVERSITY OF UTAH

Project: LIMA SUBSTATION
Project Location: NEAR OPAL, WY.
Project Number:

Log of Boring LS #1
Sheet 2 of 2

Depth, feet	Elevation, feet	Run No.	Box No.	Recovery, %	Frac. Freq.	R Q D, %	Fracture Drawing/ Number		Lithology	MATERIAL DESCRIPTION	Packer Tests	SOIL SAMPLES Type	SOIL SAMPLES Number	SOIL SAMPLES Blows per foot	Drill Rate, feet/hour	FIELD NOTES/ LAB DATA
30	6685	8	1	65	0	65		M	LS	LIMESTONE, GREENISH GRAY, THINLY BEDDED, FINE GRAINED, FRESH, STRONG, DAMP.					5	
		9	2	90	0	80		M		SANDSTONE, LIGHT TO DARK GREENISH GRAY, THINLY BEDDED, FINE GRAINED, FRESH, WEAK; MECHANICAL FRACTURING.					5	
35	6680						/40	1								
		10	2	95	0.6	40	⌐	M 2	SS	SANDSTONE, GREENISH BROWN TO DARK GREENISH GRAY, THINKLY BEDDED, FINE TO MED. GRAINED, FRESH, WEAK, MECHANICAL FRACTURING, NATURAL FRACTURING, MOIST. 1: 40, SH, VN, NO, NO, PL, SR, M 2: JOG, SH, VN, NO, NO, ST, SR, M 3: 0, SH, VN, NO, NO, PL, SR, M (NAT. FRACTURES APPEAR RUSTY)					5	
								3								
40	6675							4								
		11	3	80	0.4	40	/75	5 M		SANDSTONE TO LIMESTONE, DARK GREENISH GRAY, FINE GRAINED, THINLY BEDDED, FRESH, WEAK TO STRONG, DAMP TO MOIST, NATURAL & MECHANICAL FRACTURING. 4: 0, SH, VN, NO, NO, PL, SR, M 5: 75, SH, VN, NO, NO, PL, SR, M (NAT. FRACTURES APPEAR RUSTY)					3.5	SECTION OF HIGHLY WTH., V.W., CRUMBLY LIMESTONE
45	6670	12	3	100	0	80		M	LS	LIMESTONE, DARK GREENISH GRAY, FINE GRAINED, THINLY BEDDED, FRESH, STRONG, DAMP, MECHANICAL FRACTURING.					10	
50	6665	13	4	65	0	8		M		LIMESTONE, DARK GREENISH GRAY, FINE GRAINED, THINLY BEDDED, FRESH, STRONG, DAMP, MECHANICAL FRACTURING.					5	
55	6660	14	4	100	0	0		M		LIMESTONE, VERY DARK GREENISH GRAY, FINE TO VERY FINE GRAINED, THINLY BEDDED, HIGHLY WEATHERED, VERY WEAK, MOIST, MECHANICAL FRACTURING.					2	

GENERAL NOTES:
1. SAMPLING WAS CONDUCTED WITH SINGLE BARREL SAMPLER. SAMPLE WAS REMOVED FROM SAMPLER BY TAPPING TUBE WITH HAMMER, WHICH LIKELY AFFECTED RQD THAT WAS SUBSEQUENTLY MEASURED WHILE SAMPLE WAS IN CORE BOX.
1. INITIAL INTENT WAS TO DRILL TO A DEPTH OF 60-FT, BUT DRILLING WAS TERMINATED AT 56-FT DUE TO SLOW DRILLING RATE.
2. SLOW DRILLING RATES AT 55 FT. ARE LIKELY DUE TO INCREASED MOISTURE, WHICH IS NOT CONDUCIVE TO AIR-ROTARY. INCREASED MOISTURE AT THIS DEPTH MAY INDICATE PRESENCE OF NEAR BY WATER TABLE.

ABBREVIATIONS:
SH -- SHEAR DISCONTINUITY TYPE
VN -- VERY NARROW JOINT (<0.05 IN)
NO -- NO INFILLING
PL -- PLANAR FRACTURE SURFACE
SR -- SLIGHTLY ROUGH FRACTURE SURFACE
M -- MODERATE DISCONTINUITY SPACING (0.7 - 2.0 FT)

Fig. 4-4. Boring/coring Log LS #1 for Lima Substation site – 30 to 56 ft

4.3 Rock Coring

Rock coring was performed during two separate visits, the first being a continuation of the site visit described in Section 4.2. After reaching harder rock with the macro sampler, rock coring was conducted using an air-rotary technique and a 1.87-in. ID, NQ single-barrel rock core sampler. Drilling rates remained relatively constant at about 4 to 5 ft/hr. Sampling was conducted at 5-ft intervals to a depth of about 56 ft. The rock core was transferred to storage boxes (Fig. 4-5) upon extruding the sample from the core barrel by lightly tapping the sampling barrel with a hammer. With the rock core in the core boxes, a detailed core log was prepared, which included RQD, drilling rate, rock type, color, texture, grain size, etc. (Figs. 4-3 and 4-4). The core was placed in the box and not sealed or coated in any manner to preserve moisture content. Coring continued through July 7, 2010, stopping at about 40 ft at 7:00 p.m., and resuming the following day until about 1:00 p.m. Coring was terminating at a depth of 56 ft because a higher level of moisture was encountered, which greatly affected drilling rates using air-rotary drilling (~2 ft/hr).

Additional core samples were obtained during the third site visit on November 3–5. This coring was done by Mountain States Drilling of Salt Lake City, Utah with a CME 55 wire-line drill rig (Fig. 4-6) using an air-rotary technique and a 2.16-in ID, NX double-barrel sampler. The primary purpose of this phase of the investigation was to perform rock PMT at depths ranging between 17.5 and 60 ft in two coreholes. In addition, higher quality, intact rock core samples were obtained for additional laboratory testing and better characterization of the subsurface material. The goal was to obtain core sample to a depth of about 60 ft from both boreholes, but due to unanticipated drilling

Fig. 4-5. Rock core from LS #1 immediately after transfer to a carboard core box

Fig. 4-6. CME 55 wire-line drill rig setup for LS #4 and LS #5 on November 4, 2010

issues discussed below, samples were only obtained for the first corehole, LS #4, while the second corehole, LS #5 (see Fig. 4-1) was drilled with a standard tri-cone bit.

The sampling method used for LS #4 was similar to that described above for LS #1, but the coring, handling, and preservation methods were significantly improved in an effort to preserve natural conditions and to characterize the rock better. Sampling started at about 12:00 noon on November 3, and ended at about 3:00 p.m. on November 4. Core sampling started at a depth of 9 ft and continued to a depth of 59 ft. Approximately 8 ft of samples were obtained in the weathered material found in the upper 17 ft of the profile. Drilling rates for these dates ranged between 5 and 15 ft/hr, which were significantly faster than those experienced for LS #1. The improved drilling rate was a result of several factors including bit type, drilling technique, and use of a double barrel sampler. Upon removing the sample from the core hole, the double-barrel sampler was placed in a horizontal position, split in half, and the sample was measured for recovery and rock quality (Fig. 4-7). The samples were then carefully transferred to waxed NX rock core boxes, which had plywood fixed to the base to increase rigidity of the box. The rock core was taken inside a tent and prepared in accordance with ASTM D5079 – 08 with slight variances as discussed below.

After preparing a detailed coring log for LS #4 (Figs. 4-8 and 4-9), individual intact rock core specimens were wrapped first in saran wrap, then in cheese cloth, and then liquid paraffin wax was applied with a brush. This procedure provided an effective moisture barrier to maintain natural moisture within the rock core, and confinement to stabilize the sample. Each sample was then placed carefully in a core box for subsequent transportation to the Geotechnical Laboratory at the University of Utah in Salt Lake City,

Fig. 4-7. Fresh rock core in sample barrel (44 to 49 ft.)

THE UNIVERSITY OF UTAH

Project: LIMA SUBSTATION
Project Location: NEAR OPAL, WYOMING
Project Number:

Log of Boring LS #4
Sheet 1 of 2

Date(s) Drilled: 11/3/10 - 11/4/10	Logged By: THOMAS TIMPSON	Checked By:
Drilling Method: CORING	Drill Bit Size/Type:	Total Depth Drilled (feet): 59
Drill Rig Type: CME 55 - AIR ROTARY	Drilled By: MSD -- DON MOERMAN	Hammer Weight/ Drop (lbs/in.):
Apparent Groundwater Depth: ___ ft ATD ___ ft after ___ hrs ___ ft after ___ hrs		Surface Elevation (feet): 6715
Comments:	Borehole Backfill:	Elevation Datum:

Depth, feet	Elevation, feet	ROCK CORE: Run No.	Box No.	Recovery, %	Frac. Freq.	R Q D, %	Fracture Drawing/ Number		Lithology	MATERIAL DESCRIPTION	Packer Tests	SOIL SAMPLES: Type	Number	Blows per foot	Drill Rate, feet/hour	FIELD NOTES/ LAB DATA
0	6715	NO SAMPLE OBTAINED														
5	6710															
10	6705	1	1	97	0	N/A	N/A		CLAYEY SAND (SC)	CLAYSTONE W/ SAND W/ SAND & LIME, DARK GREENISH GRAY, VERY DENSE FINE GRAINED, HIGHLY WEATHERED, MOIST. NOTE: RUNS 1 & 2 WERE OBTAINED USING A DOUBLE ROCK CORE BARREL WITH GOOD RECOVERY. VERY BRITTLE, DIFFICULT TO TRANSFER TO CORE BOX. TAKES FORM OF SOFT ROCK BUT IS VERY BRITTLE.					20	
15	6700	2	1	90	0.2	N/A	N/A			PORTIONS OF WEAK LIMESTONE, THINLY BEDDED W/ NATURAL FRACTURING. -- CLAYSTONE W/ SAND W/ SAND & LIME, DARK GREENISH GRAY, VERY DENSE FINE GRAINED, HIGHLY WEATHERED, MOIST.					20	
20	6695	3	2	68	0.2	18		M	LIMESTONE	LIMESTONE, LIGHT GREENISH GRAY, THINLY BEDDED, FINE GRAINED, HIGHLY WEATHERED, STRONG, DAMP, MECHANICAL & NATURAL FRACTURES, VERY WEAK ALONG BEDDING PLANES					5	HIGHLY FRACT IN 1ST 18"
25	6690	4	2	86	0.8	20	90	M 1 4		LIMESTONE, LIGH GREENISH GRAY, THINLY BEDDED, FINE GRAINED, HIGHLY WEATHERED, MOD. STRONG, MOIST, MECHANICAL & NATURAL FRACTURES, VERY WEAK ALONG BEDDING PLANES 1-4: 90, SH, T, NO, NO, WA, SR, M (BLACK & BROWNISH) M: HORIZONTAL ALONG WEAK BEDDNING PLANES -- ABUNDANT					10	SWITCHED DRILL BIT DUE TO SLOW RATES -- BET. AIR CIRC.
30	6685															

Fig. 4-8. Coring Log LS #4 for Lima Substation site – 9 to 30 ft

THE UNIVERSITY OF UTAH

Project: LIMA SUBSTATION
Project Location: NEAR OPAL, WY.
Project Number:

Log of Boring LS #4
Sheet 2 of 2

Depth, feet	Elevation, feet	ROCK CORE: Run No.	Box No.	Recovery, %	Frac. Freq.	R Q D, %	Fracture Drawing/ Number	Lithology	MATERIAL DESCRIPTION	Packer Tests	SOIL SAMPLES: Type	Number	Blows per foot	Drill Rate, feet/hour	FIELD NOTES/ LAB DATA
30	6685														
		5	3	88	1.4	68	20-45		SANDSTONE, DARK GREENISH GRAY, THINLY BEDDED, FINE GRAINED, FRESH, WEAK, MOIST, MECHANICAL & NATURAL FRACTURING 5-10: 20-45, SH, VN, NO, NO, PL, SR, M (DARK GRAY WITH RUSTY OVERLAY) M: ALONG HORIZ. BEDDING PLANES					15	
35	6680						20								
		6	3 & 4	100	0.8	67	45	SS	SANDSTONE, DARK GREENISH TO BROWNISH GRAY, THINLY BEDDED, FINE GRAINED, FRESH, WEAK, MOIST NATURAL FRACTURING 11-15: 20-75, SH, T, NO, NO, PL, SR, M (RUSTY APPEARANCE)					12	
							75								
40	6675						75								CONDENS. BUILDUP (MORNING)
		7	4	60	0.2	48	45		LIMESTONE, LIGHT GREENISH GRAY, FINE GRAINED, THINLY BEDDED, FRESH, MODERATELY STONG, DAMP, MECHANICAL & NATURAL FRACTURING. 16: 45, SH, T, NO, NO, PL, SR, W, (CLEAN)					5	SECTION OF HIGHLY WTH., V.W., CRUMBLY LIMESTONE
45	6670														
		8	4 & 5	98	0	68		LS	LIMESTONE, LIGHT GREENISH GRAY, FINE GRAINED, THINLY BEDDED, FRESH, MODERATELY STRONG, DAMP, MECHANICAL FRACTURING ALONG HORIZONTAL BEDDING					15	
50	6665														
		9	5	72	0	60			LIMESTONE, LIGHT GREENISH GRAY, FINE GRAINED, THINLY BEDDED, FRESH, MODERATELY STRONG, DAMP, MECHANICAL FRACTURING ALONG HORIZONTAL BEDDING					15	
55	6660														
		10	5	76	0	17			LIMESTONE, DARK GREENISH GRAY, FINE TO VERY FINE, THINLY BEDDED, MODERATELY WEATHERED, M.S., VERY MOIST, MECHANICAL FRACTURING ALONG HORIZ. BEDDING. NOTE: SIGNIFICANTLY MORE MOIST AT 54-FT. BTWN 54-FT AND 55-FT, DARK GREEN, BROKEN FLAKY/SHALY LIKE MATERIAL ADDITIONAL MOISTURE AND WEATHERING MY BE DUE TO CLOSE PROXIMITY OF WATER TABLE.					10	

GENERAL NOTES:

1. SAMPLING WAS CONDUCTED WITH A DOUBLE-BARREL ROCK CORING SAMPLER FROM 9-FT TO 59-FT. UPON BRINGING THE SAMPLE TO THE SURFACE, THE SAMPLING TUBE WAS SPLIT OPEN FOR INSPECTION OF THE SAMPLE, AT WHICH TIME PHOTOGRAPHS, RECOVERY, AND RQD WERE TAKEN. THE SAMPLE WAS THEN TRANSFERRED TO THE CORE BOX WITH CARE. HOWEVER, DUE TO THE WEAK NATURE OF SOME OF THE ROCK, SOME OF THE CORE DID BREAK ALONG BEDDING PLANES, AS CAN BE SEEN IN BOXES.

ABBREVIATIONS:

SH -- SHEAR DISCONTINUITY TYPE
NO -- NO INFILLING
SR -- SLIGHTLY ROUGH FRACTURE SURFACE
T -- TIGHT JOINT (0 IN)
VN -- VERY NARROW JOINT (<0.05 IN)
PL -- PLANAR FRACTURE SURFACE
M -- MODERATE DISCONTINUITY SPACING (0.7 - 2.0 FT)

Fig. 4-9. Coring log LS #4 for Lima Substation site – 30 to 59 ft

Utah. Photographs of full core boxes from LS #1 and LS #4 can be seen in Figs. 4-10 through 4-18. The depths shown in these figures are approximate.

The samples from this subsequent investigation (LS #4) obtained using a double-barrel sampler and improved drilling techniques had better overall recovery and higher RQD values than those obtained with the single-barrel sampler (LS #1). This improvement was a direct result of the improved drilling technique, and demonstrates the impact that drilling and sampling techniques can have on the results of the investigation. Recovery and RQD are important parameters in determining the properties of the rock mass. Accordingly, if sampling is conducted with poor techniques, then the quality of results of the investigation will consequently reflect similar quality.

4.4 Pressuremeter Testing

The purpose of the second site visit on July 30, 2010 was to conduct PMTs to a depth of about 60 ft and borehole shear tests (BST) to a depth of 17.5 ft. However, the PMT equipment mobilized to the site had insufficient capacity to test adequately the harder rock layers. Consequently, PMT was conducted primarily in the weaker, weathered material in the upper 17 ft of the profile. One attempt was made to test the upper part of a limestone layer found at a depth of 24.5 ft. Dr. Trevor Smith of In-Situ Tech. Inc. conducted the tests using a Roctest Texam PMT. Mountain States Drilling performed the drilling for boreholes LS #2 and LS #3 with a CME 55 truck-mounted wire-line drill rig using mud-rotary drilling. An attempt was made to perform the BST in borehole LS #2, but the presence of gravel between 3 and 5 ft and a hole full of mud below 5 ft prevented lowering of the BST head below about 5 ft. Consequently, no BSTs were conducted. PMTs were performed at depths of 5.5, 11.5, 16.5, and 24.5 ft. The

Fig. 4-10. Core box #1 for LS #1

Fig. 4-11. Core box #2 for LS #1

Fig. 4-12. Core box #3 for LS #1

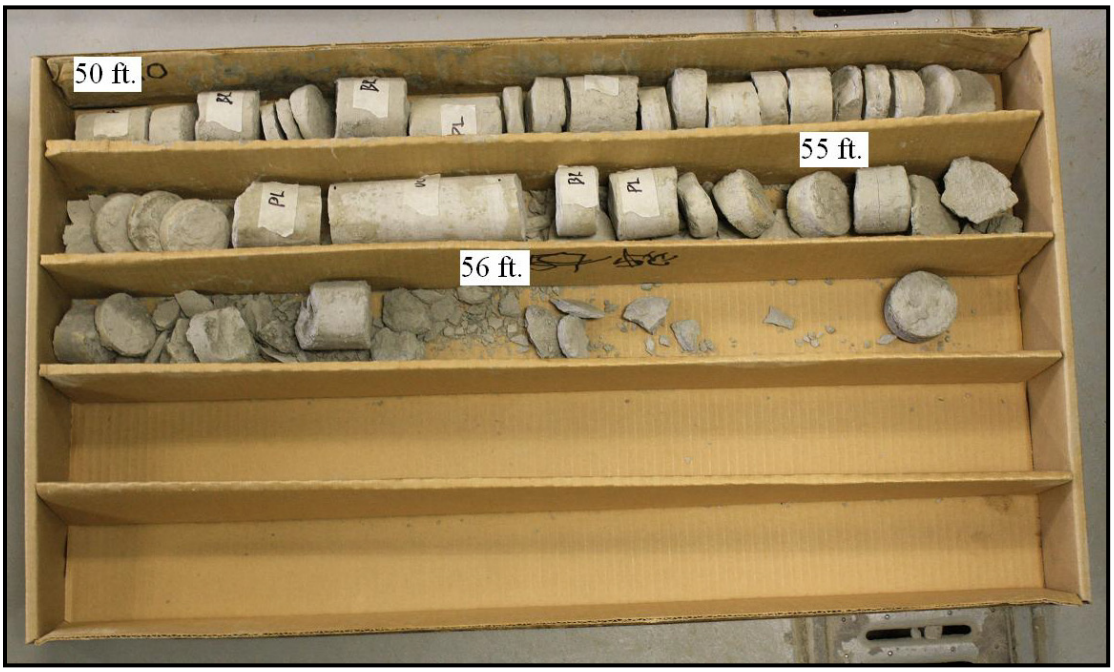

Fig. 4-13. Core box #4 for LS #1

Fig. 4-14. Core box #1 for LS #4 with waxed specimens

Fig. 4-15. Core box #2 for LS #4 with waxed specimens

Fig. 4-16. Core box #3 for LS #4 with waxed specimens

Fig. 4-17. Core box #4 for LS #4

Fig. 4-18. Core box #5 for LS #4

general procedure for conducting a test was as follows: (1) drill with a 3-7/8-in. tri-cone bit to a depth about 2 ft above the desired test location; (2) remove drill bit and proceed with 3-in. bit an additional 4 ft; (3) remove the bit, attach PMT probe, and lower until the probe is centered in the 3-in. x 4-ft cavity; (4) conduct the test (see Smith 2010). Testing was concluded at 5:00 p.m. The corrected PMT curves from these tests are shown in Figs. 4-19 through 4-22, and the calculated results are summarized in Table 4-1 (from Smith 2010).

Rock PMTs were performed during the third site visit on November 3–5, 2010. The goal was to conduct tests at intermittent intervals using two boreholes drilled to a depth of about 60 ft. In-Situ Soil Testing performed the testing using a Roctest Enerpac hydraulic piston, a Roctest Acculog-IX electronic readout, and a Roctest Probex probe. Seven tests were conducted in each corehole for a total of fourteen tests. Rather than testing alternatively with drilling, each hole was drilled to final depth (59 ft) prior to testing. Then testing was done starting at the bottom of the hole and moving upward with each successive test. In coring the first hole (LS #4), In-Situ Soil Testing confirmed that the coring bit used (3-1/16 in. diameter) was the correct size for the PMT probe. However, due to slow drilling rates, when harder rock was encountered, Mountain States Drilling switched to a 3-1/8-in. diameter bit and cored to a depth of 59 ft. This was not realized until conducting the first PMT at a depth of 57 ft, when the inflated probe membrane barely made contact with the cavity wall near maximum volume injection. Membrane expansion into the cavity wall was therefore limited in this hole. In spite of this problem, testing was resumed by carefully using somewhat higher volume injection and testing at prespecified increments.

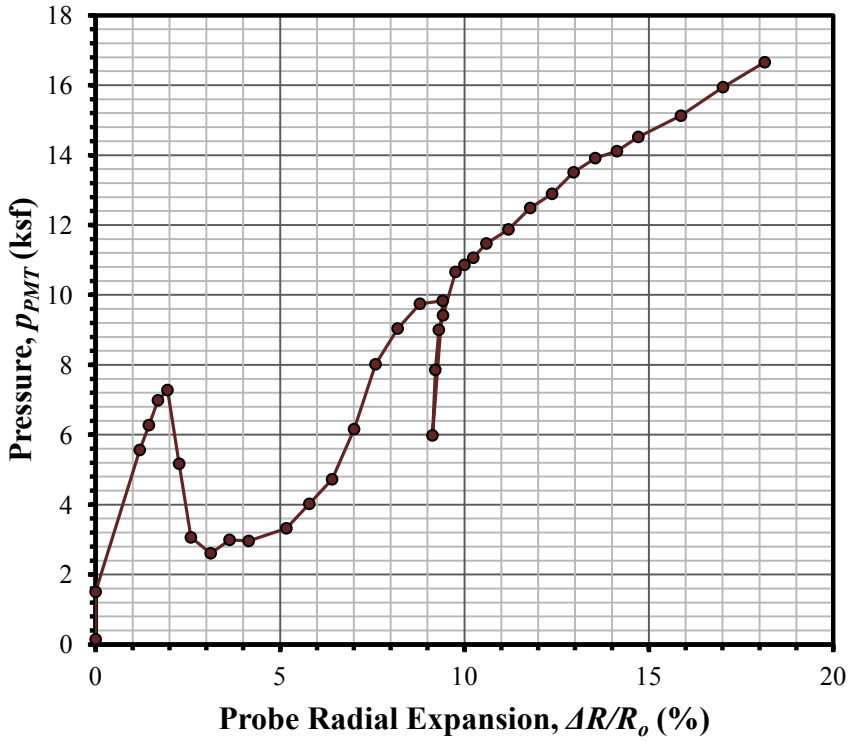

Fig. 4-19. PMT results for LS #3 at 5.5 ft (reproduced from Smith 2010)

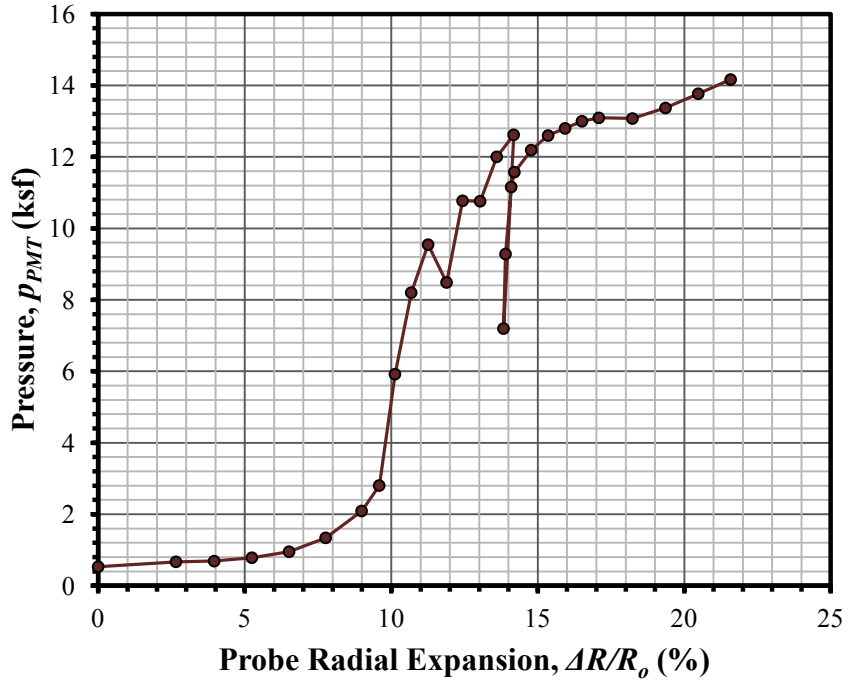

Fig. 4-20. PMT results for LS #3 at 11.5 ft (reproduced from Smith 2010)

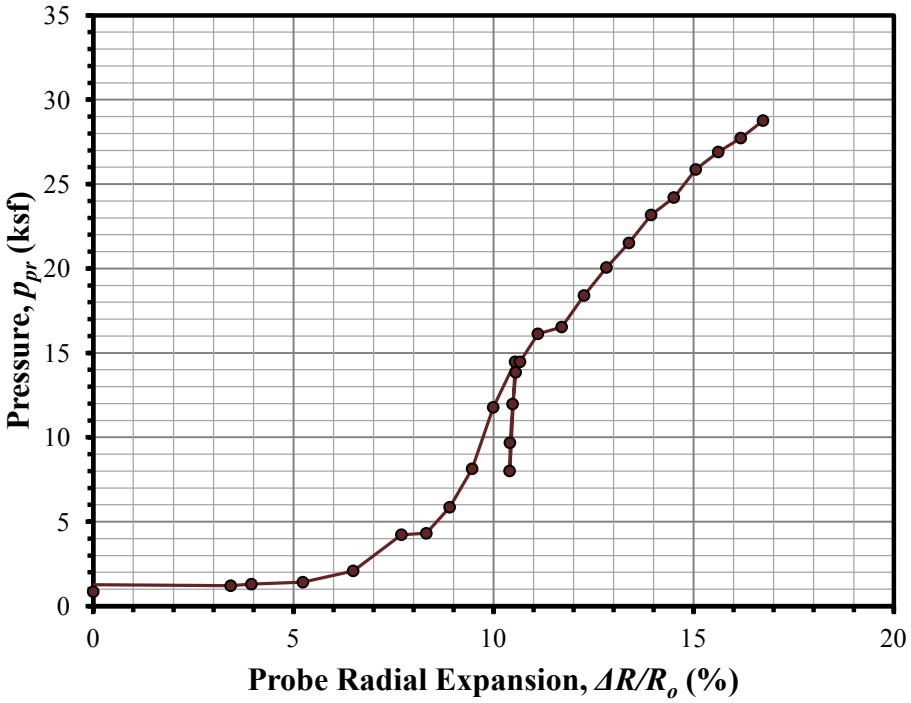

Fig. 4-21. PMT results for LS #3 at 16.5 ft (reproduced from Smith 2010)

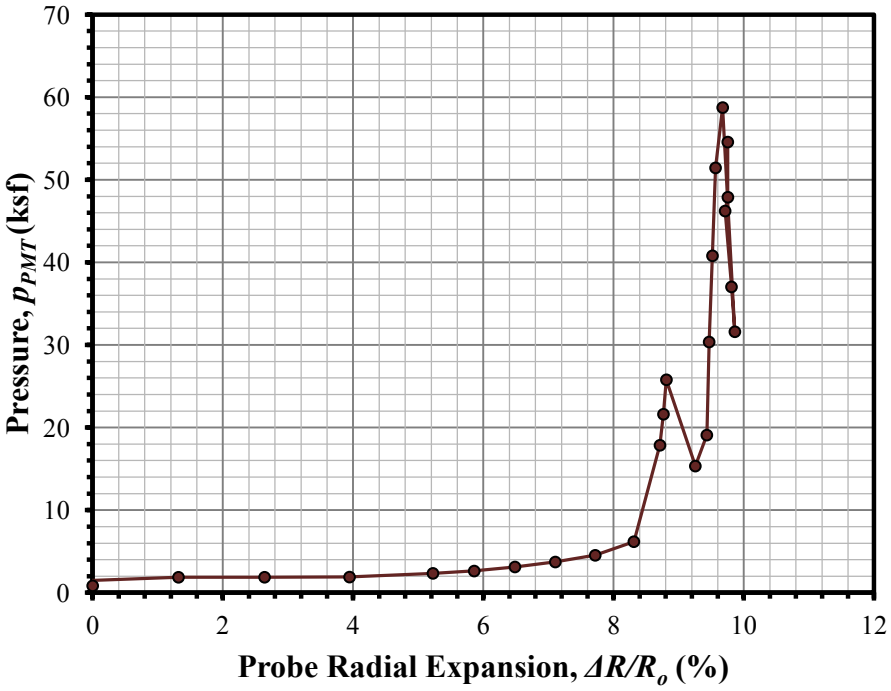

Fig. 4-22. PMT results for LS #3 at 24.5 ft (reproduced from Smith 2010)

Table 4-1. PMT Results as Reported by Smith (2010)

Test Depth, z (ft)	Initial Modulus, E_o (ksf)	Reload Modulus, E_R (ksf)	Net Limit Pressure, P_L* (ksf)	E_o/P_L*	Undrained Shear Strength, s_u (ksf)
5.5	490	1325	21.3	23.0	2.50
11.5	820	1320	13.6	60.3	1.80
16.5	900	2760	35.5	25.4	3.7
24.5	>6000	-	>100	-	-

Subsequently, the plan was to core the second hole using the 3-1/16-in. OD bit, but this bit did not allow for sufficient venting using air circulation to facilitate efficient drilling. Consequently, because another core bit of the correct size was not readily available, a 2-15/16-in diameter tri-cone bit was used to bore to a depth of 59 ft. This size of hole resulted in a hole that was slightly undersized for the PMT probe, so the hole was reamed using the 3-1/16-in OD core bit. This process resulted in a borehole (LS #5) that accommodated the PMT probe; however, because tri-cone drilling was employed, no rock core could be obtained. Nonetheless, because of the good recovery and high quality of core obtained from borehole LS #4, not having this additional core from LS #5 was not a significant concern. Testing was conducted in the same manner for borehole LS #5 as for LS #4, working from the bottom up. Testing was concluded at about 4:00 p.m. on November 5, 2010. The results from this second set of PMT are shown in Figs. 4-23 through 4-35 (not included are data for two tests at 13.0 ft because the results are suspect).

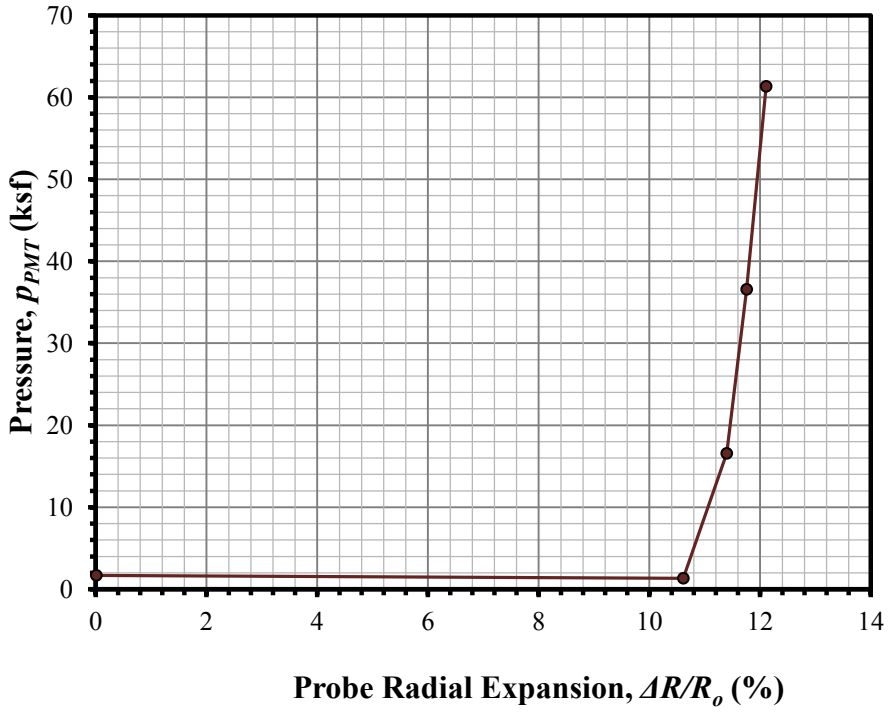

Fig. 4-23. Rock PMT results for LS #4 at 21.0 ft (from In-Situ Soil Testing 2010)

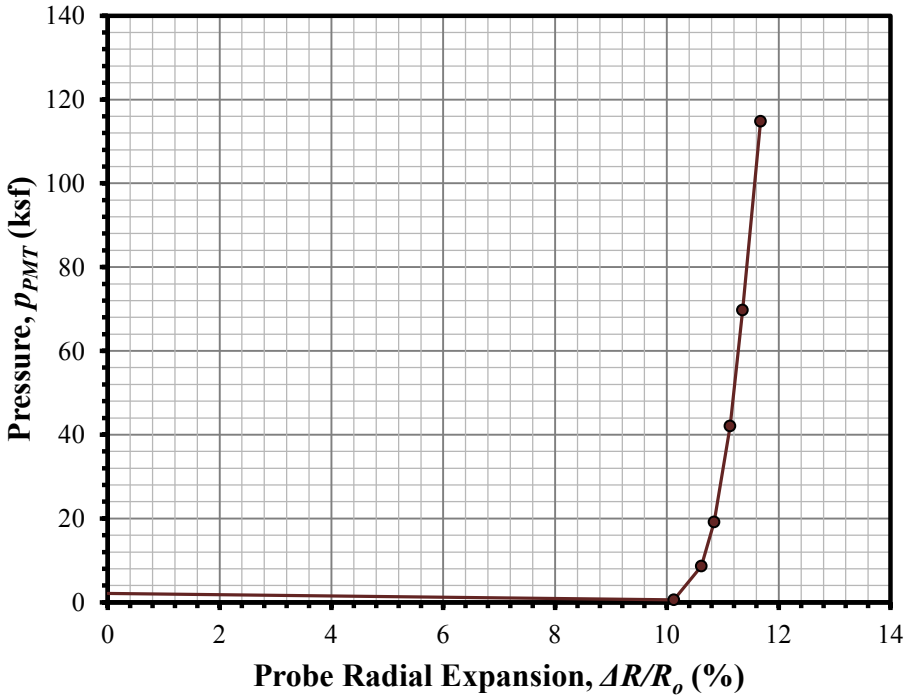

Fig. 4-24. Rock PMT results for LS #4 at 27.0 ft (from In-Situ Soil Testing 2010)

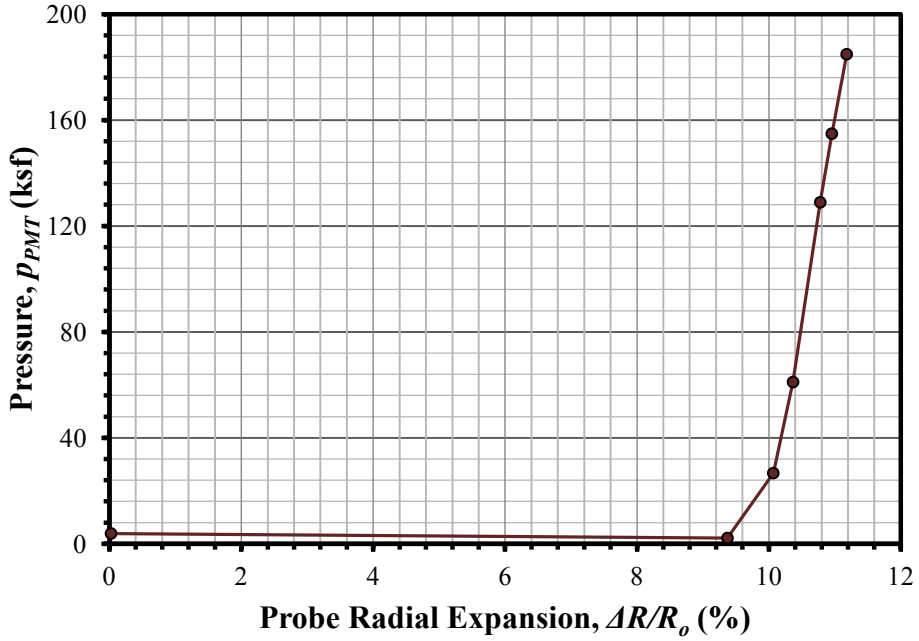

Fig. 4-25. Rock PMT results for LS #4 at 36.1 ft (from In-Situ Soil Testing 2010)

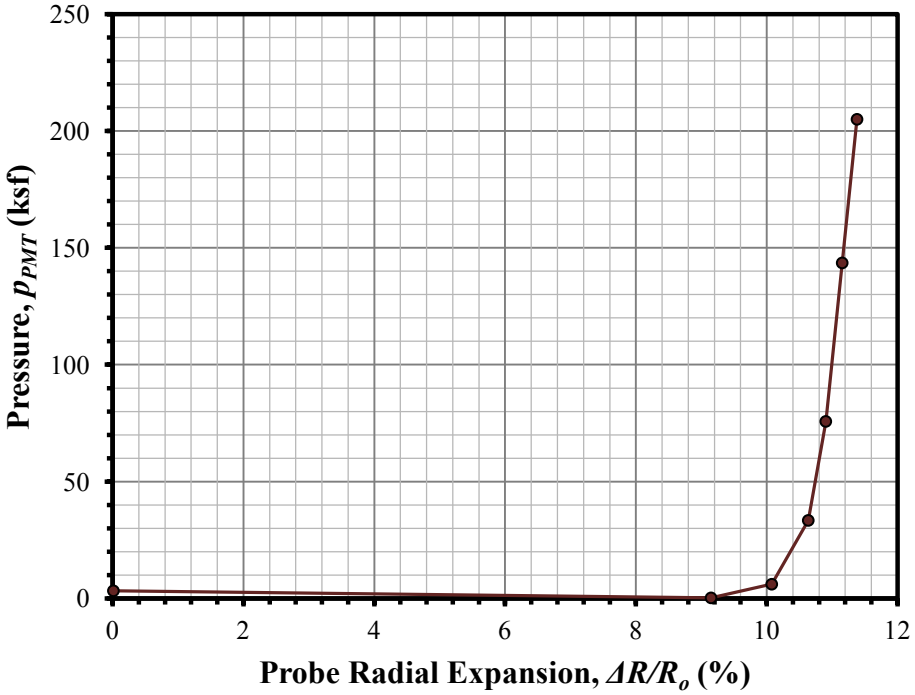

Fig. 4-26. Rock PMT results for LS #4 at 48.1 ft (from In-Situ Soil Testing 2010)

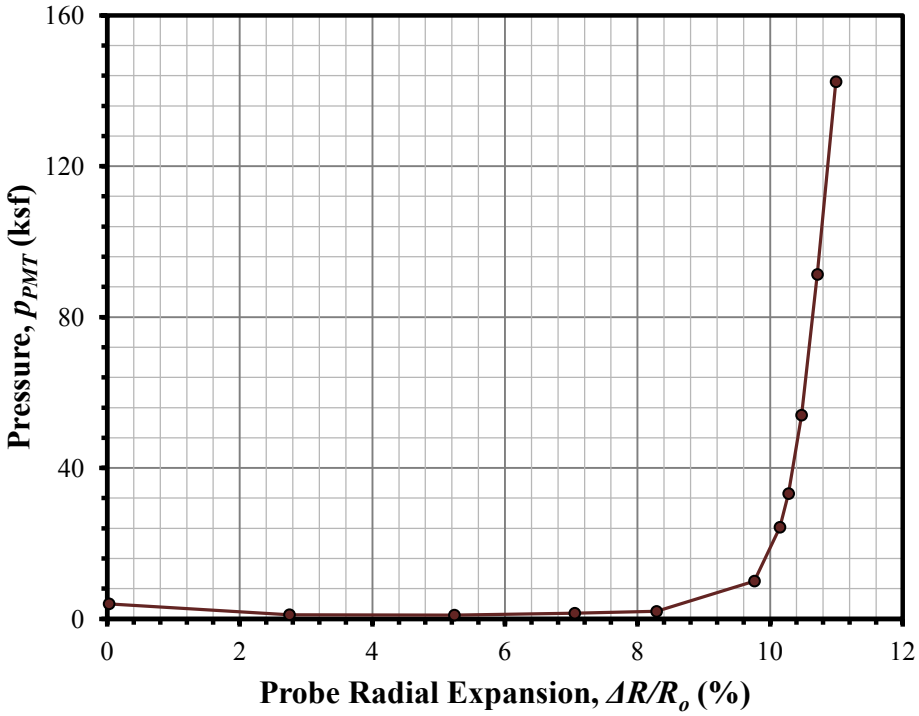

Fig. 4-27. Rock PMT results for LS #4 at 53.1 ft (from In-Situ Soil Testing 2010)

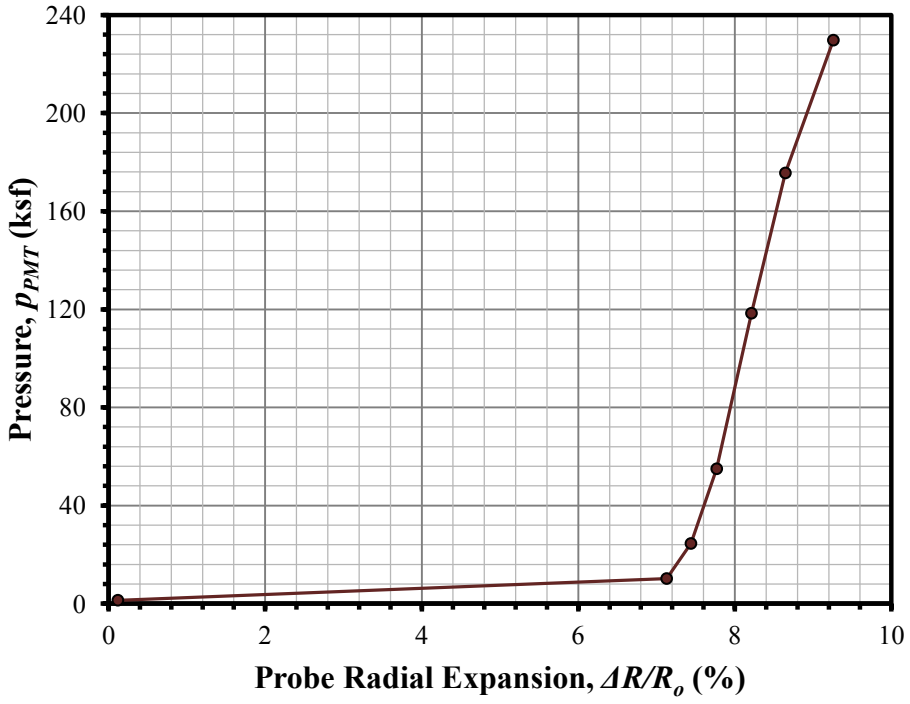

Fig. 4-28. Rock PMT results for LS #5 at 21.0 ft (from In-Situ Soil Testing 2010)

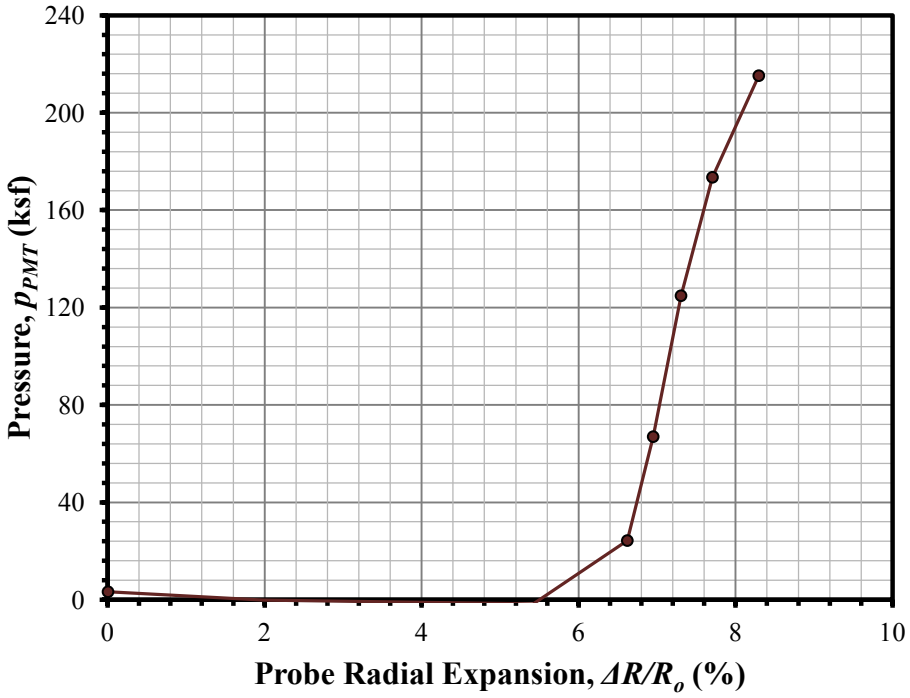

Fig. 4-29. Rock PMT results for LS #5 at 24.0 ft (from In-Situ Soil Testing 2010)

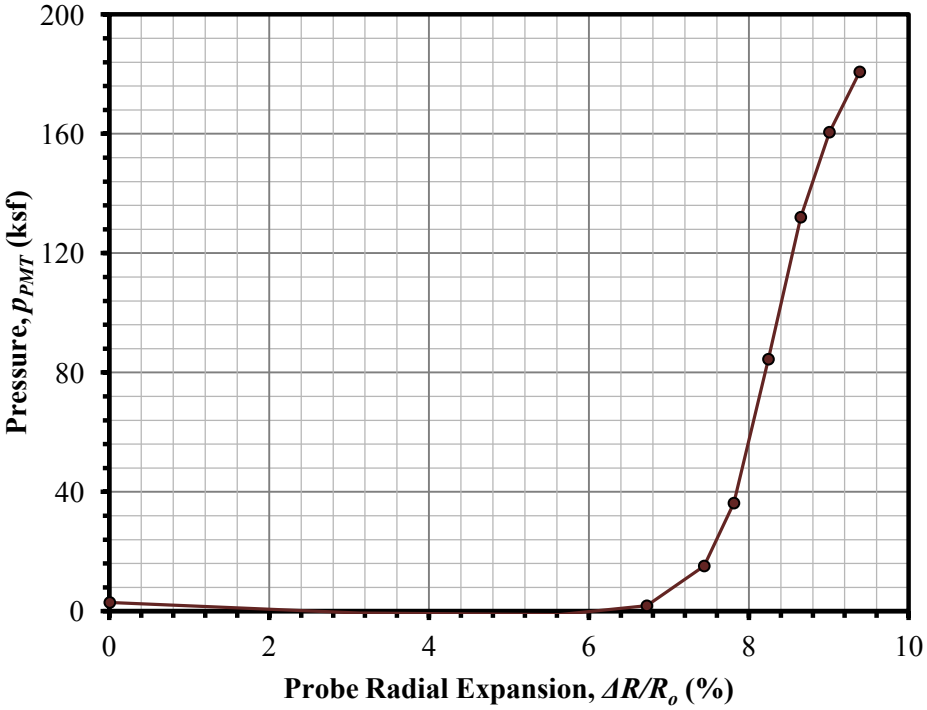

Fig. 4-30. Rock PMT results for LS #5 at 26.8 ft (from In-Situ Soil Testing 2010)

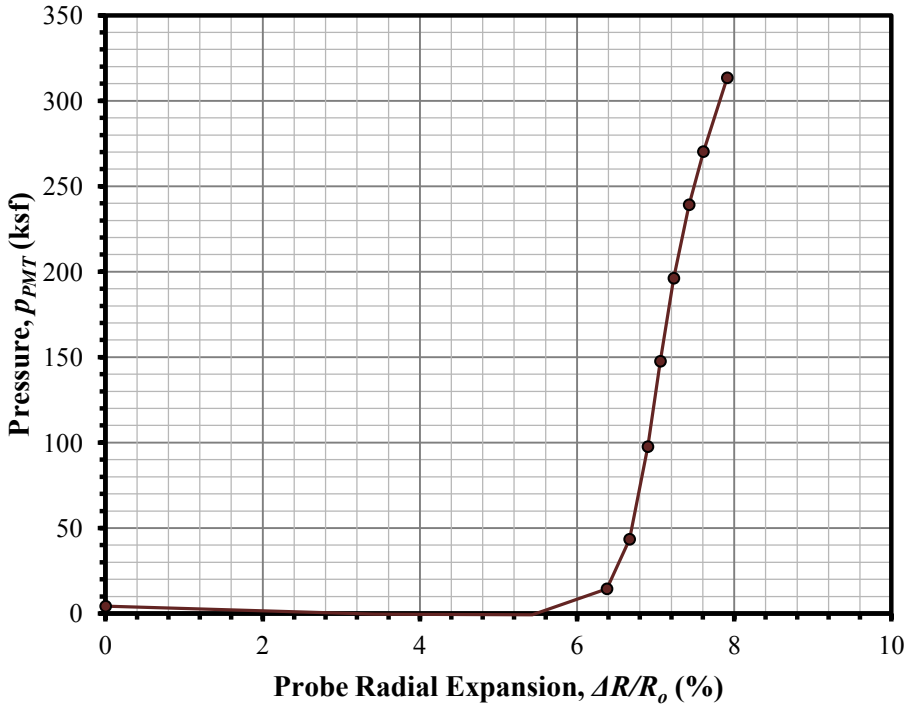

Fig. 4-31. Rock PMT results for LS #5 at 31.8 ft (from In-Situ Soil Testing 2010)

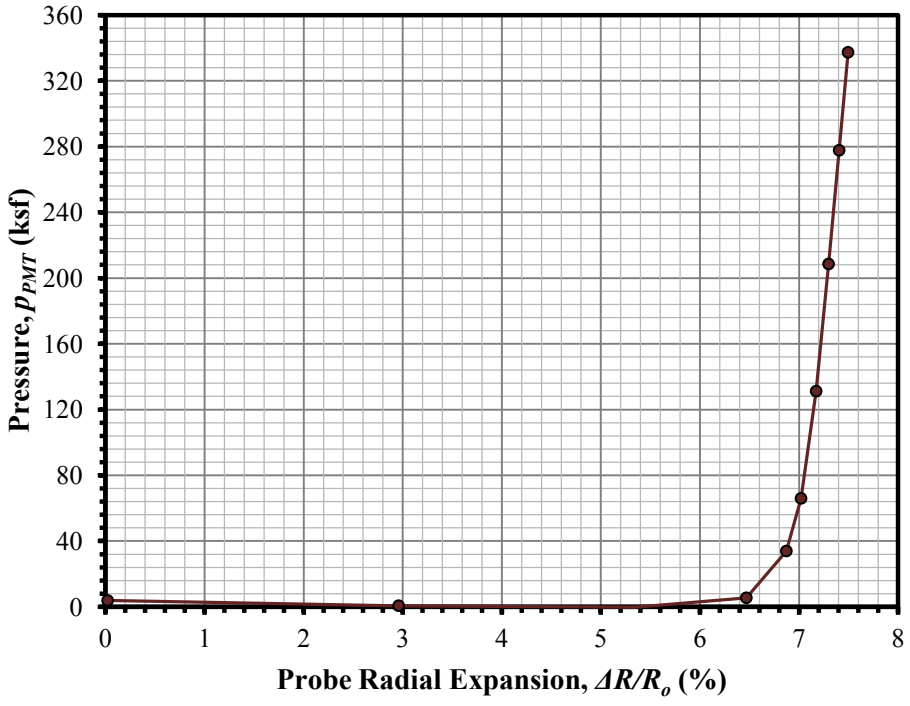

Fig. 4-32. Rock PMT results for LS #5 at 42.8 ft (from In-Situ Soil Testing 2010)

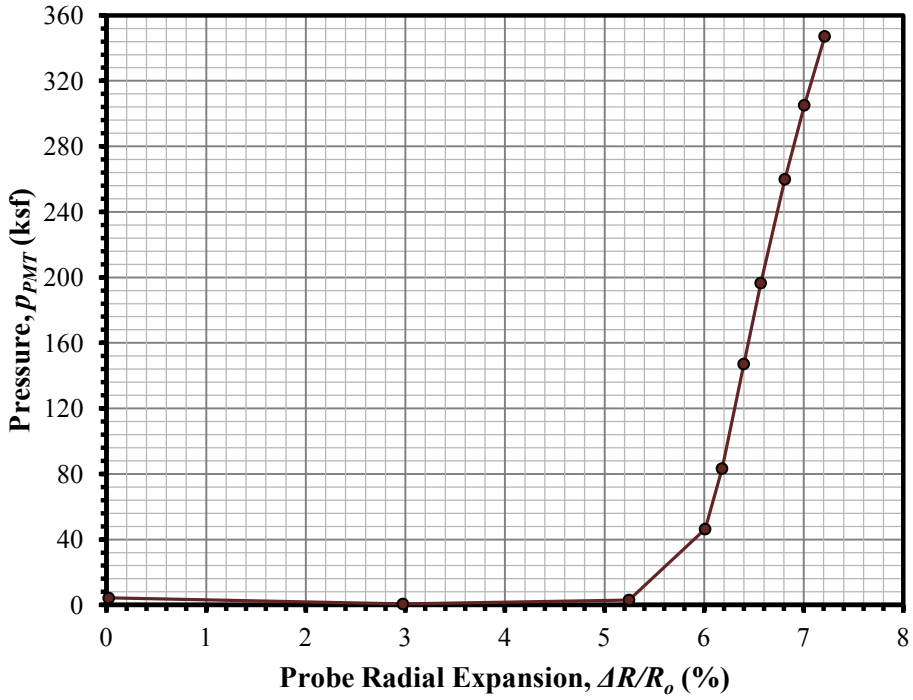

Fig. 4-33. Rock PMT results for LS #5 at 49.9 ft (from In-Situ Soil Testing 2010)

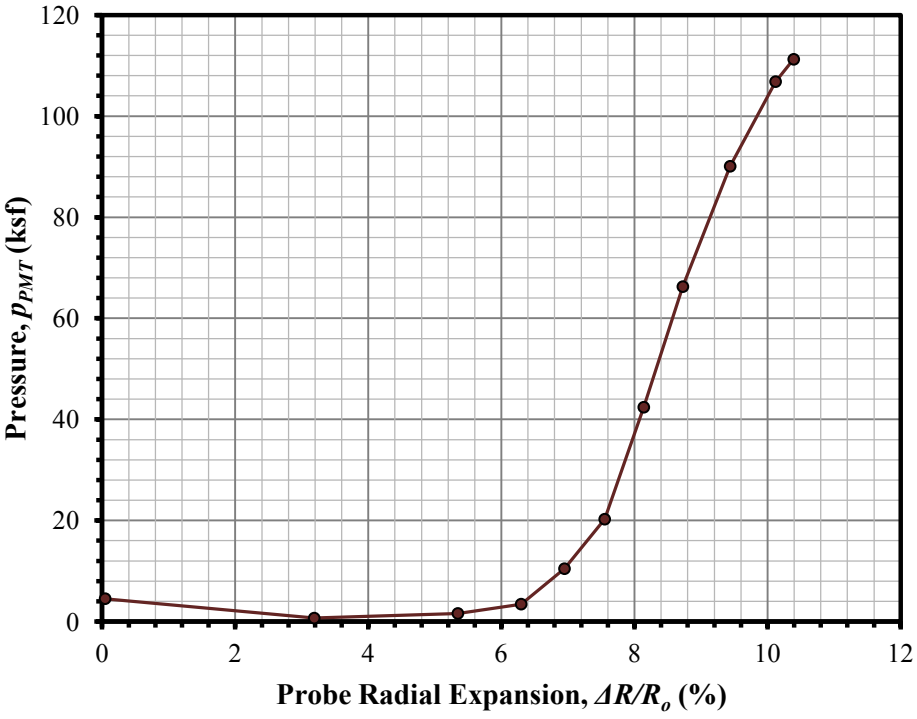

Fig. 4-34. Rock PMT results for LS #5 at 56.8 ft (from In-Situ Soil Testing 2010)

Fig. 4-35. Rock PMT setup (November 4, 2010)

4.1 Summary

In this chapter, the details and extent of the geotechnical field investigation conducted at the Lima Substation site are discussed. In all, three site visits were made to obtain soil and rock core samples, and to perform in-situ testing for strength and deformation characteristics of the subsurface material. Two runs of core sample were obtained to a depth of about 60 ft. The core from one run was sealed and handled so as to maintain in-situ conditions while the other was allowed to air-dry in storage. This difference in handling and preservation resulted in a difference of water content at the time of testing in the laboratory. The effect of these differences will be examined in Chapter 6. Soil and rock PMTs were performed to a depth of 60 ft to obtain data representing the in-situ strength and lateral deformation-displacement characteristics of the subsurface material. These data will subsequently be used as the primary means of evaluating the pertinence of various empirical methods employed in rock mechanics for

this site, as these data are considered the most reliable data obtained during the field investigation to estimate the lateral deformation characteristics of the subsurface materials at the site.

5 LABORATORY INVESTIGATION

5.1 Overview

The laboratory investigation for Lima Substation utilized the samples obtained during the field investigations to characterize the strength and deformation properties and in-situ conditions of the subsurface geomaterials. The samples collected during the field investigation included disturbed gravelly soil within 5 ft of the ground surface, disturbed samples to 17.5 ft from LS #1 obtained using a macro sampler, rock core from 17.5 ft to 56 ft from LS #1, and rock core obtained from 9 ft to 59 ft from LS #4. One particular advantage to using rock coring (see Section 4.3) in the upper weathered zone (as was done for LS #4 from 9 ft to 19 ft) was that undisturbed samples were obtained. Therefore, with adequate care, these samples could be tested in UAC.

Based on the results of drilling and coring, the strata were defined by depth and type as three general layers: (1) 0 to 6 ft as a relatively loose/soft gravelly soil material; (2) 6 to 19 ft as a very dense/stiff, weak, damp, weathered rock; (3) and deeper than 19 ft as harder, stronger rock material. The upper soil layer was characterized for strength and soil type using methods such as direct shear, particle size analysis, water content determination, and Atterberg limit analysis. The same classification tests were performed on the weathered rock between 5.5 ft and 17.5 ft, as this material could be mechanically broken down with a reasonable level of effort. Defining the strength properties for the rock mass, however, was more difficult, as the strength of intact specimens does not

necessarily represent the strength of the rock mass. Such is the case if macro features such as fracturing, bedding, and other discontinuities are present within the rock mass.

Consequently, to characterize the rock mass adequately, the goal was to perform several strength and index tests to obtain data pertaining to the intact rock and the discontinuities of the rock mass. These tests included visual observations and measurements, strength testing, and index parameters. Visual observations and measurements include RQD, fracture spacing, fracture orientation, fracture surface roughness, bedding joints, and general rock texture. UAC tests were the only strength tests conducted for the intact rock specimens. However, several index tests were also conducted on the intact rock, including point-load, rebound hardness, Brazilian tension, unit weight, and water content tests.

This chapter discusses the various strength and index tests conducted during the laboratory investigation. Tests were conducted using both ASTM standards and ISRM Suggested Methods (ISRM 1981) as references for procedure. Some results are presented here in tabular form, but the bulk of the data will be presented in Chapter 6, which will include laboratory data versus depth, correlations between parameters, variability assessment, and interpretation of the results for selection of design properties.

5.2 Unit Weight Determination

Because of the continuous nature of the core, it was possible to determine representative unit weight (γ) for each layer. For the soil layers within the upper 17 ft, γ was determined using samples from the macro sampler for boring LS #1. In addition, double-barrel core sample obtained from a depth of 9 to 19 ft from borehole LS #4 was used to determine γ.

For the undisturbed rock core, measurements of γ were made using the specimens prepared for uniaxial compression (UAC) and point-load (P-L) index tests (discussed later), which were essentially right-circular cylinders of solid material. Volume measurements were made using the caliper method prescribed by ISRM (1981). Unit weight data will be presented and discussed in Chapter 5.

5.3 Water Content Determination

Water content (w) was determined at the time of testing for the majority of specimens tested in the laboratory. The goal was to test the specimens with w as close to in-situ conditions as possible. For the upper soil/weathered rock layers, w was determined immediately upon removing material from the macro sampler. For the core obtained from borehole LS #1, proper field measures had not been taken to preserve natural conditions during laboratory storage, and consequently natural moisture conditions could not be measured because the samples were air-dried for an extended period of time. However, laboratory, air-dried w was still determined for these samples. The core obtained from borehole LS #4, on the other hand, was handled and preserved in a manner (Section 4.3) to be representative of in-situ moisture conditions. For this corehole, all samples were prepared in such a way that γ, UAC strength (q_u), and w measurements were all conducted immediately upon removal of the wax coating. Data for w are presented in Chapter 5.

5.4 Particle Size and Atterberg Limit Analysis

Particle size analyses were performed for the soil and weathered rock layers within the upper 17.5 ft. These tests were done in accordance with ASTM D422–63,

making use of a 152H hydrometer for analysis of smaller sized particles. The weathered rock was mechanically broken into individual particles using laboratory hand tools.

Atterberg limit tests were conducted on each sample for which particle size analyses were performed. ASTM D4318–05 was used as the reference for procedure in performing these tests. This testing was done to define the plasticity index (PI) of the soil using plastic and liquid limits (PL and LL). The results of these tests (Fig. 5-1) were used in conjunction with those of particle size analyses to classify each soil layer in accordance with the Unified Soil Classification System (USCS) and American Association of State Highway and Transportation Officials (AASHTO) classification systems.

5.5 Direct Shear Testing

Six (6) direct shear (DS) tests were performed to determine the effective peak internal friction angle (ϕ'_p) of the gravelly, clayey sand found within 5 ft of the ground surface. The soil used for these tests was obtained with a hand auger during the first site visit. Because the samples were disturbed, it was necessary to reconstitute it to a representative, in-situ γ of 86.7 pcf (Section 6.4.1). The level of saturation was computed to be about 20% with *w* of 8%, with an assumed specific gravity of 2.65. At this level of saturation, it was assumed that the soil is drained when sheared. Each of the six tests was conducted at a different normal stress, ranging from 1.5 to 6.3 psi (10 to 40 kPa). The results of direct shear testing are shown in Fig. 5-2 and Table 5-1. From these results, an effective cohesion intercept, c', of 2.5 psi, and an effective angle of internal friction, ϕ'_p, of 44.5° were determined.

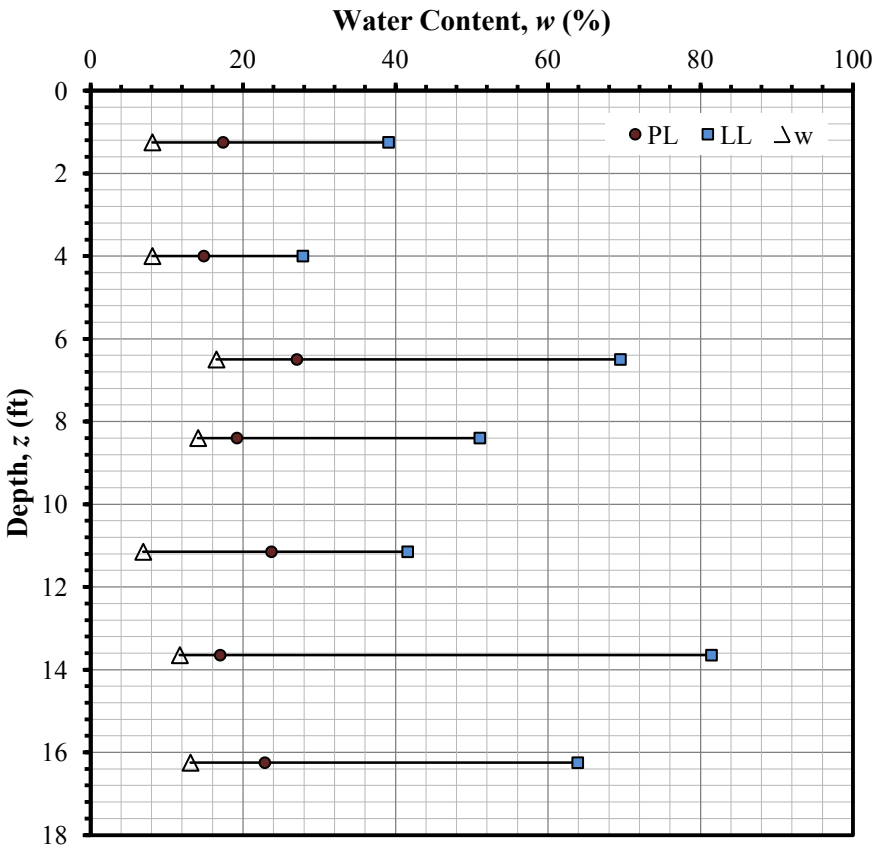

Fig. 5-1. Atterberg limits and natural water content of subsurface material between 0 and 17.5 ft

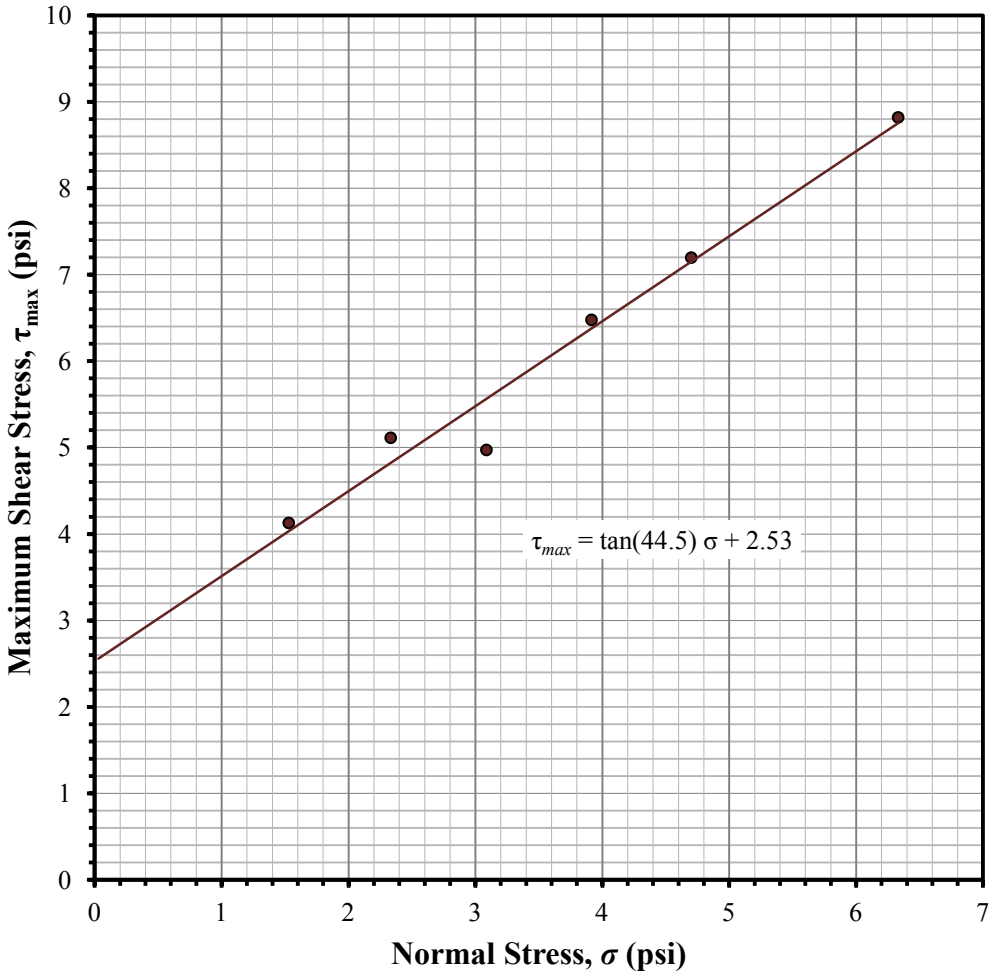

Fig. 5-2. Results of direct shear testing on soil from upper 5 ft

Table 5-1. Results of Direct Shear Testing on Soil from Upper 5 ft.

Normal Stress, σ (psi)	Maximum Shear Stress, τ_{max} (psi)
1.53	4.13
2.33	5.11
3.09	4.97
3.92	6.48
4.70	7.20
6.33	8.82

5.6 Uniaxial Compression Testing

The strength of the intact rock was determined by testing samples obtained from LS #1 and LS #4 in uniaxial compression (UAC). Because the core from each borehole was not handled and preserved in the same manner, the strength parameters calculated for the core obtained from the two boreholes were significantly different, even if the rock core(s) had similar type, fabric, appearance, and texture. As previously mentioned in Section 4.3, no special effort was made to preserve the natural condition of the core obtained from LS #1, while significant effort was made in this regard for the core from LS #4. As a result, there were significant differences in w at the time of testing, and those specimens with lower w had greater strength for the same rock type. The impact of w on laboratory-measured strength values will be discussed in more detail in Chapter 6.

UAC tests were conducted on intact rock core specimens from LS #1 (NQ, d = 1.87 in) and from LS #4 (NX, d = 2.16 in). The majority of the effort required to conduct these tests was in the preparatory process, which was dictated by the procedures and strict shape tolerance prescribed in ASTM D4543-08. The first step in the testing process was to select appropriate samples representative of the rock layers within the strata. The samples were then cut to length/diameter ratios ranging between 2 and 2.5. An l/d of 2.5 was used when possible as to minimize shape effects (Pariseau 2007). Cutting was done using a typical tile saw and minimal amounts of water as cutting fluid.

With each specimen cut to length, the two ends of the cylinder were prepared to within a reasonable tolerance of parallelism. This final hewing is typically done using mechanically operated precision equipment. However, due to the nature of the rock core and its susceptibility to degrade upon exposure to water and impact, this method was not effective and consequently was not used. Therefore, hand tools such as a file, sandpaper,

and other laboratory tools were used to trim the samples within reasonable tolerance levels. As seen in Fig. 5-3, trimming was accomplished by first orienting the longitudinal axis of the specimen horizontally in a rigid U-block. Using the square nature of the U-block, the specimens were trimmed to right circular cylinders with sand paper and a file. As indicated in Fig. 5-4, calipers were used as a quick visual check on the parallelism between the two ends. Once it appeared the sample ends were close to conformance, a more detailed tolerance check was performed.

The tolerance was checked with a dial gauge with a precision of 0.0001 in. With the specimen oriented up-right on a flat, level, stainless steel surface, and the dial gauge in contact with the upper end, the specimen was shifted horizontally while taking gauge readings every 1/8 in. along the diameter (Fig. 5-5). This process was completed across two diameters on each end of the specimen. The results of a typical tolerance check are shown graphically in Fig. 5-6. ASTM D4543-08 prescribes a parallelism tolerance of 0.25°, and that no point on each end surface can vary from a best fit plane by more than 0.001 in. If the tolerance results deviated significantly from these prescribed values, additional hewing was done in an effort to conform to the standard. A significant effort was made to bring each sample within conformance, but the acceptable tolerance was not completely satisfied for all specimens. However, the deviation was within reasonable limits for each.

Upon completion of sample preparation, specimens were tested for UAC strength (q_u) using a Satec Series Instron loading cell. This device measures load and vertical displacement. ASTM D7012 – 07 was used as a reference for procedure. This testing was done by placing the test specimen between two parallel steel loading platens, and

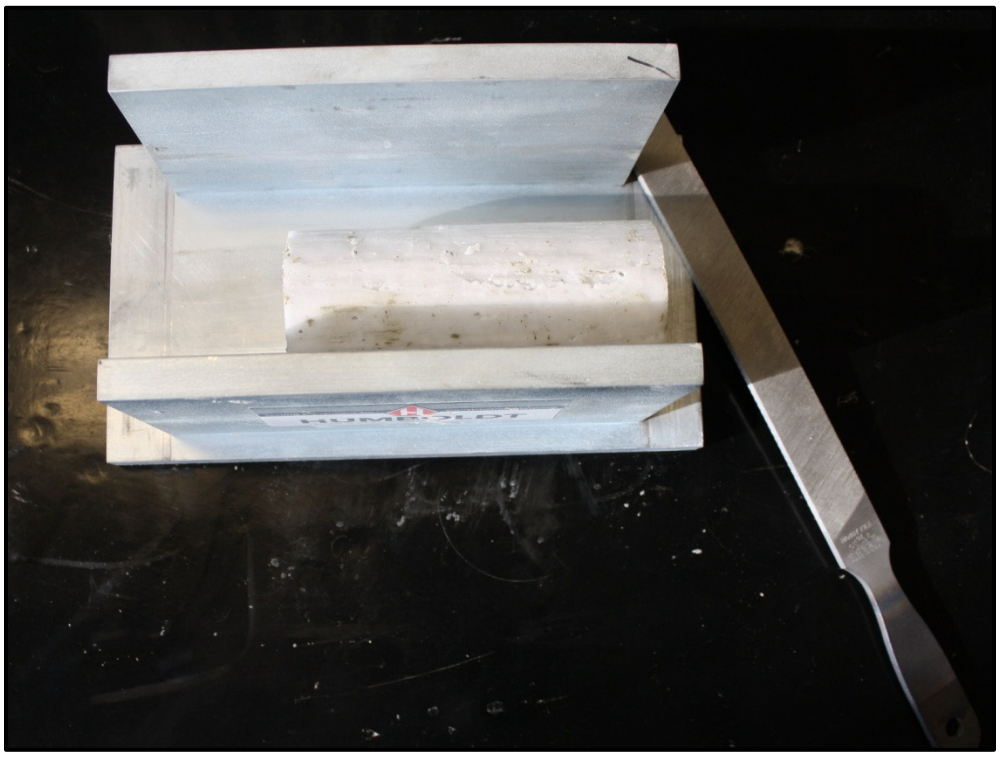

Fig. 5-3. Setup used for trimming rock core samples

Fig. 5-4. Calipers used for quick check of end parallelism

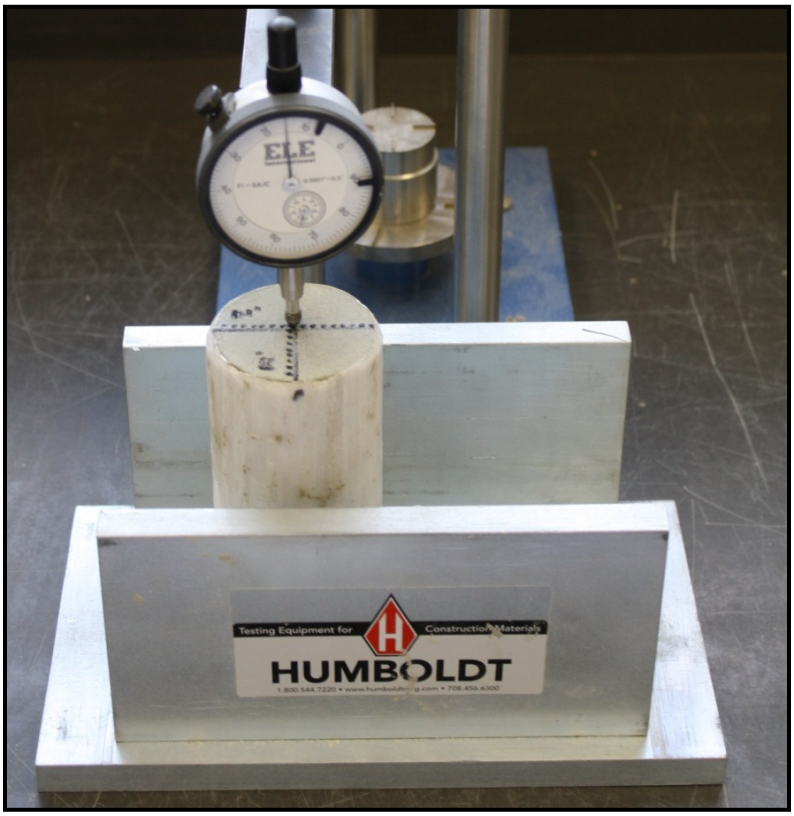

Fig. 5-5. Setup for tolerance check

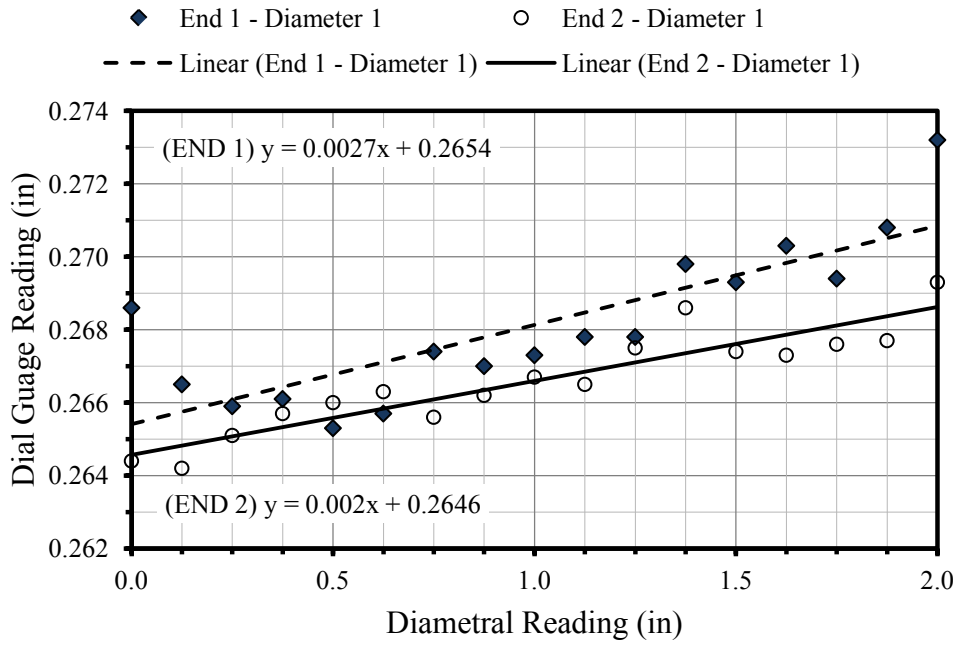

(a)

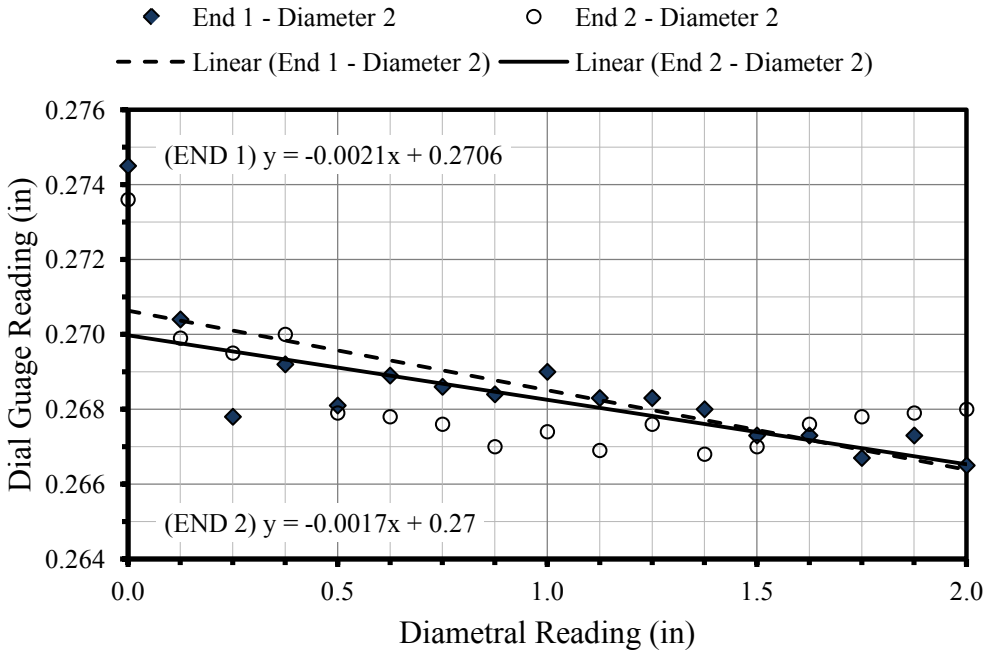

(b)

Fig. 5-6. Tolerance check for specimens UC-5 from LS #4 (a) diameter 1 and (b) diameter 2

loading the specimen to failure at a constant deformation rate (Fig. 5-7). A typical test was completed within 3 to 15 min at an applied displacement rate of 0.01 in/min. Load and axial displacement were measured through the duration of each test. Typical failure modes for this test include spalling, vertical fracture, single shear fracture, or multiple fractures (Pariseau 2007). Each of these failure modes occurred in one or more of the specimens tested. The nature of fracturing varied with respect to rock characteristics (rock type, bedding, and isotropy). A combination of single vertical fracture and spalling is shown in Fig. 5-8. Typical levels of strain at failure ranged between 1.0 and 2.5%, and those for compressive strength ranged from 170 to 10,000 psi. Tabulated results of laboratory UAC testing are shown in Tables 5-2 and 5-3. These data are presented in graphical form in Chapter 6 in conjunction with additional analysis and interpretation of the results.

5.7 Point-Load Index

The point-load index ($I_{s(50)}$) test is a simple test used to estimate the compressive strength of intact rock. It is typically used because it can be readily performed on samples of various shapes and forms, and consequently it is relatively inexpensive in comparison to UAC or other more sophisticated tests (Bieniawski 1975). The test is conducted by loading a rock specimen of known dimension between two conical loading platens (Fig. 5-9). These platens are hydraulically compressed into the specimen until failure, which should result in a fracture surface passing through the two loading points; otherwise, the results of the test are to be disregarded (ASTM D5731–08). At failure, the

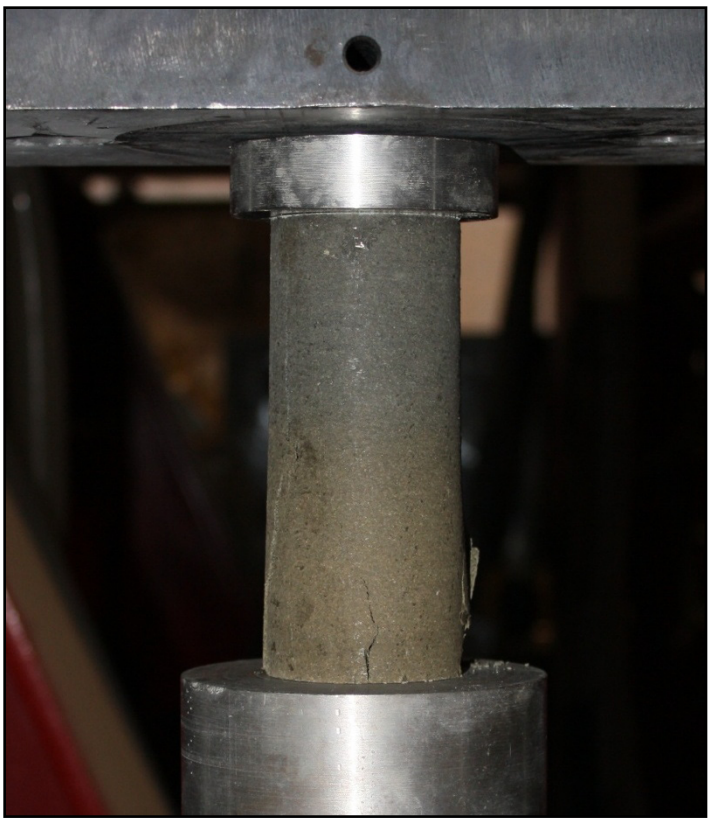

Fig. 5-7. Rock core specimen tested in UAC (UC-5 from LS #4)

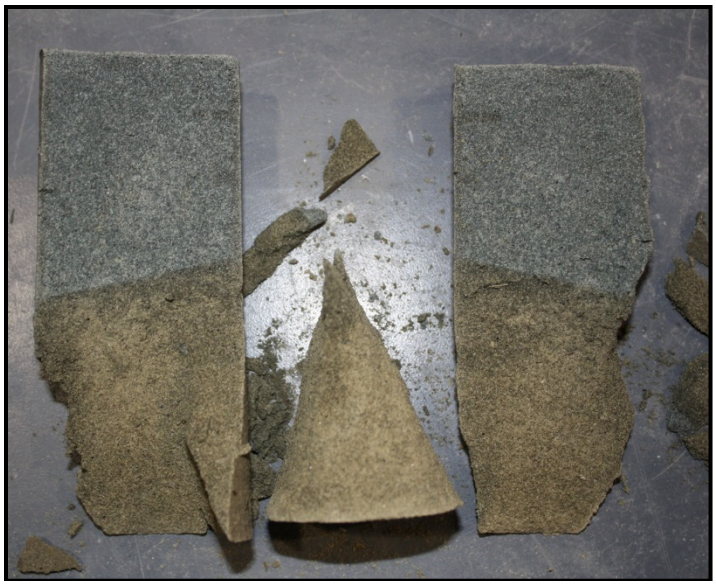

Fig. 5-8. Specimen failure under UAC (UC-5 from LS #4)

Table 5-2. Results of UAC Testing for LS #1

Specimen ID	Depth, z (ft)	Uniaxial Compressive Strength, q_u (ksi)	Tangent Modulus at 50% q_u, E_{t50} (ksi)	E_{t50}/q_u
UC-1	22.5	10.3	1160	110
UC-2	27.5	7.25	533	74
UC-3	33.0	3.33	181	54
UC-4	34.0	3.47	334	96
UC-5	35.0	2.55	174	68
UC-6	36.0	3.51	341	97
UC-7	37.0	3.68	334	91
UC-8	38.5	3.63	241	66
UC-9	39.5	3.31	258	78
UC-10	43.0	6.95	626	90
UC-11	44.0	4.05	450	110
UC-12	46.5	4.60	294	64
UC-13	47.0	7.24	732	100
UC-14	47.5	6.25	568	91
UC-15	48.0	6.65	610	92
UC-16	49.5	4.57	268	59
UC-17	54.0	7.32	522	71

Table 5-3. Results of UAC Testing for LS #4

Specimen ID	Depth, z (ft)	Uniaxial Compressive Strength, q_u (ksi)	Tangent Modulus at 50% q_u, E_{t50} (ksi)	E_{t50}/q_u
UC-1	12.0	0.165	15.0	91
UC-2	14.0	0.388	21.0	54
UC-3	15.0	0.233	13.0	56
UC-4	16.0	0.265	20.0	75
UC-5	17.5	3.34	428	130
UC-6	22.0	8.62	1130	130
UC-7	23.0	2.26	310	140
UC-8	24.0	4.48	487	110
UC-9	28.5	6.50	1040	160
UC-10	31.0	0.592	30.0	51
UC-11	33.0	2.71	362	130
UC-12	34.0	0.876	48.0	55
UC-13	34.5	1.60	243	150
UC-14	35.0	2.76	372	140
UC-15	36.0	1.05	61.0	58
UC-16	37.0	1.18	105	89
UC-17	40.0	1.09	94.9	87
UC-18	42.0	3.54	443	130
UC-19	43.0	2.17	349	160
UC-20	44.5	3.97	592	150
UC-21	45.0	3.08	248	80
UC-22	46.5	3.55	342	96
UC-23	47.0	4.75	579	120
UC-24	49.0	2.63	218	83
UC-25	51.0	2.90	193	67
UC-26	52.0	1.41	188	130
UC-27	54.0	3.14	301	96
UC-28	56.0	0.533	51.0	96
UC-29	58.0	1.59	99.2	63

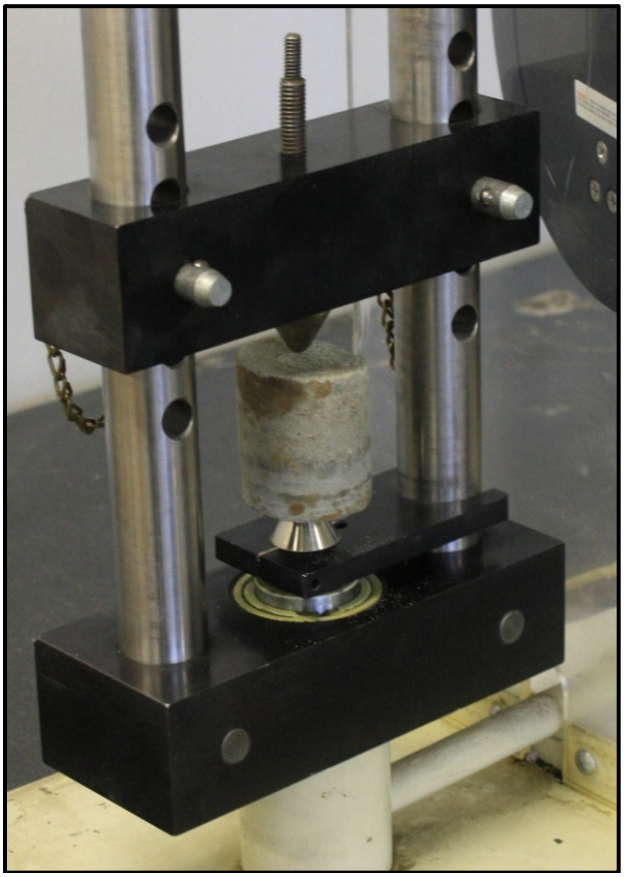

Fig. 5-9. Typical setup for point-load test – axial loading

load and distance between platens are measured, from which the point-load index is derived using the following equation (Eq. 5-1):

$$I_S = \frac{P}{D_e^{\,2}} \tag{5-1}$$

where:

P = measured load at failure

D_e = equivalent diameter of the specimen

I_s = point-load index

D_e is derived by converting the area of the fracture surface into an equivalent circle and finding the corresponding diameter. I_s is corrected to $I_{s(50)}$ to minimize variability due to size effects. $I_{s(50)}$ is the measured point load index normalized to an equivalent diameter of 1.97 in. (50 mm) using the following expression from ASTM D5731–08:

$$I_{S(50)} = (D_e / 1.97)^{0.45} I_S \tag{5-2}$$

where D_e is in inches.

The UAC strength (q_u) of a given material is typically more than an order of magnitude greater than the point-load index measured for the same material. Typical factors used to estimate q_u from $I_{s(50)}$ range between 21 and 29, but other correlations have been developed beyond using simple factors [e.g. Bieniawski (1975), and Gunsallus and Kulhawy (1984)].

Point-load testing was conducted in accordance with ASTM D573–08 on approximately 100 rock core specimens obtained from both LS #1 and LS #4. Specimens were loaded axially (Fig. 5-9) and diametrically to produce index values representing each direction. With index values in both directions, an estimate of the degree of anisotropy may be determined by taking the ratio between the two ($I_{a(50)} = I_{s(50)\parallel} / I_{s(50)\perp}$) . An axial load orientation assures an axial fracture oriented perpendicular to bedding planes. This failure is consistent with the failure mode that typically develops in UAC. This facilitated a meaningful comparison between point-load test results and uniaxial strength tests (Section 6.4.5). Any specimen not failing along a vertical plane located between the loading points was disregarded. (This improper failure was the case for several specimens that first fractured along bedding planes during axial loading.)

Specimens were cut and prepared as right-circular cylinders with length/diameter ratios *(l/d)* ranging between 0.5 and 1.0. For samples from LS #4, a value of 1.0 was targeted when possible to minimize shape effects, as shape effects can have a significant influence on the results (Broch and Franklin 1972).

Values obtained for point-load index perpendicular to bedding planes ranged between 65 and 600 psi as indicated in Tables 5-4 and 5-5. Values for point-load index parallel to bedding planes ranged between 16 and 680 psi, as shown in Tables 5-6 and 5-7 along with a computed anisotropy index for each test depth. These results are further analyzed in more detail in Section 6.4.5.

5.8 Rebound Hardness Index

The rock rebound hardness index (R_N) is used to evaluate rock quality and may be correlated with q_u. R_N is determined by depressing a plunger with a spring loaded piston

Table 5-4. Results of Point-Load Index Testing for LS #1 – Perpendicular to Bedding Planes

Specimen ID	Depth, z (ft)	Load at Failure, $P_┤$ (lb)	Equivalent Diameter, D_e^2 (in^2)	Point-load Index, $I_{s┤}$ (psi)	Size Correction Factor, $(D_e/1.97)^{0.45}$	Corrected Point-load Index, $I_{s(50)┤}$ (psi)
PL-1	18	1380	2.59	531	0.924	481
PL-2	18	1590	5.58	285	1.06	307
PL-4	21	1030	2.81	366	1.07	338
PL-3	21	917	5.26	174	1.00	185
PL-5	22	738	5.35	138	0.812	147
PL-8	28	11300	3.93	330	0.929	329
PL-10	31	1160	1.59	733	0.943	595
PL-11	32	559	2.88	194	0.910	180
PL-12	33	805	3.09	261	0.874	246
PL-13	34	894	2.63	340	1.01	310
PL-14	34	604	2.20	274	0.984	240
PL-15	35	771	4.12	187	1.01	189
PL-17	36	738	3.72	199	1.03	195
PL-18	37	1200	4.27	280	0.917	284
PL-19	37	1030	4.62	223	0.978	230
PL-20	39	559	2.72	205	1.05	188
PL-21	39	1010	3.62	278	0.952	272
PL-22	40	1300	4.89	265	0.896	277
PL-24	42	637	3.21	199	1.04	189
PL-25	42	928	2.45	379	0.820	339
PL-27	43	1390	4.84	286	1.04	299
PL-28	45	850	1.66	512	1.00	420
PL-29	45	1500	4.70	319	0.889	331
PL-30	46	716	3.97	180	0.885	180
PL-31	48	1140	2.37	480	0.962	427
PL-31	48	1010	2.33	432	1.02	383
PL-32	48	335	3.36	100	0.904	95.9
PL-33	49	1110	4.38	253	0.889	258
PL-35	50	559	2.55	219	1.01	198
PL-35A	51	727	2.37	307	0.968	273
PL-37	51	738	4.24	174	0.924	176
PL-39	54	1017	3.46	294	1.06	285

Table 5-5. Results of Point-Load Index Testing for LS #4 – Perpendicular to Bedding Planes

Specimen ID	Depth, z (ft)	Load at Failure, $P_{\perp}$ (lb)	Equivalent Dia., D_e^2 (in^2)	Point-load Index, $I_{s\perp}$ (psi)	Size Correction Factor, $(D_e/1.97)^{0.45}$	Corrected Point-load Index, $I_{s(50)\perp}$ (psi)
PL-3	22	894	5.35	167	1.07	178
PL-5	23	771	3.03	255	0.939	239
PL-8	27	861	3.94	218	1.00	218
PL-11	29	1400	3.30	423	0.958	405
PL-12	30	246	3.72	66.1	0.984	65.0
PL-14	31	615	3.69	167	0.982	164
PL-17	32	369	3.43	108	0.966	104
PL-18	32	302	3.69	81.8	0.982	80.4
PL-19	35	313	4.42	70.8	1.02	72.4
PL-22	36	313	4.25	73.6	1.01	74.6
PL-24	36	255	2.17	117	0.872	102
PL-30	43	525	3.62	145	0.978	142
PL-31	44	414	4.61	89.8	1.03	92.7
PL-33	44	347	3.74	92.7	0.985	91.3
PL-34	47	783	5.27	148	1.06	158
PL-38	48	1410	3.86	365	0.992	362

Table 5-6. Results of Point-Load Index Testing for LS #1 – Parallel to Bedding Planes

Specimen ID	Depth, z (ft)	Load at Failure, P (lb)	Equiv. Dia., D_e^2 (in^2)	Point-load Index, $I_s\parallel$ (psi)	Size Correction Factor, $(D_e/1.97)^{0.45}$	Corrected Point-load Index, $I_{s(50)}\parallel$ (psi)	Anisotropy Index, $I_{a(50)}$ (psi)
PL-1	18	1280	3.42	372	0.966	360	0.747
PL-2	18	1100	2.84	386	0.926	357	1.16
PL-4	21	839	3.42	245	0.966	237	0.700
PL-5	22	2010	2.72	741	0.917	679	4.61
PL-6	23	1990	3.42	581	0.966	561	3.81
PL-8	27	604	2.20	274	0.874	240	0.729
PL-14	34	514	3.42	150	0.966	145	0.605
PL-15	35	55.9	1.65	33.8	0.820	27.7	0.147
PL-18	37	89.4	2.05	43.6	0.860	37.5	0.132
PL-19	37	246	1.89	130	0.845	110	0.478
PL-22	40	55.9	2.05	27.2	0.860	23.4	0.085
PL-23	40	112	3.42	32.7	0.966	31.5	0.114
PL-25	42	55.9	3.42	16.3	0.966	15.8	0.046
PL-27	43	112	1.65	67.7	0.820	55.5	0.186
PL-28	45	537	3.42	157	0.966	151	0.360
PL-29	45	1096	2.55	430	0.904	388	1.18
PL-31	48	671	3.42	196	0.966	189	0.494
PL-33	49	55.9	1.82	30.8	0.837	25.8	0.100
PL-37	51	44.7	1.82	24.6	0.837	20.6	0.117
PL-38	54	55.9	3.42	16.3	0.966	15.8	0.055

Table 5-7. Results of Point-Load Index Testing for LS #4 – Parallel to Bedding Planes

Specimen ID	Depth, z (ft)	Load at Failure, P (lb)	Equiv. Dia., D_e^2 (in^2)	Point-load Index, $I_s\|\|$ (psi)	Size Correction Factor, $(D_e/1.97)^{0.45}$	Corrected Point-load Index, $I_{s(50)}\|\|$ (psi)	Anisotropy Index, $I_{a(50)}$ (psi)
PL-4	23	224	4.20	53.2	1.01	53.8	0.225
PL-13	30	101	2.32	43.3	0.885	38.3	0.589
PL-15	31	201	1.99	101	0.855	86.4	0.528
PL-16	31	134	3.33	40.3	0.959	38.7	0.236
PL-20	35	112	2.11	53.1	0.866	45.9	0.635
PL-23	36	134	3.85	34.9	0.991	34.6	0.463
PL-25	38	436	3.91	112	0.995	111	1.08
PL-26	38	168	3.73	45.0	0.984	44.3	0.433
PL-27	38	179	3.52	50.8	0.972	49.4	0.483
PL-28	38	78.3	3.35	23.4	0.961	22.5	0.219
PL-35	47	67.1	2.85	23.6	0.926	21.8	0.138
PL-43	51	67.1	4.20	16.0	1.01	16.1	--

perpendicular to a rock surface. After reaching a certain level of depression, the piston is released to impact the rock surface. R_N is expressed as a percentage and is given by the ratio of the rebound height after impact to the initial height prior to impact (Basu and Aydin 2004).

The index was determined using an NR-9 Schmidt rebound hammer by Forney's Inc. (Fig. 5-10). ASTM D5873–05 and ISRM (1981) were standards of reference. Ideally, testing should be conducted on large block samples to minimize size effects. However, it is common to do testing on rock core, and most conveniently on the cylindrical surface as it is relatively smooth and requires little preparation. Aydin and Basu (2005) recommend testing along the diameter be conducted on NX core or larger. However, despite the notion that the test is nondestructive, it was found in this study that diametrical impact (orthogonal to cylindrical surface, parallel to bedding planes) often

Fig. 5-10. NR-9 Schmidt rebound hammer

caused the core to cleave along bedding planes. Therefore, testing was done orthogonal to bedding planes, as significantly less damage was incurred. ASTM indicates that the testing surface should be 6 in. wide, while ISRM (1981) recommends using a 2.4 in. wide surface. However, the core from LS #4 had a diameter of only 2.1 in., and therefore shape effects may have had a pronounced effect on the results.

Specimens prepared for rebound hardness testing were NQ and NX core cut in lengths of about 1.5 in. Testing was performed on both ends of the specimen as the sample was secured to the ground. The hammer was oriented vertically downward, and

testing was concluded if the specimen fractured. Despite the recommendation of ASTM D5873–05 to conduct a minimum of 10 tests, several of the samples fractured prior to reaching this number. However, several samples within the same rock layer were tested, so a representative number was obtained for each depth.

There are two corrections that are typically applied to the readings to obtain the final value of R_N (the 'N' indicating the use of an N-type hammer). The first correction applies a calibration factor to the measured *R*-value. This factor is defined as the ratio between the *R*-value (provided by the manufacturer) obtained from testing an anvil in the factory to the actual value measured when testing the same anvil in the laboratory. Because no anvil was available for the hammer used, the calibration factor was assumed to be 1, and no adjustment in this regard was applied.

The second correction accounts for the hammer orientation with respect to horizontal to which R_N is to be normalized. This correction is typically supplied by the manufacturer. However, this information was not available in this case, but Basu and Aydin (2004) indicate that these values are typically based on testing conducted on select materials, and therefore may not be valid for every case. Therefore, this correction was applied using the theoretical approach of Basu and Aydin (2004), which gives the correction graphically as a function of the measured R-value (Basu and Aydin 2004, Fig. 4). The results of rebound hardness testing are shown in Tables 5-8 and 5-9.

5.9 Tensile Strength Testing

The uniaxial tensile strength was determined indirectly using the Brazilian tensile strength test. In addition to providing some indication of tensile strength, the Brazilian tensile strength can be used to correlate with q_u. As for the point-load test, the Brazilian

Table 5-8. Results of Rebound Hardness Testing for LS #1 (d = 1.85 in.)

Specimen ID	Depth, z (ft)	Sample Size, n	Corrected Rebound Hardness Index, R_N	CoV (%)
SH-1	23	5	38	10
SH-2	25	7	31	7.6
SH-3	33	8	23	14
SH-4	36	10	22	8.0
SH-5	37	9	26	7.4
SH-6	40	10	26	8.3
SH-7	43	2	25	9.1
SH-8	45	6	28	13
SH-9	49	5	27	9.1
SH-10	50	4	21	7.7

Table 5-9. Results of Rebound Hardness Testing for LS #4 (d = 2.05 in.)

Specimen ID	Depth, z (ft)	Sample Size, n	Corrected Rebound Hardness Index, R_N	CoV (%)
SH-1	21	4	33	4.8
SH-2	20	4	25	4.3
SH-3	25	4	30	8.9
SH-4	29	4	52	5.4
SH-5	30	10	39	6.3
SH-6	31	10	27	7.6
SH-7	32	10	28	7.4
SH-8	35	10	26	6.0
SH-9	37	10	25	7.1
SH-10	37	5	24	5.8
SH-11	39	9	23	11.0
SH-12	40	9	21	6.2
SH-15	46	5	25	1.9
SH-16	47	10	33	4.8
SH-17	49	7	30	8.8
SH-18	50	10	25	7.2
SH-19	53	6	23	8.3
SH-20	56	4	17	11.5

tension test is widely used because it is simple and inexpensive, as opposed to determining tensile strength directly. ASTM D3957–08 was used as the reference for procedure. The indirect tensile strength is determined by loading a disc-shaped specimen diametrically until failure, and is given by the following equation:

$$\sigma_t = \frac{2P}{\pi dl} \tag{5-3}$$

where:

P = measured load at failure

l = the specimen length,

d = specimen diameter

A total of 39 Brazilian tension tests were successfully conducted, 21 from LS #1 and 18 from LS #4, neglecting those specimens that did not fracture correctly. The desired mode of failure is a fracture along the diameter of the specimen (Fig. 5-11), which is believed to be caused by induced tensile stress (Goodman 1980). Upon loading, several specimens fractured along horizontal bedding planes prior to fracturing diametrically (Fig. 5-12), and results from these tests were consequently disregarded. Values of *l/d* ranged between 0.5 and 0.75 for all specimens. Testing was conducted using a Satec series Intron loading cell, which measures load and deformation. Loading was applied at about 0.04 in./min., and failure was typically attained after about 1 min. The results of the Brazilian tension tests are summarized in Tables 5-10 and 5-11.

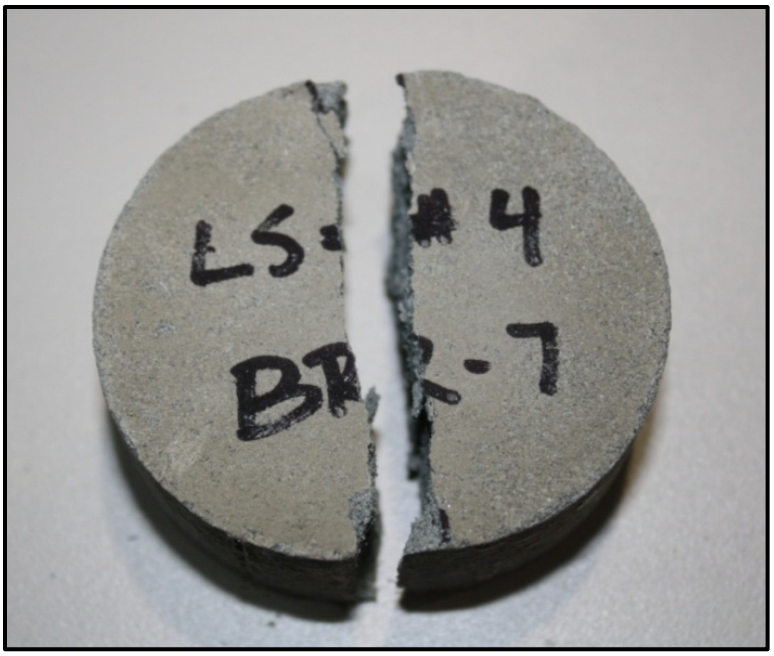

Fig. 5-11. Diametral fracture for Brazilian tension test

Fig. 5-12. Disregarded Brazilian specimen – fracture along bedding planes

Table 5-10. Results of Brazilian Tension Testing for LS #1

Specimen ID	Depth, z (ft)	Length, l (in)	Diameter, d (in)	Load, P (lb)	Tensile Strength, σ_t (psi)
BR-1	18	0.930	1.84	1520	564
BR-4	31	1.06	1.85	1940	629
BR-10	33	1.08	1.83	1060	342
BR-11	34	1.28	1.81	1540	422
BR-12	37	1.10	1.87	772	239
BR-13	38	0.750	1.85	852	391
BR-15	39	0.850	1.83	1110	455
BR-16	39	0.830	1.82	1090	458
BR-18	40	1.04	1.84	1360	452
BR-19	40	1.32	1.85	2340	611
BR-20	40	0.880	1.84	2050	805
BR-22	42	0.980	1.85	2020	710
BR-23	43	0.650	1.86	1990	1050
BR-25	46	1.24	1.86	1610	444
BR-26	46	1.12	1.84	880	272
BR-28	48	0.910	1.86	1760	661
BR-29	48	0.970	1.86	1300	460
BR-30	49	0.890	1.85	1240	479
BR-31	49	1.15	1.86	1360	406
BR-33	50	1.19	1.83	812	237

Table 5-11. Results of Brazilian Tension Testing for LS #4

Specimen ID	Depth, z (ft)	Length, l (in)	Diameter, d (in)	Load, P (lb)	Tensile Strength, σ_t (psi)
BR-1	21	0.820	2.05	1880	712
BR-2	27	0.970	2.04	1990	640
BR-3	31	1.11	2.03	1120	317
BR-4	31	0.910	2.03	1120	387
BR-5	31	1.23	2.03	1390	354
BR-7	36	0.900	2.03	963	336
BR-8	36	0.940	2.02	911	305
BR-9	36	1.07	2.03	907	266
BR-10	37	0.760	2.03	741	306
BR-10B	37	1.24	2.03	1380	349
BR-11	42	0.930	2.05	1000	335
BR-12	43	0.880	2.04	651	231
BR-13	43	0.970	2.04	1350	435
BR-15	48	1.22	2.05	1540	392
BR-16	48	0.890	2.04	650	228
BR-17	48	0.960	2.05	816	264
BR-18	49	1.26	2.05	1240	306
BR-22	53	1.01	2.05	1310	403

5.10 Summary

In this chapter, details of the geotechnical laboratory investigation conducted using the subsurface material obtained during the geotechnical field investigation (Chapter 4) were discussed. Laboratory testing included several strength and index tests that were conducted on intact rock core, tested both under laboratory air-dry conditions and in-situ moisture conditions. The results from the laboratory investigation will be discussed in more detail in Chapter 6.

6 FIELD AND LABORATORY DATA REDUCTION

6.1 Overview

The data from the field and laboratory investigations are presented in more detail in this chapter, with the goal to reduce the data to appropriate parameters that may be used in engineering design. First, a description of the material observed within 60 ft of the ground surface will be given in conjunction with detailed coring logs. In addition, the engineering properties observed in the laboratory are plotted versus depth. From these plots, the observed data may be compared by property and by layer. To assess material variability, the data are categorized based on the associated material, subsurface layer, and index or engineering property. With the data grouped in this way, a statistical analysis is performed with each set to produce a mean, coefficient of variation (CoV), and an associated 70% confidence interval of the true mean.

The results of the laboratory investigation include a relatively large dataset of strength and index properties of the intact rock. Correlations between q_u and several index properties exist in the literature (Section 2.3.1) and may be used to estimate rock strength. In Chapter 7, these correlations will be examined in terms of their predictions of actual strength. Because these existing correlations were developed based on site-specific data, they may not apply in every case. Therefore, in the case that it may be justified based on the scale of the project, site-specific correlations should be developed

to estimate strength more accurately and reliably. Appropriately, the laboratory data collected in this study are analyzed in this section to develop site-specific correlations.

It is important to note the directional aspect of engineering properties obtained in relation to the orientation of the loads enforced on the foundation materials. This study is conducted in the context of laterally loaded foundations. For the most part, the investigation was limited to making observations and determining strength properties with respect to the vertical direction. Consequently, minimal data representing the horizontal strength of the material are known, which should be considered in selecting the final design parameters. The one exception is the PMT data, which are utilized in this section to estimate the lateral deformation modulus of the rock mass, in addition to developing load-displacement (*p*-*y*) curves. This PMT data will be used in subsequent sections to evaluate methods of estimating deformation characteristics of the rock mass.

6.2 Subsurface Profiles

Subsurface materials and conditions were logged versus depth for site explorations LS #1 and LS #4, which are presented in Figs. 6-1 through 6-4. These coring logs depict a general description of subsurface material boundaries, type, color, texture, and moisture, in addition to several strength and rock quality parameters. The two exploration logs were made from coreholes drilled about 8 ft apart, and consequently exhibit similar stratification of material type. Hence, these logs and the associated properties should only be taken to represent subsurface conditions within the immediate vicinity of the drilling operations.

PROJECT: PACIFICORP RESEARCH | DRILLING FIRM / OPERATOR: INBERG-MILLER | DRILL RIG: CME 85 TRUCK | STATION / OFFSET: | EXPLORATION ID: LS #1

TYPE: STRUCTURE | SAMPLING FIRM / LOGGER: U OF U / THOMAS T. | HAMMER: | ALIGNMENT: LIMA SUBSTATION

PID: 99999 BR ID: N/A | DRILLING METHOD: AIR-ROTARY / NQ | CALIBRATION DATE: N/A | ELEVATION: 6715.0 (MSL) EOB: 56.0 ft. | PAGE: 1 OF 2

START: 7/7/10 END: 7/8/10 | SAMPLING METHOD: SINGLE BARREL -- NQ | ENERGY RATIO (%): | COORD: 41.720000000, -110.370000000

MATERIAL DESCRIPTION AND NOTES	LITH	ELEV. 6715.0	DEPTH (ft)	RUN ID	REC (%)	RQD (%)	Rate (ft/h)	F.F. (/ft)	Lab ID	Unit Wt. (pcf)	qu/(C,AF) (psi/deg)	WC (%)	GRADATION (%) GR	CS	FS	F	ATTERBERG LL	PL	PI	SOIL CLS.
TOP SOIL																				
SOFT TO MEDIUM STIFF, LIGHT BROWN, **LEAN CLAY WITH SAND**, FINE TO VERY FINE GRAINED, DAMP		6714.5	1 2	Macro-1	80	--	--	--	C-1	86.8	(2.5,44.5)	8.1	4	10	14	72	39	17	22	CL A-7-6
MEDIUM DENSE TO DENSE, LIGHT BROWN TO WHITE, **CLAYEY SAND WITH GRAVEL**, COURSE TO FINE GRAINED, DAMP		6712.5	3 4 5						C-2	90.7	(2.5,44.5)	2.6	22	12	20	46	28	15	13	SC A-6
LIMESTONE, OLIVE GREEN, HIGHLY WEATHERED, WEAK, VERY FINE GRAINED, THINLY BEDDED, FRIABLE, DAMP.		6709.5	6 7	Macro-2	90	--	--	--	C-3	115	-	17	0	0	1	99	69	27	42	CH A-7-6
SANDY CLAYSTONE, DARK GREENISH GREY, HIGHLY WEATHERED, WEAK, FINE TO VERY FINE GRAINED, THINLY BEDDED, CALCAREOUS, FIRABLE, DAMP.		6707.5	8 9 10						C-4	127	-	14	0	0	35	65	51	19	32	CH A-7-6
			11 12	Macro-3	100	--	--	--	C-5	134	-	6.9	0	0	42	58	42	24	18	CL A-7-6
CLAYSTONE, DARK GREENISH GREY, HIGHLY WEATHERED, WEAK, VERY FINE GRAINED, THINLY BEDDED, CALCAREOUS, FRIABLE, DAMP.		6702.5	13 14 15						C-6	134	-	12	0	0	14	86	81	17	64	CH A-6
			16 17	Macro-4	100	--	--	--	C-7	137	-	13	0	0	5	95	64	23	41	CH A-7-6
LIMESTONE, LIGHT GREENISH GREY, SLIGHTLY WEATHERED, MODERATELY STRONG, FINE GRAINED, THINLY BEDDED, DAMP.		6697.5	TR 18	NQ-5	50	15	4	0												
CLAYSTONE, DARK GREENISH GREY, HIGHLY WEATHERED, WEAK, VERY FINE GRAINED, THINLY BEDDED, CALCAREOUS, CONGLOMERATE, FRIABLE, MOIST, MECHANICAL FRACTURING.		6696.5	19																	
LIMESTONE, LIGHT GREENISH GREY, SLIGHTLY WEATHERED, MODERATELY STRONG, FINE GRAINED, THINLY BEDDED, DAMP. @22.0'; 17.5' - 23' -- STRONG, HOMOGENEOUS, OBLIQUE NATURAL FISSURES.		6695.0	20 21 22 23 24 25	NQ-6	80	30	4	0	UC-1	154	10,000	1.2	--	--	--	--	--	--	--	CORE
@26.0'; 23' - 31' -- MODERATELY STRONG PERPENDICULAR TO BEDDING PLANES, ANISOTROPIC, FRIABLE ALONG HORIZONTAL BEDDING PLANES, DAMP, MECHANICAL FRACTURING.			26 27 28 29	NQ-7	10	10	5	0	UC-2	139	7300	1.7	--	--	--	--	--	--	--	CORE

Fig. 6-1. Coring log for investigation LS #1 – 0 to 30 ft

PID: 99999 | BR ID: N/A | PROJECT: PACIFICORP RESEARCH | STATION / OFFSET: | START: 7/7/10 | END: 7/8/10 | PG 2 OF 2 | LS #1

MATERIAL DESCRIPTION AND NOTES	LITH	ELEV. 6685.0	DEPTH (ft)	RUN ID	REC (%)	RQD (%)	Rate (ft/h)	F.F. (/ft)	Lab ID	Unit Wt. (pcf)	qu/(C,AF) (psi/deg)	WC (%)	GRADATION (%) GR	CS	FS	F	ATTERBERG LL	PL	PI	SOIL CLS.
LIMESTONE, LIGHT GREENISH GREY, SLIGHTLY WEATHERED, MODERATELY STRONG, FINE GRAINED, THINLY BEDDED, DAMP. *(continued)*			31	NQ-8	65	65	5	0												
SANDSTONE, DARK GREENISH GREY, SLIGHTLY TO MODERATELY WEATHERED, MODERATELY STRONG, HOMOGENEOUS, FINE GRAINED, THINLY BEDDED, CALCAREOUS, FRIABLE, DAMP, MECHANICAL FRACTURING, RUSTIC NATRUAL FRACTURING.		6683.0	32																	
@35.0'; & @ 33: GRADES GREENISH BROWN.			33	NQ-9	90	80	5	0	UC-3	131	3300	3.3	--	--	--	--	--	--	--	CORE
@36.0'; 1: 40, SH, VN, NO, PL, SR, C.			34						UC-4	136	3500	2.3	--	--	--	--	--	--	--	CORE
@37.0'; 2: JOG, SH, VN, NO NO, ST, SR, C.			35						UC-5	129	2500	3.3	--	--	--	--	--	--	--	CORE
@38.0'; & @ 33: GRADES BLUISH GREY			36						UC-6	129	3500	2.5	--	--	--	--	--	--	--	CORE
3: 0, SH, VN, NO, NO, PL, SR, C.			37						UC-7	131	3600	2.8	--	--	--	--	--	--	--	CORE
@39.0'; 4: 0, SH, VN, NO, NO, PL, SR, C.			38	NQ-10	95	40	5	0.6												
@40.0'; 5: 75, SH, VN, NO, NO, PL, SR, C.			39						UC-8	128	3600	2.8	--	--	--	--	--	--	--	CORE
			40						UC-9	130	3300	3.4	--	--	--	--	--	--	--	CORE
LIMESTONE, DARK GREENISH GREY, FRESH WEATHERED, MODERATELY STRONG, FINE TO VERY FINE GRAINED, THINLY BEDDED, DAMP, MECHANICAL FRACTURING.		6674.0	41																	
@42.0'; 41' - 42' -- LOW RECOVERY, VERY BRITTLE, FRIABLE, FLAKY.			42	NQ-11	80	40	3.5	0.6												
			43						UC-10	138	7000	1.8	--	--	--	--	--	--	--	CORE
@45.0'; - 46.5' -- ABUNDANT MECHANICAL FRACTURING.			44						UC-11	138	2000	2.5	--	--	--	--	--	--	--	CORE
			45																	
			46						UC-12	138	2300	2.1	--	--	--	--	--	--	--	CORE
			47						UC-13	135	7200	1.1	--	--	--	--	--	--	--	CORE
@48.0'; 46.5' - 50' -- COMPETENT ROCK, SOME MECHANICAL FRACTURING.			48	NQ-12	100	80	10	.4	UC-14	147	3100	1.5	--	--	--	--	--	--	--	CORE
			49						UC-15	146	6700	1.1	--	--	--	--	--	--	--	CORE
			50						UC-16	136	2200	1.9	--	--	--	--	--	--	--	CORE
@52.0'; 50' - 55' -- ABUNDANT MECHANICAL FRACTURING.			51																	
			52	NQ-13	65	8	5	0												
			53																	
			54						UC-17	145	3600	2.6	--	--	--	--	--	--	--	CORE
SHALE, DARK GREENISH GREY, MODERATELY TO HIGHLY WEATHERED, WEAK, VERY FINE GRAINED, THINLY BEDDED, MECHANICAL FRACTURING, MOIST.		6660.0	55	NQ-14	100	0	2	0												
		6659.0	56 B																	

ABREVIATIONS:

SH -- SHEAR DISCONTINUITY TYPE
NO – NO INFILLING
SR -- SLIGHTLY ROUGH FRACTURE SURFACE
T -- TIGHT JOINT (0 IN.)
VN -- VERY NARROW JOINT (<0.05 IN.)
PL – PLANAR FRACTURE SURFACE
M – MODERATE DISCONTINUITY SPACING (0.7 - 2.0 FT.)

GR – GRAVELLY SOIL
CS – COURSE GRAIN + MEDIUM GRAIN SAND
FS -- FINE GRAINED SAND
LL -- LIQUID LIMIT
PL -- PLASTIC LIMIT
PI -- PLASTICITY INDEX
LITH. – LITHOLOGY

qu -- UNIAXIAL COMPRESSIVE STRENGTH
WC -- WATER CONTENT
REC – RECOVERY
RQD – ROCK QUALITY DESIGNATION
F.F. -- FRACTURE FREQENCY
C – EFFECTIVE COHESION
AF – EFFECTIVE ANGLE OF INTERNAL FRICTION

U OF U STANDARD BORING LOG - OH DOT GDT - 4/24/11 00:29 - C:\DOCUMENTS AND SETTINGS\THOMAS\MY DOCUMENTS\COLLEGE\RESEARCH\LIMA SUBSTATION\GINT\BORING LO

Fig. 6-2. Coring log for investigation LS #1 – 30 to 56 ft

U:\OF U STANDARD BORING LOG - OH DOT GDT - 4/24/11 00:29 - C:\DOCUMENTS AND SETTINGS\THOMAS\MY DOCUMENTS\COLLEGE\RESEARCH\LIMA SUBSTATION\INT\BORING LC

PROJECT: PACIFICORP RESEARCH | DRILLING FIRM / OPERATOR: MSD / DON M. | DRILL RIG: CME 55 TRUCK | STATION / OFFSET: | EXPLORATION ID: LS #4

TYPE: STRUCTURE | SAMPLING FIRM / LOGGER: U OF U / THOMAS T. | HAMMER: | ALIGNMENT: LIMA SUBSTATION

PID: 99999 BR ID: N/A | DRILLING METHOD: AIR-ROTARY / NX | CALIBRATION DATE: N/A | ELEVATION: 6715.0 (MSL) EOB: 59.0 ft. | PAGE: 1 OF 2

START: 11/3/10 END: 11/4/10 | SAMPLING METHOD: DOUBLE BARREL -- NX | ENERGY RATIO (%): | COORD: 41.720000000, -110.370000000

MATERIAL DESCRIPTION AND NOTES	LITH	ELEV. 6715.0	DEPTH (ft)	RUN ID	REC (%)	RQD (%)	Rate (ft/h)	F.F. (/ft)	Lab ID	Unit Wt. (pcf)	qu/(C,AF) (psi/deg)	WC (%)	GRADATION (%) GR	CS	FS	F	ATTERBERG LL	PL	PI	SOIL CLS.
NO SAMPLE OBTAINED.			1–8																	
CLAYSTONE, GREENISH GREY, HIGHLY WEATHERED, WEAK, FINE TO VERY FINE GRAINED, THINLY BEDDED, CALCAREOUS, FRIABLE, MOIST.		6706.0	9–12	NX-1	97	73	20	0	UC-1	133	170	9.87	--	--	--	--	--	--	--	CORE
@13.0'; 9' - 19': GRADES BETWEEN LIGHT & DARK GREENISH GREY.			13–16	NX-2	90	72	20	0.2	UC-2	127	80	9.43	--	--	--	--	--	--	--	CORE
									UC-3	145	390	7.9	--	--	--	--	--	--	--	CORE
									UC-4	134	230	8.66	--	--	--	--	--	--	--	CORE
									UC-5	137	270	12.2	--	--	--	--	--	--	--	CORE
			17R																	
LIMESTONE, LIGHT GREENISH GREY, SLIGHTLY WEATHERED, MODERATELY STRONG, DENSE, HOMOGENEOUS,, FINE GRAINED, THINLY BEDDED, DAMP, OBLIQUE NATURAL FISSURES.		6698.0	18						UC-6	151	3300	5.52	--	--	--	--	--	--	--	CORE
SANDY CLAYSTONE, DARK GREENISH GREY, HIGHLY WEATHERED, WEAK, DENSE,, FINE GRAINED, THINLY BEDDED, CALCAREOUS, FRIABLE, DAMP.		6697.0																		
LIMESTONE, LIGHT GREENISH GREY, SLIGHTLY WEATHERED, MODERATELY STRONG, FINE GRAINED, THINLY BEDDED, DAMP.		6696.0	19–23	NX-3	68	18	5	0.2	UC-7	158	8600	3.7	--	--	--	--	--	--	--	CORE
@22.0'; 21' - 23.5' -- MODERATELY STRONG, HOMOGENEOUS, OBLIQUE NATURAL FRACTURING 1-4: 90, SH, T, NO, NO, WA, SR, M.									UC-8	154	2200	6.8	--	--	--	--	--	--	--	CORE
									UC-9	146	4500	6.93	--	--	--	--	--	--	--	CORE
@24.0'; 23.5' - 31' -- MODERATELY STRONG PERPENDICULAR TO BEDDING PLANES, ANISOTROPIC, FRIABLE ALONG BEDDING PLANES, DAMP, MECHANICAL FRACTURING.			24–28	NX-4	86	20	10	0.8												
			29						UC-10	155	6500	4.54	--	--	--	--	--	--	--	CORE
		6686.0																		

Fig. 6-3. Coring log for investigation LS #4 – 9 to 30 ft

PID: 99999 | BR ID: N/A | PROJECT: PACIFICORP RESEARCH | STATION / OFFSET: | START: 11/3/10 | END: 11/4/10 | PG 2 OF 2 | LS #4

MATERIAL DESCRIPTION AND NOTES	LITH	ELEV. 6685.0	DEPTH (ft)	RUN ID	REC (%)	RQD (%)	Rate (ft/h)	F.F. (/ft)	Lab ID	Unit Wt. (pcf)	qu/(C,AF) (psi/deg)	WC (%)	GRADATION (%) GR	CS	FS	F	ATTERBERG LL	PL	PI	SOIL CLS.
SANDSTONE, DARK GREENISH GREY, MODERATELY WEATHERED, WEAK, HOMOGENEOUS, FINE GRAINED, THINLY BEDDED, MOIST, MECHANICAL FRACTURING, NATURAL FRACTURING. *(continued)*			31	NX-5	68	68	15	1.4	UC-11	138	590	16	--	--	--	--	--	--	--	CORE
			32																	
@33.0'; 5-10: 20-45, SH, VN, NO, NO, PL, SR, M (DARK GREY WITH RUSTIC APPEARANCE).			33						UC-12	146	2700	9.35	--	--	--	--	--	--	--	CORE
			34						UC-13	140	870	14	--	--	--	--	--	--	--	CORE
@35.0'; 29' - 41': GRADES BETWEEN GREENISH BROWN, DARK GREENISH GREY, & BLUISH GREY.			35	NX-6	100	67	12	0.8	UC-14	142	1600	11.3	--	--	--	--	--	--	--	CORE
									UC-15	141	2800	9.82	--	--	--	--	--	--	--	CORE
			36						UC-16	141	1100	13	--	--	--	--	--	--	--	CORE
			37						UC-17	140	1100	13	--	--	--	--	--	--	--	CORE
@38.0'; 11-15: 20-75, SH, T, NO, NO, PL, SR, M (RUSTIC APPEARANCE).			38																	
@39.0'; SLOW DRILLING RATE PARTIALLY CAUSED BY OVERNIGHT CONDENSATION BUILDUP.			39																	
			40						UC-18	139	1100	12.9	--	--	--	--	--	--	--	CORE
			41																	
			42	NX-7	60	48	5	0.2	UC-19	145	3500	10.3	--	--	--	--	--	--	--	CORE
LIMESTONE, LIGHT GREENISH GREY, FRESH WEATHERED, MODERATELY STRONG, FINE TO VERY FINE GRAINED, THINLY BEDDED, DAMP, MECHANICAL FRACTURING, NATURAL FRACTURING.		6673.0	43						UC-20	144	2100	12	--	--	--	--	--	--	--	CORE
			44																	
@43.0'; 16: 45, SH, T, NO, NO, PL, SR, W, (CLEAN).									UC-21	150	4000	7.14	--	--	--	--	--	--	--	CORE
@44.0'; PRESENCE OF SMALL GRAVEL PARTICLES IN TEST SPECIMEN.			45						UC-22	148	2800	8.7	--	--	--	--	--	--	--	CORE
@45.0'; - 47.5: MECHANICAL FRACTURING.			46																	
				NX-8	98	68	15	0	UC-23	146	3600	6.90	--	--	--	--	--	--	--	CORE
@47.0'; 41' - 47': LENGTHS OF COMPETENT ROCK.			47						UC-24	149	4700	6.0	--	--	--	--	--	--	--	CORE
			48																	
			49						UC-25	146	2600	8.8	--	--	--	--	--	--	--	CORE
			50																	
			51						UC-26	147	2900	8.63	--	--	--	--	--	--	--	CORE
				NX-9	72	60	15	0	UC-27	146	1400	8.05	--	--	--	--	--	--	--	CORE
			52																	
			53																	
SHALE, DARK GREENISH GREY, MODERATELY TO HIGHLY WEATHERED, WEAK, VERY FINE GRAINED, THINLY BEDDED, MOIST, FLAKY, FRIABLE, MECHANICAL FRACTURING.		6661.0	54						UC-28	155	3100	6.0	--	--	--	--	--	--	--	CORE
			55																	
			56	NX-10	76	17	10	0	UC-29	138	530	14	--	--	--	--	--	--	--	CORE
			57																	
			58						UC-30	144	1600	10.8	--	--	--	--	--	--	--	CORE
		6656.0	59 B																	

ABREVIATIONS:

SH -- SHEAR DISCONTINUITY TYPE
NO -- NO INFILLING
SR -- SLIGHTLY ROUGH FRACTURE SURFACE
T -- TIGHT JOINT (0 IN.)
VN -- VERY NARROW JOINT (<0.05 IN.)
PL -- PLANAR FRACTURE SURFACE
M -- MODERATE DISCONTINUITY SPACING (0.7 - 2.0 FT.)
GR -- GRAVELLY SOIL
CS -- COURSE GRAIN + MEDIUM GRAIN SAND
FS -- FINE GRAINED SAND
LL -- LIQUID LIMIT
PL -- PLASTIC LIMIT
PI -- PLASTICITY INDEX
qu -- UNIAXIAL COMPRESSIVE STRENGTH
WC -- WATER CONTENT
REC -- RECOVERY
RQD -- ROCK QUALITY DESIGNATION
LITH -- LITHOLOGY
F.F. -- FRACTURE FREQUENCY
C -- EFFECTIVE COHESION
AF -- ANGLE OF INTERNAL FRICTION

Fig. 6-4. Coring log for investigation LS #4 – 30 to 59 ft

Following is a general description of the subsurface conditions as shown in Figs. 6-1 through 6-4. Note that the subsurface layer boundaries indicated in these figures are approximate. The soil within about 6 ft of the ground surface is lean clay with sand and gravel. A very dense/stiff, heavily cemented sandy clay material was encountered between 6 and 17 ft, and is classified as a weak, weathered rock material. Another thin layer of this weak rock exists between about 18 and 19 ft, with an intermediate moderately strong limestone layer between 17 and 18 ft. The weathered rock grades from medium to very high plasticity (Fig. 5-1). However, the in-situ *w*, which ranges between 6 and 17%, was determined to be less than the plastic limit.

Four distinct layers of rock were encountered between 19 and 59 ft (Figs 6-1 through 6-4): (1) A layer of limestone of moderate strength exists between about 19 and 29 ft; (2) between about 29 and 42 ft, a weak sandstone layer was encountered with *w* ranging between about 13 and 16%; (3) the sandstone layer was followed by a layer of relatively competent, moderately strong limestone between 42 and 54 ft, which indicated a relatively low range of *w* between 6 and 12%; (4) below a depth of 54 ft to the end of exploration at 59 ft, a weak, slightly weathered, and relatively moist layer of flaky, friable, calcareous shale was encountered. No free standing water surface was encountered.

As indicated on coring logs LS #1 and LS #4 (Figs. 6-1 through 6-4), within certain intervals the rock core experienced high levels of mechanical fracturing during coring. This is indicative of relatively low strength along horizontal bedding planes of the rock, and therefore a high to moderate level of strength anisotropy was exhibited. This anisotropy was further demonstrated in the laboratory for depths ranging between 6

and 17 ft, 24 and 29 ft, and below 54 ft, as pieces of rock core were cleaved by hand with little effort. Rock core within certain depths, however, demonstrated great strength along bedding planes, indicating less anisotropic behavior. Examples include the limestone between 20 and 24 ft, the sandstone between 29 and 42 ft, and portions of the lower limestone layer. In addition, several portions of the rock core exhibited natural fracturing unassociated with bedding planes. The strength of the rock mass is largely dependent on the frequency, orientation, and surface characteristics of natural discontinuities. Descriptions of the fractures encountered during exploration are detailed in the boring logs presented in Figs. 6-1 through 6-4. Details of these discontinuities will be discussed later in regard to rock mass strength (Section 7.3).

6.3 Index and Engineering Properties versus Depth

As previously discussed in Chapter 5, the strength and index tests conducted during the laboratory investigation include UAC, point load index, Brazilian tension, rebound hardness index, and unit weight and water content determination. The results of each of these tests for material from LS #1 and LS #4 are plotted versus depth in Figs. 6-5 through 6-7. As discussed in Chapter 5, material from LS #1 was tested under air-dried conditions, while that of LS #4 was tested under in-situ moisture conditions. This difference affected the measured strength and index properties of the materials obtained from the two investigations, as can clearly be seen in the following figures.

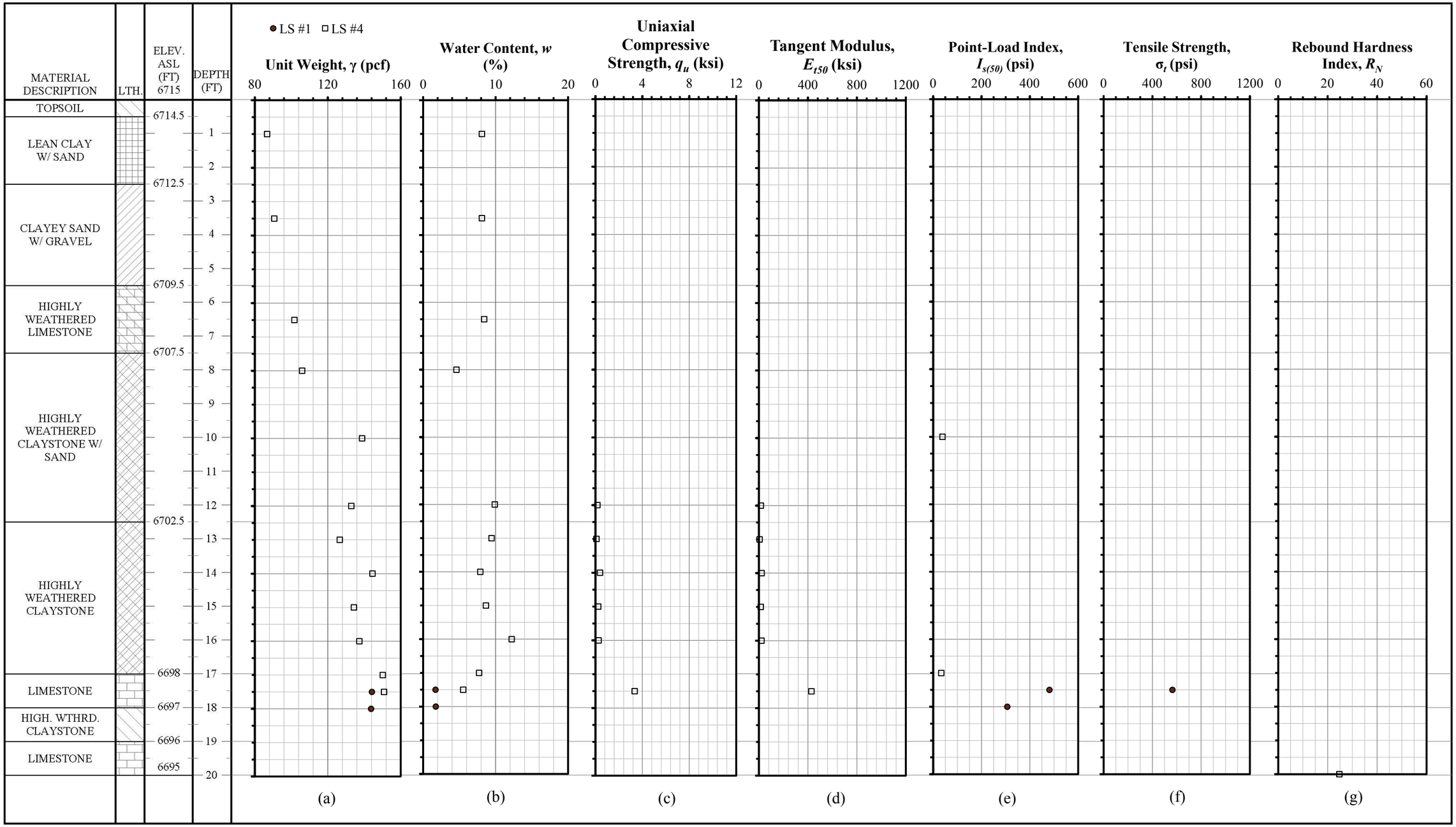

Fig. 6-5. Index and engineering properties versus depth – 0 to 20 ft

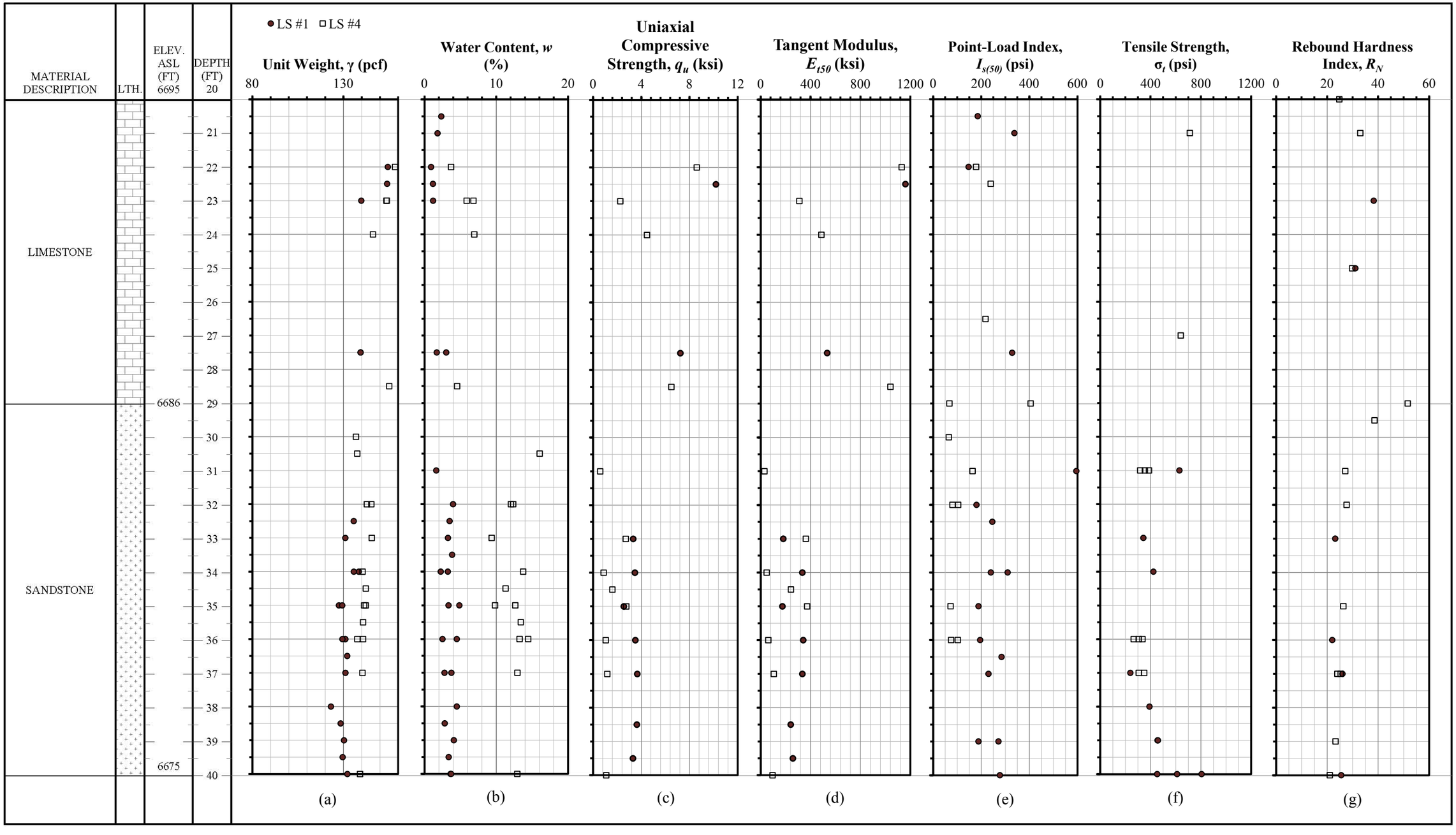

Fig. 6-6. Index and engineering properties versus depth – 20 to 40 ft

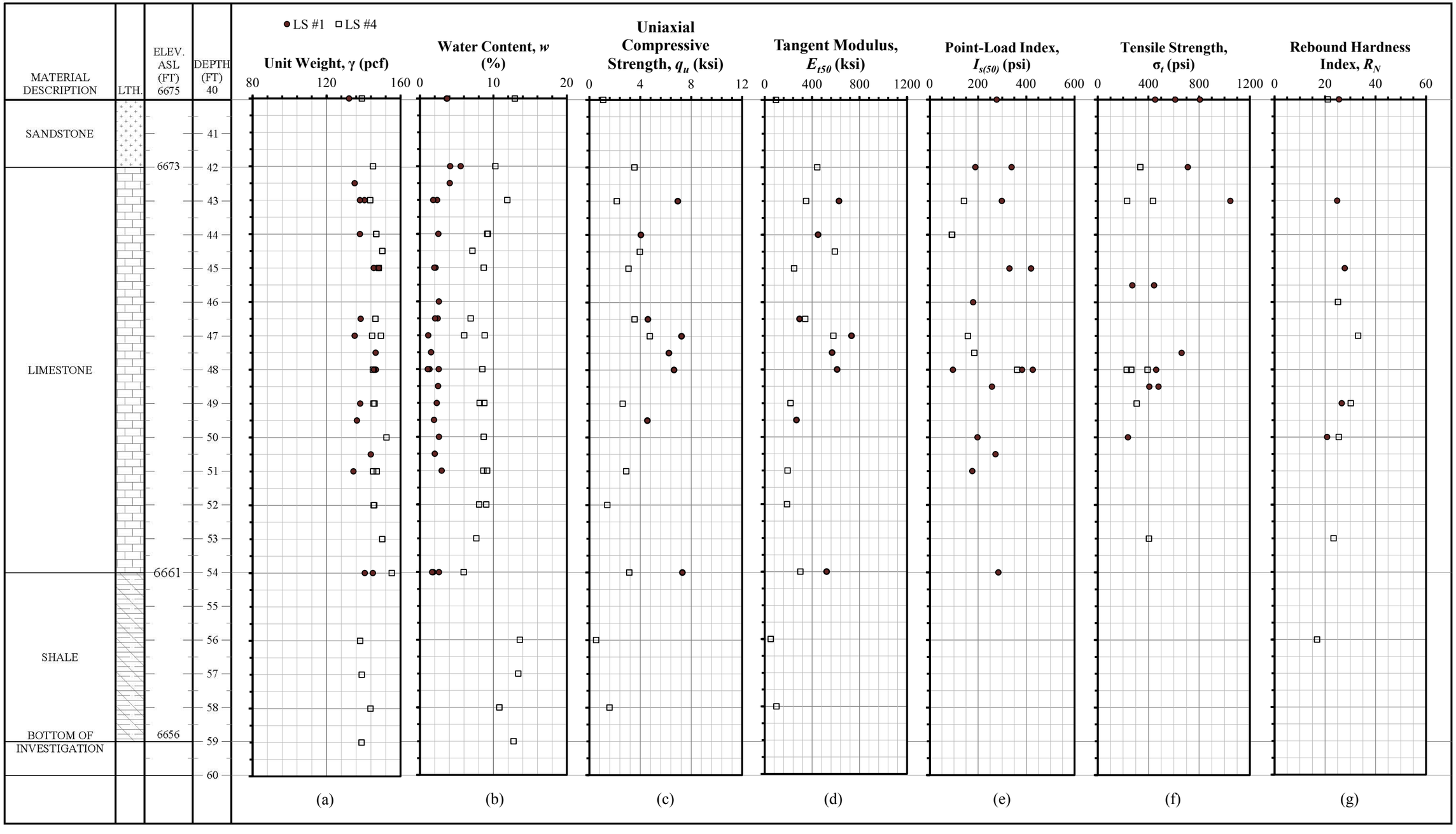

Fig. 6-7. Index and engineering properties versus depth – 40 to 60 ft

6.4 Data Variability and Site-Specific Correlations

As expected, the test results exhibit considerable scatter (Figs. 6-5 through 6-7), indicating variability in the material properties. Associated with this variability is a level of uncertainty as to the "true" properties of the material – whether the experimental results are biased high or low in terms of actual strength. This section discusses the statistical variability associated with each set of raw data collected in the laboratory, which will subsequently be used to determine best-estimate engineering properties. Accuracy of the data in terms of their use with existing correlations to predict strength will be discussed in Chapter 7.

To describe the variability associated with the collected data, the test results were first classified and grouped based on material type and layer. One method used to determine a representative or best-estimate design value is to simply calculate the mean of the observed data. However, for design purposes, it is important to consider the uncertainty associated with the observed mean to describe the variability of the data (Gill et al. 2004). For each set of data, the mean, coefficient of variation (CoV), and 70% confidence interval were determined. A 70% confidence interval was selected because it approximately represents the mean plus or minus one standard deviation estimate. The confidence interval was calculated using the Student's *t*-test. This method adjusts the confidence interval for small sample size effects ($n < 20$), which were present in the data sets due to limited sampling. It should also be noted that the following statistical analyses represent layers up to 13 ft thick, each of which exhibit natural heterogeneity to a certain extent. Therefore, relatively high variability may be expected for the data within each layer.

In addition to assessing variability, site-specific, empirical correlations developed between q_u and each index property will be presented in this section. It is assumed that the results from UAC testing produce the most reliable estimate of q_u. These correlations were made taking q_u as the dependent variable because it is the most common design parameter used in most design models (Pariseau 2007). Similar empirical correlations used to predict q_u exist in the literature. These correlations are generally used to estimate strength for rock classification purposes and are not intended for use in design. In addition, like most empirical correlations, they are generally applicable to site-specific conditions. In the case that large-scale construction is to take place at a site, it is advisable that such correlations be validated prior to use, and that site-specific correlations be developed if sufficient data can be collected. The correlations produced in this study were developed by matching q_u with the applicable index property at corresponding depths. Using the plotted results, a best-fit regression analysis was applied to each data set. Correlations developed in the literature will be analyzed in Section 7.2 to assess the predictive capability of each method, similar to that done by Gunsallus and Kulhawy (1984).

6.4.1 Unit Weight (γ)

Unit weight (γ) is plotted versus depth for both LS #1 and LS #4 in Figs. 6-5 (a) through 6-7 (a). The values for γ range between about 86 pcf for the alluvial soil at the surface to about 158 pcf for portions of the limestone layers. The unit weight data were separated into datasets based on material rock layer. These data sets correspond to the weathered claystone layer, the upper limestone layer, the sandstone layer, the lower limestone layer, and the shale layer below 54 ft (Figs. 6-5 through 6-7). The statistics for

γ for LS #4 are shown for each of these layers in Table 6-1. (Only data for LS #4 are shown because it is most representative of field conditions.) The mean values of γ range between 88.7 pcf and 152.6 pcf for the various layers. The coefficient of variation (CoV) for the data ranges between 1.8 and 3.1%. The variability is low in this case because the unit weight is strictly a function of mass and geometric characteristics, and is not influenced by the mechanical characteristics of the rock.

UAC strength data is plotted versus γ in Fig. 6-8 for LS #1 and LS #4. These data were correlated by matching data observed in the laboratory at corresponding depths. This figure shows a significant difference in the regression line for the two datasets – the data for LS #1 representing air-dry conditions and the data for LS #4 representing moist conditions. The best correlation for each dataset was obtained by exponential regression analysis, which is consistent with correlations developed in the literature. However, both data sets indicate values significantly below a similar correlation developed by Smorodinov et al. (1970). The coefficient of determination (R^2) for the regression analyses is 0.713 for samples from LS #1 and 0.771 for samples from LS #4.

Table 6-1. Statistical Results for Unit Weight Data – LS #4

Subsurface Layer	Top (ft)	Bottom (ft)	Sample Size, *n*	Observed Mean Unit Weight, γ_{ave} (pcf)	CoV (%)	70% Confidence Interval	
						Lower, γ_L (pcf)	Upper, γ_U (pcf)
Clayey Sand	0	6	2	88.7	3.1	84.9	92.6
Upper Claystone	6	12	2	103.8	2.9	99.7	108.0
Lower Claystone	12	19	6	135.7	4.5	132.9	138.6
Upper Limestone	19	29	7	152.6	2.6	150.9	154.3
Sandstone	29	42	14	141.0	1.9	140.2	141.7
Lower Limestone	42	54	19	147.3	2.0	146.6	148.1
Shale	54	59	4	140.0	1.8	138.4	141.6

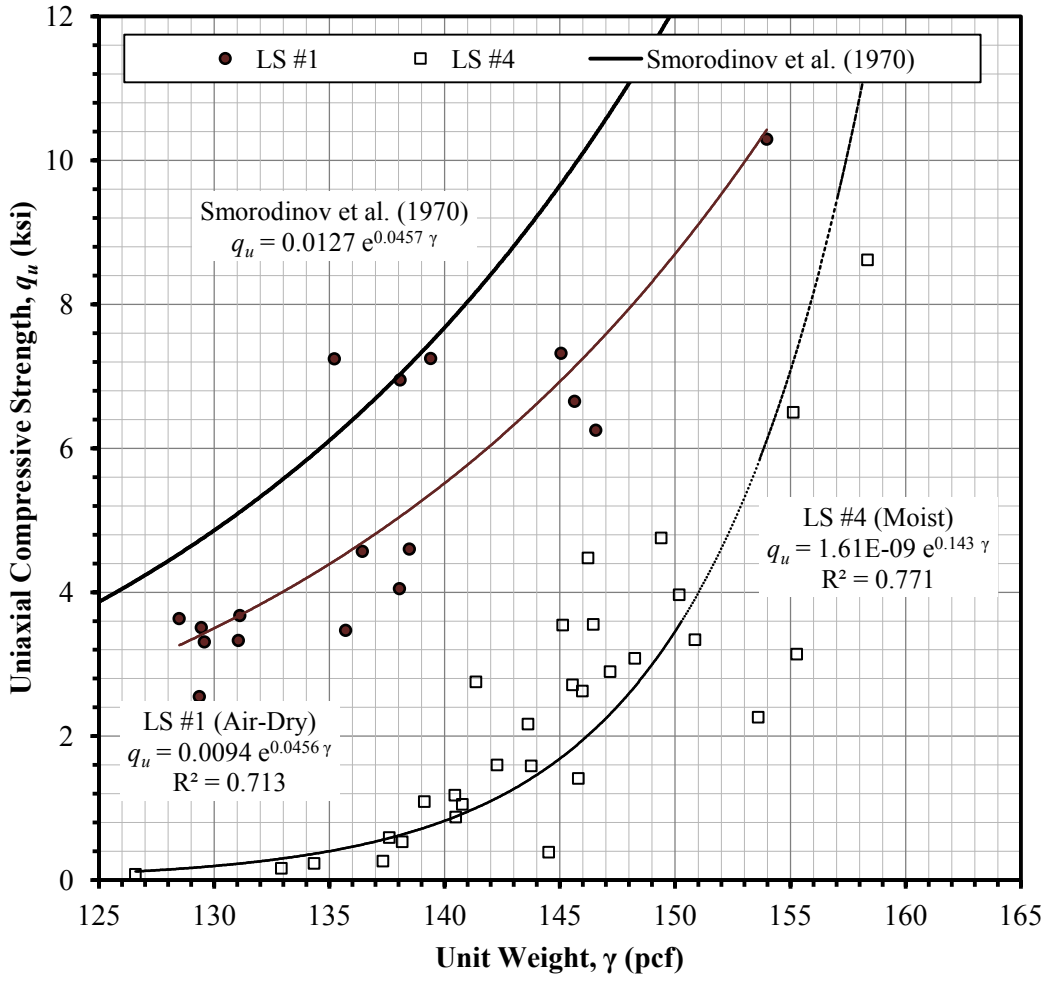

Fig. 6-8. Correlation between UAC strength and unit weight

6.4.2 Water Content (*w*)

Water content (*w*) is shown plotted versus depth in Figs. 6-5 (b) through 6-7 (b) for LS #1 and LS #4. Moisture content ranges between about 4 and 16% for samples tested from LS #4. Because samples from LS #1 were air-dried in the laboratory, values of *w* ranged between about 1 and 4%. The descriptive statistics for moisture content of samples from LS #4 are shown in Table 6-2. It follows that the mean value ranged between 5.87 and 12.6% and the CoV ranged between 10 and 42%.

Table 6-2. Statistical Results for Water Content Data – LS #4

Subsurface Layer	Top (ft)	Bottom (ft)	Sample Size, n	Observed Mean Water Content, w_{ave} (%)	CoV (%)	70% Confidence Interval	
						Lower, w_L (%)	Upper, w_U (%)
Clayey Sand	0	6	1	8.10	--	--	--
Upper Claystone	6	12	2	6.50	42	2.75	10.2
Lower Claystone	12	19	5	9.61	17	8.74	10.5
Upper Limestone	19	29	7	5.87	24	5.26	6.47
Sandstone	29	42	13	12.6	14	12.1	13.2
Lower Limestone	42	54	19	8.45	16	8.11	8.79
Shale	54	59	4	12.6	10	11.8	13.4

As can be seen in Fig. 6-9, q_u is inversely proportional to w. As previously discussed, there is a significant difference in the strength characteristics between the rock samples obtained from the two site investigations. The two datasets were not analyzed together because of the strong influence of w on strength, which was influenced by the sample handling and storage. The correlation for LS #1 has a higher coefficient of determination of 0.835 due to the smaller variability resulting from air drying, while that for LS #4 was less at 0.770, because these latter samples were closer to in-situ moisture conditions than the air-dried samples.

6.4.3 Uniaxial Compressive Strength (q_u)

Values of uniaxial compressive (UAC) strength (q_u) for rock samples from LS #1 and LS #4 are shown plotted versus depth in Figs. 6-5 (c) through 6-7 (c). Observed values for this strength parameter range between about 0.1 and 11 ksi. The statistics of the data collected for rock from LS #1 and LS #4 are shown in Table 6-3. The observed mean q_u for samples from LS #1 range between 3.35 and 8.77 ksi, while that for samples

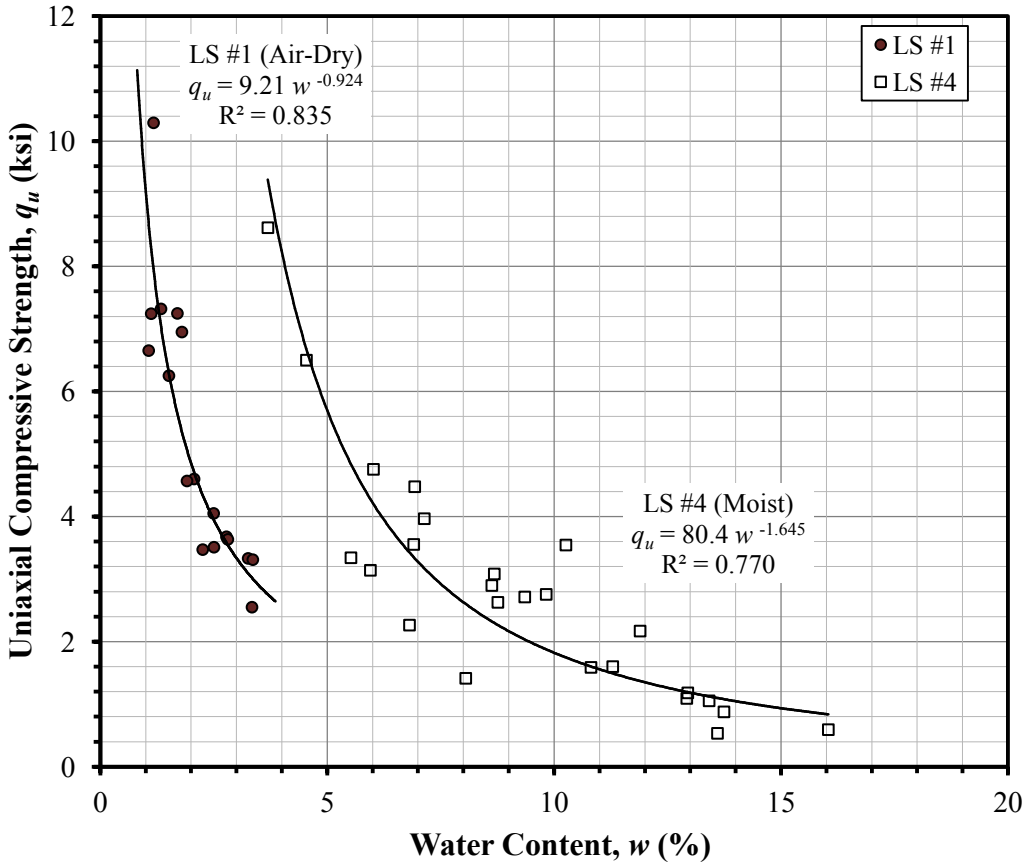

Fig. 6-9. Correlation between UAC strength and water content

Table 6-3. Statistical Results for UAC Data

Borehole/ Subsurface Layer	Top (ft)	Bot. (ft)	Sample Size, n	Observed Mean UAC Strength, $q_{u,ave}$ (ksi)	CoV (%)	70% Confidence Interval Lower, q_{uL} (ksi)	70% Confidence Interval Upper, q_{uU} (ksi)
Borehole LS #1							
Up. Limestone	19	29	2	8.77	25	5.78	11.8
Sandstone	29	42	7	3.35	11	3.19	3.52
Lo. Limestone	42	54	8	5.81	23	5.28	6.34
Borehole LS #4							
Claystone	9	19	4	0.263	36	0.204	0.321
Up. Limestone	19	29	5	5.04	50	3.69	6.39
Sandstone	29	42	8	1.48	55	1.16	1.81
Lo. Limestone	42	54	10	3.11	30	2.79	3.44
Shale	54	59	2	1.06	70	0.0252	2.10

from LS #4 range between 0.263 and 5.04 ksi. This marked difference in average strength values is also due to the difference in water content at the time of testing, and other physical and chemical changes that may have occurred during the drying process. The CoV for q_u data ranges between 11 and 25% for samples from LS #1 and between 30 and 70% for samples from LS #4. Factors impacting variability include differences in material fabric, water content, isotropy, and heterogeneity. Typical mean q_u values for limestone and sandstone are about 11 ksi and 9 ksi, respectively (Kulhawy 1975). Consequently, because the mean values of strength for rock core tested in this study are significantly lower than typical mean values of strengths for similar rock, the rock at Lima Substation may be considered to be relatively weak.

6.4.4 Elastic Modulus (E_{t50})

The elastic modulus (E_{t50}) is shown plotted versus depth for rock core from LS #1 and LS #4 in Figs. 6-5 (d) through 6-7 (d). This factor was determined from the UAC data and was taken to be the slope of the line tangent to the stress-strain curve at a normal stress equal to 50% of the peak normal stress. Observed E_{t50} values range between 13 and 1200 ksi. Statistical results for E_{t50} are shown in Table 6-4. Mean values of E_{t50} range between 266 and 846 ksi for LS #1 and between 17.3 and 679 ksi for samples from LS #4. The CoV ranged between 27 and 52% for samples from LS #1 and between 22 and 86% for samples from LS #4. In comparison, the variability of E_{t50} for samples from LS #4 is within about the same range as that of q_u.

The ratio between the stiffness and strength properties of intact rock (E_{t50} / q_u) is commonly used for correlation purposes. Statistics regarding this ratio are shown in Table 6-5. Typical values of modulus ratio for sandstone and shale are about 100, while

Table 6-4. Statistical Results for Elastic Modulus Data

Borehole/ Subsurface Layer	Top (ft)	Bottom (ft)	Sample Size, n	Observed Mean Modulus, E_{t50} (ksi)	CoV (%)	70% Confidence Interval	
						Lower, E_{t50L} (ksi)	Upper, E_{t50U} (ksi)
Borehole LS #1							
Up. Limestone	19	29	2	846	52	231	1460
Sandstone	29	42	7	266	27	235	297
Lo. Limestone	42	54	8	509	32	444	573
Borehole LS #4							
Claystone	9	19	4	17.3	22	14.8	19.7
Up. Limestone	19	29	5	679	56	478	880
Sandstone	29	42	8	164	86	109	220
Lo. Limestone	42	54	10	345	43	293	397
Shale	54	59	2	75.1	45	27.8	122

Table 6-5. Statistical Results for Modulus Ratio Data

Borehole/Subsurface Layer	Top (ft)	Bottom (ft)	Sample Size, n	Observed Mean Ratio, E_{t50}/q_u	CoV (%)	70% Confidence Interval	
						Lower, E_{t50}/q_u	Upper, E_{t50}/q_u
Borehole LS #1							
Up. Limestone	19	29	2	93.6	30	54.2	133
Sandstone	29	42	7	78.8	21	71.7	85.9
Lo. Limestone	42	54	8	84.9	22	77.7	92.2
Borehole LS #4							
Claystone	9	19	4	69.1	25	58.1	80.0
Up. Limestone	19	29	5	133	14	123	143
Sandstone	29	42	8	94.9	42	79.0	111
Lo. Limestone	42	54	10	111	28	100	122
Shale	54	59	2	79.1	30	46.5	112

values for limestone are typically about 200, with each giving a relatively wide distribution (after Horvath and Kenney 1979; Peck 1976). For samples from LS #4, the observed mean modulus ratio for sandstone is 94.9, that for shale is 79.1, and that for limestone is 111 to 133. These values are within the ranges reported, considering the variability associated with each typical value reported in the literature (Horvath and Kenney 1979; Peck 1976). A correlation between E_{t50} and q_u is presented in Fig. 6-10, indicating that the data are well represented by linear regression.

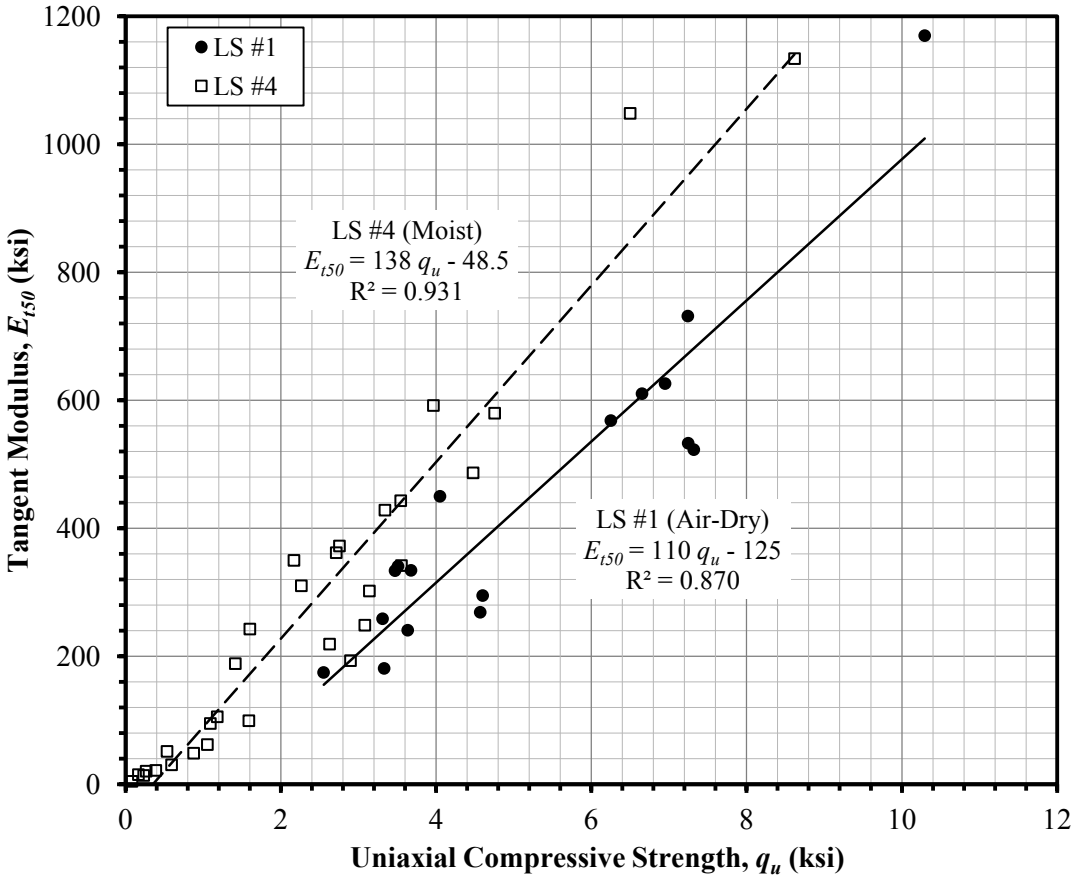

Fig. 6-10. Correlation between tangent modulus and UAC strength

6.4.5 Point Load Index ($I_{s(50)}$)

Point-load index ($I_{s(50)}$) values measured in the laboratory for specimens from LS #1 and LS #4 are plotted versus depth in Figs. 6-5 (e) through 6-7 (e). These values range between about 16 and 700 psi for all specimens tested, both axially and diametrically. The statistics for the point-load test data perpendicular (axial, $I_{s(50)\perp}$) and parallel (diametrical, $I_{s(50)\parallel}$) to bedding planes are shown for each of the layers in Tables 6-6 and 6-7, respectively. The mean values of $I_{s(50)\perp}$ range between 95 and 298 psi, and the CoV ranges between 36 and 66%. The mean values of $I_{s(50)\parallel}$ range between 19 and 406 psi and the CoV ranges between 21 and 132%. Because $I_{s(50)}$ is used to estimate q_u, it is insightful to compare the variability between the two. The CoV for q_u ranges between 11 and 70%, which is comparable to the range for point-load index, $I_{s(50)\perp}$. The significant variability seen in the point load results may be due, in part, to shape effects. Broch and Franklin (1972) found that the shape and size of the specimen can affect the variability for testing done in the axial direction.

A linear regression analysis was performed on the data for each rock type to produce the correlations between q_u and $I_{s(50)\perp}$ presented in Fig. 6-11. The data in this figure exhibit significant scatter and variability, which results in relatively low coefficients of determination. This scatter is indicative of the poor reliability associated with estimating strength from index tests. The regression lines were assumed to pass through the origin.

The statistics for the anisotropy index [$I_{a(50)}$], which was taken as the ratio between $I_{s(50)\parallel}$ and $I_{s(50)\perp}$, are presented in Table 6-8. These values range between 0.11 and 1.36, indicating a high level of anisotropy in the rock tested, which is primarily due to the bedding planes found within the sedimentary rock. The value of $I_{a(50)}$ of 1.36

Table 6-6. Statistical Results for Point-Load Index Data Perpendicular to Bedding

Borehole / Subsurface Layer	Top (ft)	Bottom (ft)	Sample Size, n	Observed P-L Index Mean, $I_{s(50)\perp,ave}$ (psi)	CoV (%)	70% Confidence Interval	
						Lower, $I_{s(50)\perp L}$ (psi)	Upper, $I_{s(50)\perp U}$ (psi)
Borehole LS #1							
Up. Limestone	19	29	6	298	40	241	354
Sandstone	29	42	12	267	42	232	302
Lo. Limestone	42	54	14	275	36	247	304
Borehole LS #4							
Up. Limestone	19	29	4	260	38	198	323
Sandstone	29	42	7	95	36	80.1	109
Lo. Limestone	42	54	5	169	66	110	229

Table 6-7. Statistical Results for Point-Load Index Data Parallel to Bedding

Borehole/ Subsurface Layer	Top (ft)	Bottom (ft)	Sample Size, n	Observed P-L Index Mean, $I_{s(50)\parallel,ave}$ (psi)	CoV (%)	70% Confidence Interval	
						Lower, $I_{s(50)\parallel L}$ (psi)	Upper, $I_{s(50)\parallel U}$ (psi)
Borehole LS #1							
Up. Limestone	19	29	6	406	44	321	490
Sandstone	29	42	4	62.6	91	27.1	98.0
Lo. Limestone	42	54	10	91.7	130	49.7	134
Borehole LS #4							
Up. Limestone	19	29	1	53.8	--	--	--
Sandstone	29	42	9	52.3	54	42.0	62.7
Lo. Limestone	42	54	2	19.0	21	13.4	24.6

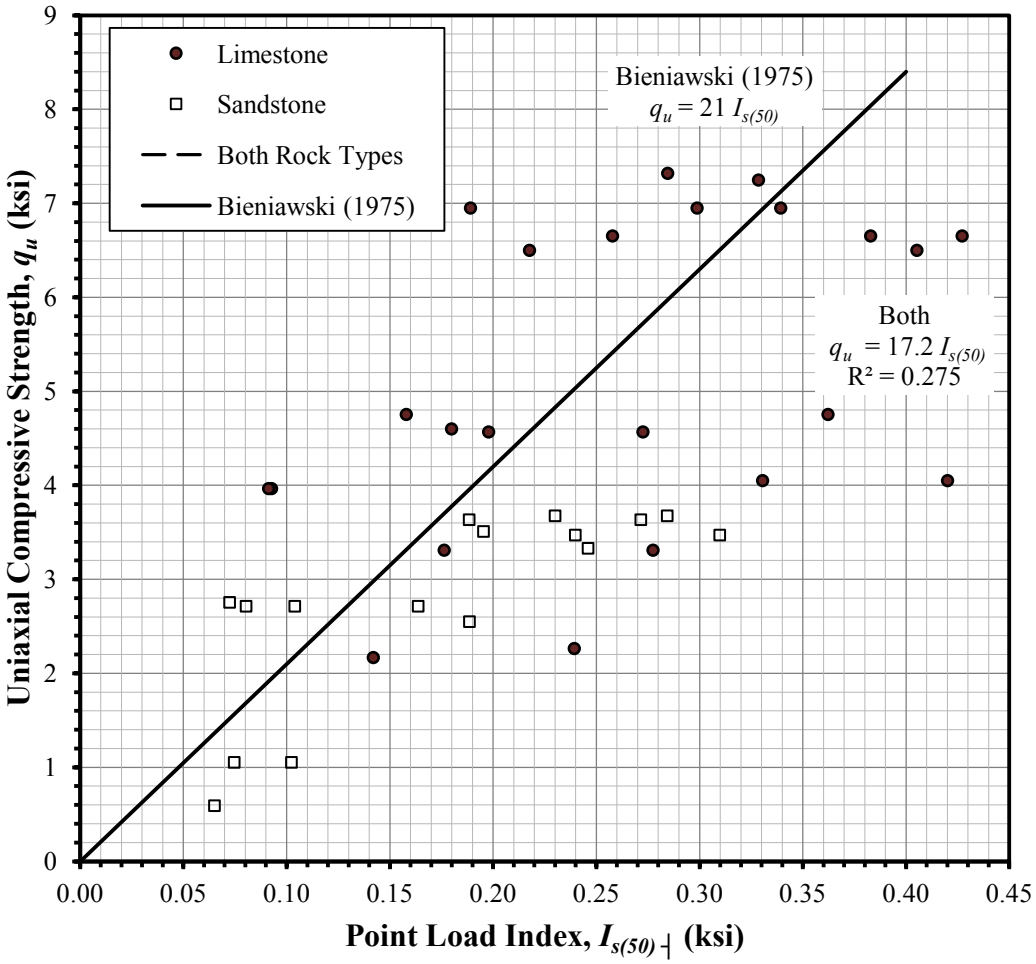

Fig. 6-11. Correlation between UAC strength and point-load index

Table 6-8. Anisotropy Index

Subsurface Layer	Top (ft)	Bottom (ft)	Degree of Anisotropy
Borhole LS #1			
Up. Limestone	17	29	1.36
Sandstone	29	42	0.23
Lo. Limestone	42	54	0.33
Borhole LS #4			
Up. Limestone	17	29	0.21
Sandstone	29	42	0.55
Lo. Limestone	42	54	0.11

exhibited in the upper limestone layer for LS #1 is likely biased because a limited number of samples were available for this case. Portions of this rock layer exhibited weak strength along bedding planes.

6.4.6 Brazilian Tension Test (σ_t)

The results of the Brazilian tension tests are plotted versus depth in Figs. 6-5 (f) through 6-7 (f). The observed values for tensile strength ranged between 200 and 1100 psi. As indicated in Table 6-9, the observed mean values for the various layers range between 324 and 676 psi, while the CoV ranges between 8 and 48% for LS #4. The variability of the data obtained using samples from LS #1 is significantly higher than those for LS #4, ranging between 34 and 48%. In addition to the difference in moisture content, this increase in variability is likely caused by the specimen size effects. The test is typically done on specimens with a minimum diameter of about 2.16 in. (NX). The diameter of specimens from LS #1 was about 1.85 in. (NQ), which may introduce size effects. For the data from LS #4, the Brazilian tension test had lower variability than that

Table 6-9. Statistical Results for Brazilian Tensile Test Data

Borehole/Subsurface Layer	Top (ft)	Bot. (ft)	Sample Size, *n*	Observed Mean Tensile Stength, $\sigma_{t,ave}$ (psi)	CoV (%)	70% Confidence Interval: Lower, $\sigma_{t,aveL}$ (psi)	70% Confidence Interval: Lower, $\sigma_{t,aveU}$ (psi)
Borehole LS #1							
Up. Limestone	19	29	1	564	--	--	--
Sandstone	29	42	10	480	34	424	537
Lo. Limestone	42	54	9	524	48	432	616
Borehole LS #4							
Up. Limestone	19	29	2	676	8	605	746
Sandstone	29	42	8	328	11	313	342
Lo. Limestone	42	54	8	324	25	293	356

for either the UAC or the point-load tests. A linear regression was performed on the observed q_u and σ_t data and is presented in Fig. 6-12. As indicated in this figure, the data exhibit scatter with a coefficient of determination of 0.556. This regression line is reasonably consistent with that found by Hassani (1979, shown in the figure), but is supported by data over a relatively narrow range and is highly influenced by minimum σ_t data over 0.6 ksi.

6.4.7 Schmidt Rebound Hardness (R_N)

Rebound hardness index (R_N) is presented versus depth in Figs. 6-5 (g) through 6-7 (g). The observed values for R_N range between 17 and 52. The mean values for the various layers presented in Table 6-10 range between 17 and 36, with CoVs between 11 and 24%. These results indicate the lowest variability of all the index tests except for γ. However, while the variability of the data seems reasonable, the magnitude of the test results may be incorrect. In addition, little variability is exhibited between layers, while the results of all other testing indicated such variability. This may be a result of the fact that the specimens tested were relatively small compared to the size recommended by ASTM. This smaller specimen size may have resulted in an undesirable dissipation of energy from the specimen to the base at impact. The low variability may also be due to the nature and sensitivity of the index test itself.

6.4.8 Comments on Variability and Site-specific Correlation

As indicated above, variability is inherent in the material tested. In summary, the CoV exhibited for UAC strength ranged between 11 and 70%, that for $I_{s(50)}$ ranged between 36 and 66%, that for σ_t ranged between 8 and 48%, and that for R_N ranged

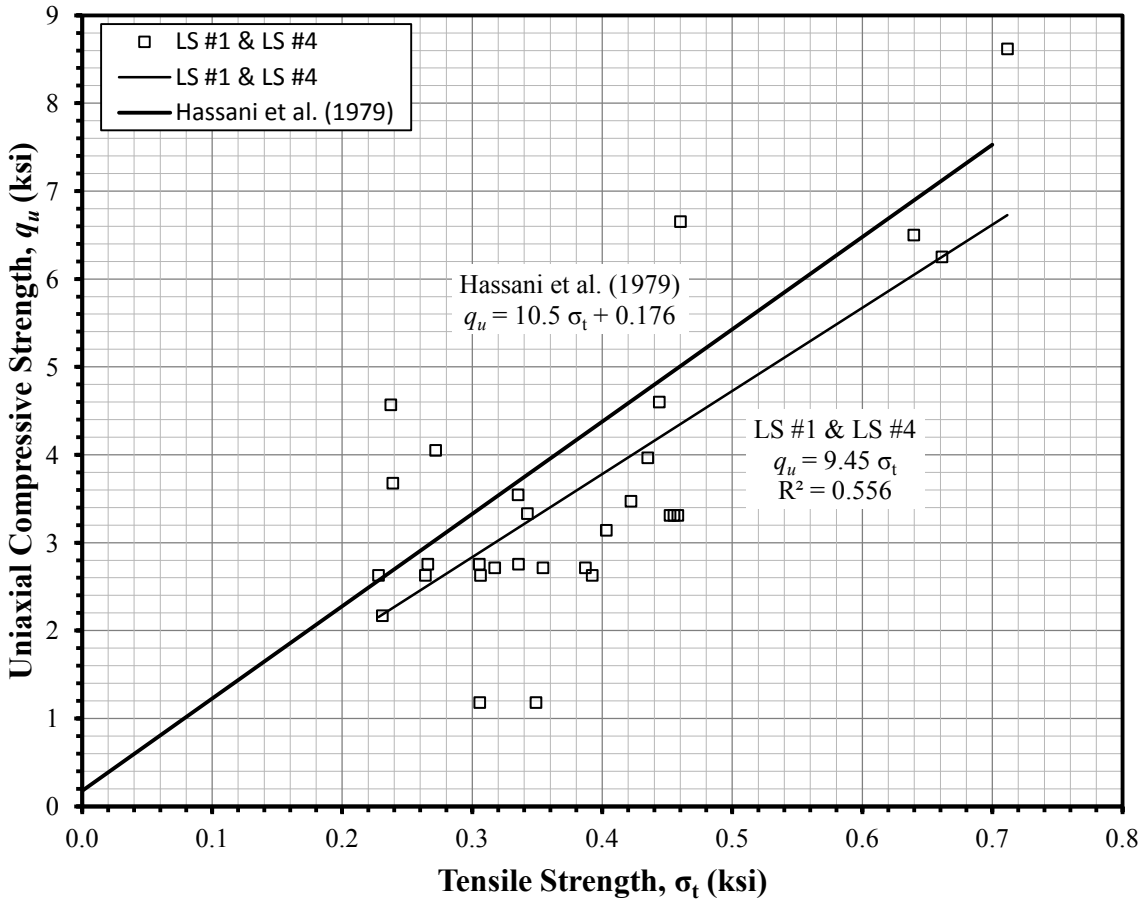

Fig. 6-12. Correlation between UAC strength and tensile strength

Table 6-10. Statistical Results for Rebound Hardness Data

Borehole / Subsurface Layer	Top (ft)	Bottom (ft)	Sample Size, n	Mean Rebound Hardness Index, R_N (psi)	CoV (%)	70% Confidence Interval	
						Lower, R_{NL} (psi)	Upper, R_{NU} (psi)
Borehole LS #1							
Up. Limestone	19	29	12	34	14	33	36
Sandstone	29	42	37	24	11	24	25
Lo. Limestone	42	54	17	25	15	24	26
Borehole LS #4							
Up. Limestone	19	29	26	36	24	34	38
Sandstone	29	42	63	25	11	25	26
Lo. Limestone	42	54	38	28	15	27	29
Shale	54	59	4	17	12	16	18

between 11 and 24%. The CoV for γ ranged between 1.8 and 3.1%, while that for *w* ranged between 10 and 42%. The lowest variability was found in the unit weight distribution, which is expected because γ is based solely on dimensional characteristics, not mechanical. The raw data for each of the index tests exhibited variability within or lower than the range exhibited by the UAC data, which was assumed to be the most accurate representation of strength. The results for R_N are suspect because little variability between layers was exhibited.

The correlations between q_u and each index property developed above are shown in Table 6-11. Based on the coefficient of determination computed for each correlation, q_u correlates equally well (R^2 = 0.770) with unit weight and water content. The correlations with point-load index exhibit the lowest coefficient, (R^2 = 0.275), while those for Brazilian tension (R^2 = 0.556) were intermediate. It should be noted that the linear regression lines for the point-load index and Brazilian tension were assumed to pass through the origin, and that this does affect the correlation coefficient. The developed equations take on a similar form to those developed in the literature, each of which will be examined in more detail in Section 7.2. The scatter associated with each of

Table 6-11. Site-Specific Correlations Developed in Present Study

Index test	Equation	Coefficient of Determination
Point-Load, $I_{s(50)}$	$q_u = 17.2\ I_{s(50)}$	$R^2 = 0.275$
Brazilian Tension, σ_t	$q_u = 9.45\ \sigma_t$	$R^2 = 0.556$
Unit Weight, γ	$q_u = 1.61E\text{-}09\ e^{0.143\ \gamma}$	$R^2 = 0.771$
Water Content, *w*	$q_u = 80.4\ w^{-1.645}$	$R^2 = 0.770$

γ in pcf q_u in ksi σ_t in ksi $I_{s(50)}$ in ksi *w* in %

these correlations should also be noted. Such correlations are typically used to estimate strength for classification purposes, and are typically not intended for use in design.

6.5 Pressuremeter Data

Pressuremeter testing can be a valuable source of information in determining the lateral deformation characteristics of subsurface material. All too often, however, financial budgets for geotechnical investigations do not allow for such testing to be conducted. Consequently, investigations are typically limited to obtaining information that can be used in conjunction with empirical correlations to estimate strength and deformation properties. This method typically introduces high levels of uncertainty. Fortunately, PMT was incorporated into this study, and the data obtained may therefore be used to predict more accurately the deformation characteristics of the rock mass. The PMT data are examined in this section to determine the lateral deformation modulus of the rock mass. In addition, this section presents the *p*-*y* curves obtained directly from the pressuremeter curves using the procedure outlined in Section 2.4.2. Both the deformation modulus and *p*-*y* curves developed in this section will subsequently be used to evaluate empirical models (Section 2.3 and 2.5) typically used in industry.

6.5.1 Initial Pressuremeter Modulus versus Depth

The PMT data from Section 4.4 was used to determine the rock mass modulus ($E_{rm} = E_o$) corresponding to each PMT depth using Eq. 2-10 from Section 2.4.1. The results for E_o from PMT are shown in Figure 6-13 and Table 6-12. Poison's ratio, v, was assumed to be 0.33 for the highly weathered rock. For the more competent rock layers,

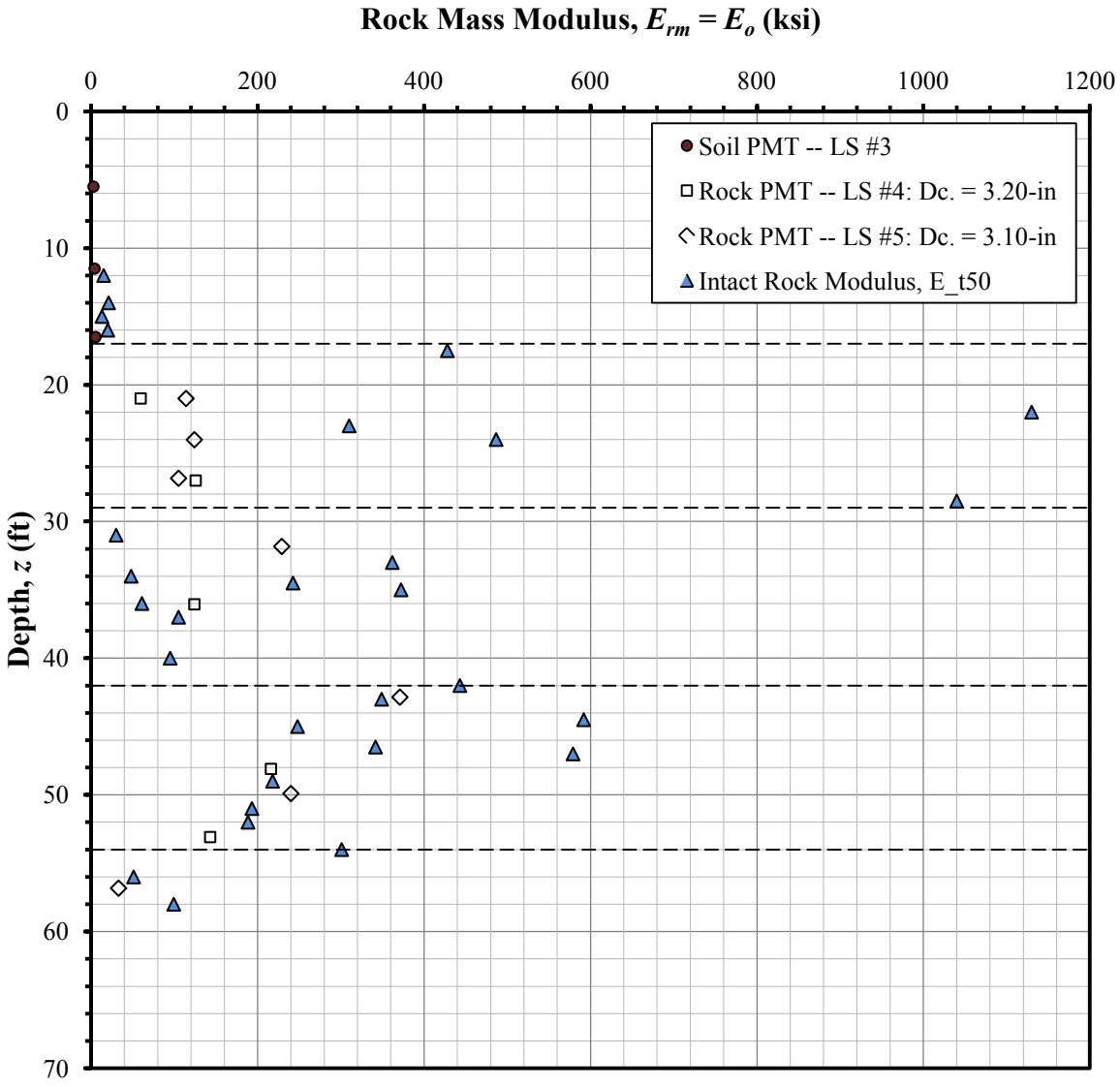

Fig. 6-13. Initial PMT modulus versus depth

Table 6-12. Results of Statistical Analysis for Initial PMT Modulus

Subsurface Layer	Top (ft)	Bottom (ft)	Sample Size, n	Observed Mean, E_o (ksi)	CoV (%)
Claystone	9	17	2	4.73	18
Upper Limestone	17	29	5	106	26
Sandstone	29	42	2	177	42
Lower Limestone	42	54	4	243	39
Shale	54	59	1	32.9	--

Poison's ratio was assumed to be typical values for intact rock as reported by Kulhawy (1975). These values are 0.14 and 0.22 for sandstone and limestone, respectively.

Also shown in Fig. 6-13 are values of E_{t50} for intact rock core measured in the laboratory. The modulus reduction factor, or the ratio between the deformation modulus for the rock mass and intact rock ($\alpha_E = E_{rm}/E_r$), is a useful parameter in design. This value is typically estimated from RQD [e.g. Zhang and Einstein (2004), and Kulhawy (1978)], or GSI and q_u (e.g. Hoek et al. 2002). However, in this case α_E may also be reasonably estimated with PMT data, taking $E_{rm} = E_o$ and $E_r = E_{t50}$. α_E was computed for each rock layer using the average results of each modulus, the results of which are shown in Table 6-13. The results indicated in Fig. 6-13, Table 6-12, and Table 6-13 are interesting in many respects, and will subsequently be used in evaluating empirical correlations typically used to estimate rock mass deformation characteristics. The computed values of α_E range between 0.16 and 1.07, but this value is typically not taken greater than 1.0.

6.5.2 *p-y* Curves Developed from PMT Data

The PMT data were also used to develop lateral load-displacement (*p-y*) curves to represent the lateral deformation response of the subsurface material corresponding to each test depth. The results for all *p-y* curves are shown in Figs. 6-14 through 6-16. These curves were developed point-by-point using the method prescribed by Briaud (1992) as outlined in Section 2.4.2. These curves are assumed to be the most accurate representation of the response of the subsurface material to lateral loading, and will subsequently be used to evaluate the *weak rock* model (Reese 1997), an empirical method used in *LPILE* to develop *p-y* curves.

Table 6-13. Results of Statistical Analysis for Rock Mass / Intact Rock Modulus

Subsurface Layer	Top (ft)	Bottom (ft)	Observed Mean, E_{t50} (ksi)	$\alpha_E = E_{o,ave}/E_{t50,ave}$
Claystone	9	17	17.3	0.27
Upper Limestone	17	29	679	0.16
Sandstone	29	42	164	1.07
Lower Limestone	42	54	345	0.70
Shale	54	59	75.1	0.44

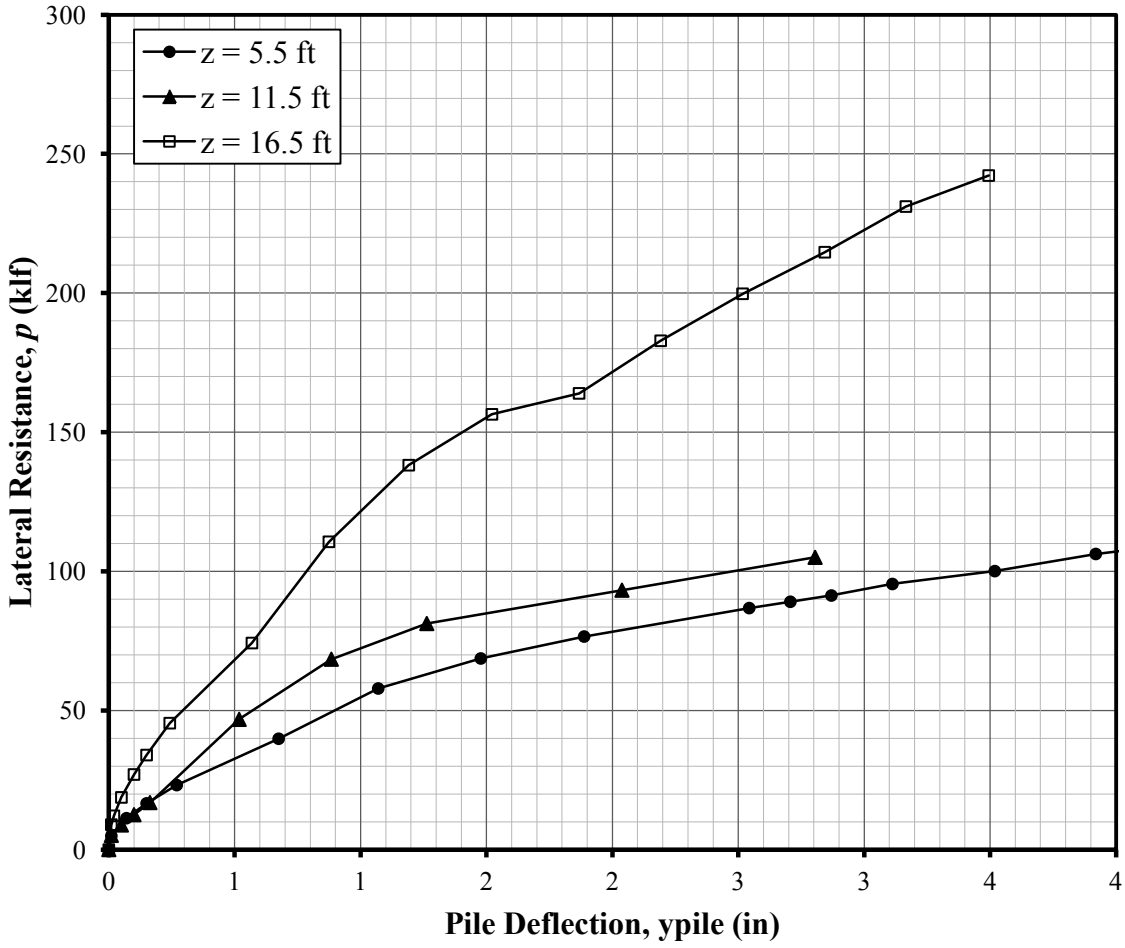

Fig. 6-14. *p-y* curves derived from PMT data from LS #3

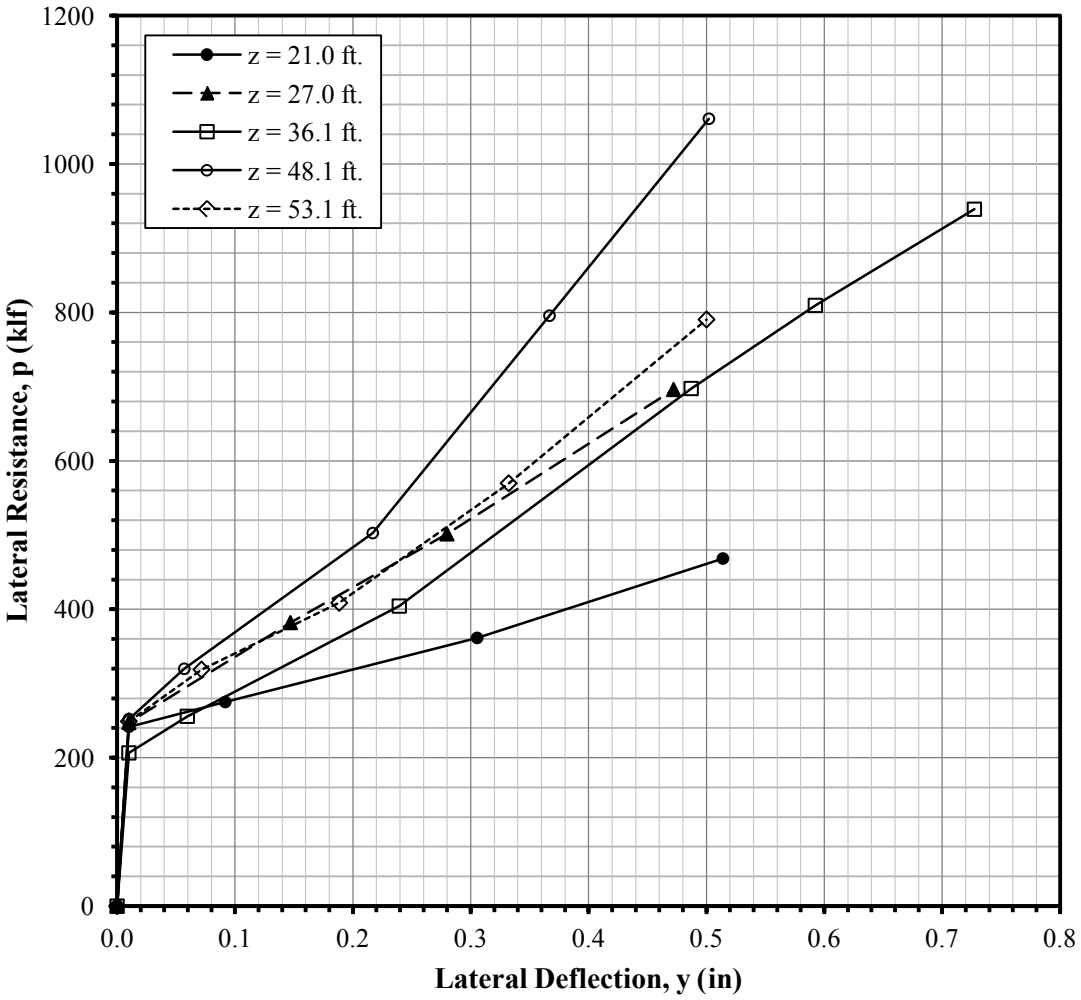

Fig. 6-15. *p-y* curves derived from rock PMT data from LS #4

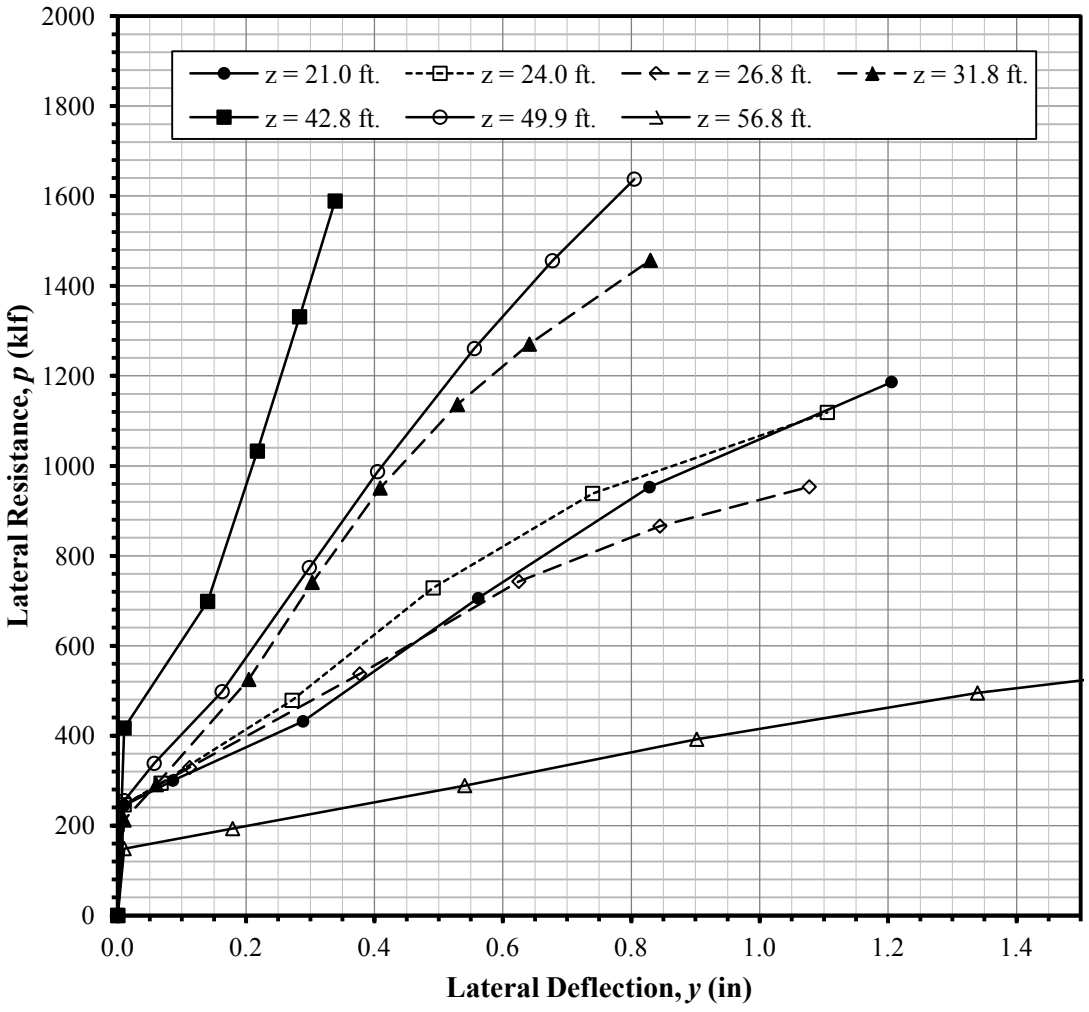

Fig. 6-16. *p-y* curves derived from rock PMT data from LS #5

6.6 Summary

The field and laboratory data obtained during the present study were presented in detail in this chapter. The data were reduced to show the variability associated with each rock type and strength and index property. It was found that the strength and index property data exhibited significant scatter and variability, which was found to be comparable between the two. In addition, site-specific correlations were developed between UAC strength and the various index properties. These correlations, however, exhibit significant scatter and are not intended for use in design, but rather to estimate the strength of the rock for classification purposes. The PMT data were used in this chapter to develop reliable deformation characteristics of the rock mass, including rock mass deformation modulus and load-displacement (*p*-*y*) curves to describe the nonlinear deformation response of the subsurface material. The data presented here will subsequently be used to evaluate existing methods and correlations.

7 EVALUATION OF EXISTING CORRELATIONS

7.1 Overview

One challenging aspect of geotechnical engineering is determining representative strength parameters to be used in design. Due to the lack of adequate high quality data, this is typically done using empirical correlations and minimal data for strength and index properties. When engineering foundations in rock, the ultimate goal is to understand the strength and deformation characteristics of the rock mass, not solely the strength of the intact rock. The strength of the rock mass is highly influenced by the presence of discontinuities such as fractures, joints, and bedding planes. Accordingly, the strength of the rock mass is typically determined using parameters of the intact rock in conjunction with the physical characteristics of the discontinuities.

In the present study, a significant quantity of data for strength and index properties of the intact rock was obtained in the laboratory. The goal of this chapter is to make use of the significant amount of data to evaluate the predictive capability of existing correlations used to estimate the strength of intact rock from index properties. There also exist correlations that relate the strength and deformation characteristics of the rock mass to those of the intact rock and the physical characteristics of the discontinuities within the rock mass. This chapter also evaluates these relationships in terms of how their predictions compare to results obtained from the PMT data. The chapter concludes by providing best estimate design parameters for the intact rock and rock mass at this site.

7.2 Intact Rock Strength versus Index Properties

Several empirical correlations have been developed in the literature between q_u and the various index parameters previously discussed (see Section 2.3.1), similar to those developed in Section 6.4. The motive behind these correlations is to provide a simple method to estimate strength of intact rock with reasonable levels of reliability and accuracy, with a relatively low level of effort. The purpose of this section is to evaluate the accuracy of these correlations and to assess the variability associated with their application.

Two laboratory strength tests that typically provide reasonable estimates of intact rock strength are uniaxial and triaxial compression. Of these two tests, triaxial compression is considered more reliable because it accounts for the confining stresses of the rock under in-situ conditions, which has been found to affect the stress-strain behavior of the rock (Kulhawy 1975). Uniaxial compression testing, however, can be more easily and economically performed, and the results are more commonly used in strength models (Pariseau 2007).

However, these two tests generally demand time and effort, and are consequently expensive to conduct, especially when a large sample size is desired. Index tests on the other hand are generally more economical, can be quickly conducted, and consequently can be used to obtain a large sample size to more adequately assess variability. The intended use of these index parameters and corresponding correlations is to estimate the strength of the rock for classification and mapping purposes (Broch and Franklin 1972), not necessarily for design. The variability exhibited in index test data can be used in conjunction with strength derived from reliable testing to produce a reasonable and reliable bound on engineering design values.

As previously discussed, this study incorporated the use of several index tests that can be used to estimate engineering properties and to assess variability. The variability of the raw data collected has previously been assessed in Section 6.4. Furthermore, these data have been used to develop site-specific correlations between q_u and index properties. In this section, correlations that have been developed in the literature (Section 2.3.1) will be evaluated in terms of accurately predicting the strength of intact rock. This method is based on the assumption that the results of UAC testing are reasonably representative of the "true strength". Therefore, to evaluate the predictive nature of the existing correlations properly, the average q_u values resulting from their application will be compared to the mean values and corresponding 70% confidence interval of the UAC data.

To evaluate the predictive capability of the index correlations, correlations that are appropriate for the specific rock type, core size, and testing method must be selected from the literature. The correlations selected (Section 2.3.1) are shown in Table 7-1 (same as Table 2-3). The results from applying each of these equations to the data obtained in the laboaratory for each index test are plotted versus depth in Figs. 7-1 and 7-2 for LS #1 and LS #4, respectively.

Table 7-1. Index Property Correlations

Index test	Equation	Source
Point Load	$q_u = 21\ I_{s(50)}$	Bieniawski (1975)
Brazilian Tension	$q_u = 10.5\ \sigma_t + 176.3$	Hassani et al. (1979)
Rebound Hardness	$q_u = 2.21\ e^{(0.07\ R_N)}$	Katz et al. (2000)
Unit Weight	$q_u = 0.0864\ e^{(0.291\ \gamma)}$	Smorodinov et al. (1970)

γ in KN/m^3 q_u, σ_t, and $I_{s(50)}$ in psi

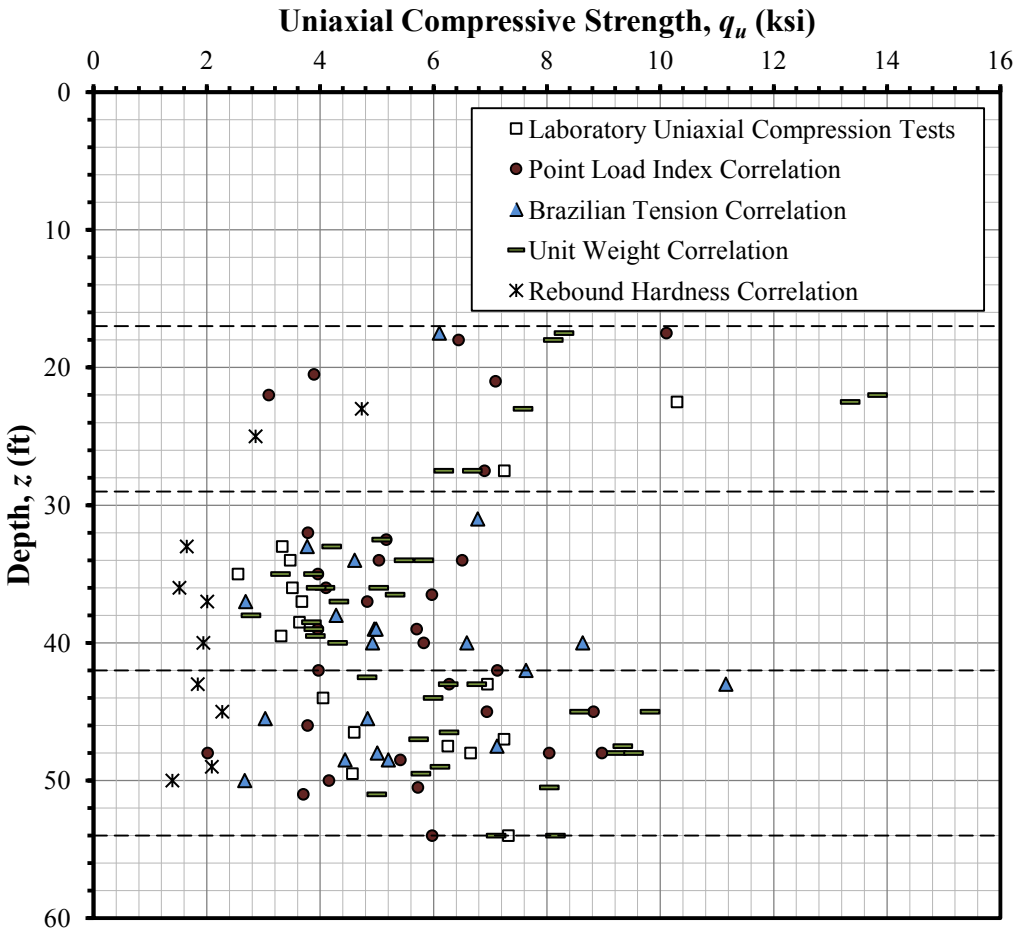

Fig. 7-1. q_u from UAC testing and index correlations for LS #1

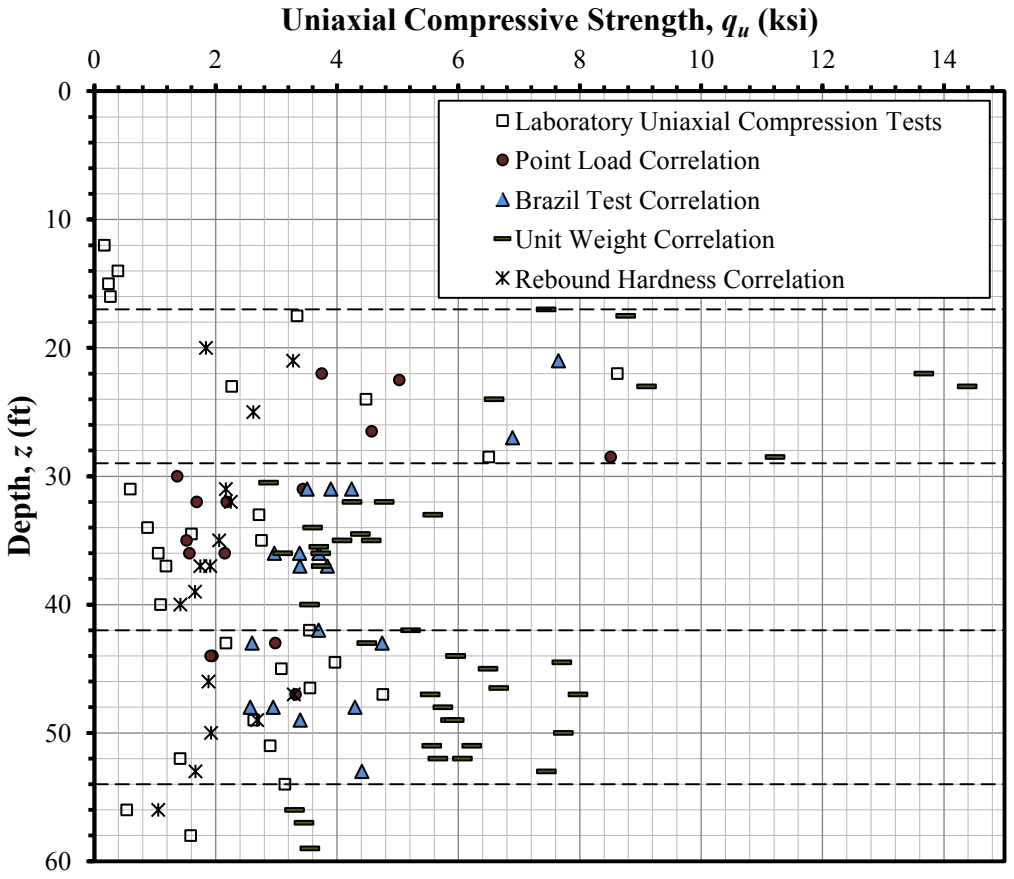

Fig. 7-2. q_u from UAC testing and index correlations for LS #4

From visual observation of Figs. 7-1 and 7-2, it is clear that the predicted strength values exhibit variability both between layers and within layers. The data representing the upper limestone layer (between 17 and 29 ft) exhibit higher levels of variability than data for the other layers. It may be inferred that some of the correlations predict q_u values within the "true" range of values (UAC strength data), and also those that predict q_u values that are biased high or low. For example, the correlation with γ consistently predicts values biased high for samples from LS #4. On the other hand, the correlation with R_N consistently predicts strength values biased low for samples from LS #1. For a closer examination of the empirical correlations, the statistics for the predicted q_u values were computed for each data set, including the mean and CoV. These statistics were then compared to the mean value and the corresponding 70% confidence interval computed for the observed UAC data. It should be noted that the confidence intervals were based on minimal data in some cases, and have been adjusted for statistical uncertainty using the Student's *t*-test. These statistics are presented in Tables 7-2 through 7-4. Table 7-2 is a duplicate of UAC data shown in Table 6-3, and is presented here so the data may be readily compared.

The results of the comparison for predictive capability are shown in Table 7-5. Of the four correlations, the correlation for $I_{s(50)}$ exhibited the best predictive capability. This correlation either predicted a mean value within or greater than the upper bound of the 70% confidence interval computed for the UAC data. The correlation with $I_{s(50)}$ worked best for the limestone layers, which exhibited higher strength than the sandstone layer. Predicted $q_{u,ave}$ from $I_{s(50)}$ for the limestone layers were within about 0.5 ksi of the mean, which is relatively close. Applying the correlation for σ_t typically resulted in

Table 7-2. Statistical Results for UAC Data with 70 % Confidence Interval

Borehole / Subsurface Layer	Top (ft)	Bottom (ft)	Sample Size, n	Observed Mean UAC Strength, $q_{u,ave}$ (ksi)	CoV (%)	70% Confidence Interval Lower, q_{uL} (ksi)	70% Confidence Interval Upper, q_{uU} (ksi)
Borehole LS #1							
Up. Limestone	19	29	2	8.77	25	5.78	11.8
Sandstone	29	42	7	3.35	11	3.19	3.52
Lo. Limestone	42	54	8	5.81	23	5.28	6.34
Borehole LS #4							
Up. Limestone	19	29	5	5.04	50	3.69	6.39
Sandstone	29	42	8	1.48	55	1.16	1.81
Up. Limestone	42	54	10	3.11	30	2.79	3.44

Table 7-3. Summary of q_u Results from Correlations with $I_{s(50)}$ and σ_t

Borehole / Subsurface Layer	q_u from P-L Index, $I_{s(50)}$: Sample Size	q_u from P-L Index, $I_{s(50)}$: Observed Mean, $q_{u,ave}$ (ksi)	q_u from P-L Index, $I_{s(50)}$: CoV (%)	q_u from Brazilian Tension, σ_t: Sample Size	q_u from Brazilian Tension, σ_t: Observed Mean, $q_{u,ave}$ (ksi)	q_u from Brazilian Tension, σ_t: CoV (%)
Borehole LS #1						
Up. Limestone	6	6.25	40	1	6.10	--
Sandstone	11	4.99	19	10	5.22	33
Lo. Limestone	14	5.78	36	9	5.68	46
Borehole LS #4						
Up. Limestone	4	5.46	38	2	7.27	7
Sandstone	7	1.99	36	8	3.62	11
Lo. Limestone	4	2.54	28	8	3.58	24

Table 7-4. Summary of q_u Results from Correlations with γ and R_N

	q_u from Unit Weight, γ			q_u from Rebound Hardness, R_N		
Borehole / Subsurface Layer	Sample Size	Observed Mean, $q_{u,ave}$ (ksi)	CoV (%)	Sample Size	Observed Mean, $q_{u,ave}$ (ksi)	CoV (%)
Borehole LS #1						
Up. Limestone	7	9.15	34	2	3.80	35
Sandstone	16	4.33	19	4	1.99	12
Lo. Limestone	17	7.21	23	4	1.91	17
Borehole LS #4						
Up. Limestone	7	10.2	26	3	2.58	28
Sandstone	13	3.99	21	7	1.89	16
Lo. Limestone	18	6.23	18	5	2.29	30

Table 7-5. Evaluation of Predictive Capability of Correlations with Index Tests

Borehole/Rock Layer	Point Load	Brazilian Tension	Unit Weight	Rebound Hardness
Borehole LS #1				
Upper Limestone	X	X	X	(-)
Sandstone	(+)	(+)	(+)	(-)
Lower Limestone	X	X	(+)	(-)
Borehole LS #4				
Upper Limestone	X	(+)	(+)	(-)
Sandstone	(+)	(+)	(+)	(+)
Lower Limestone	X	(+)	(+)	(-)

X -- within bounds of 70% confidence interval

(+) -- greater than upper bound of 70% confidence interval

(-) -- less than lower bound of 70% confidence interval

estimates beyond the upper bound of the 70% confidence interval, with the exception to the data for samples from LS #1 for the two limestone layers. For the results of q_u from σ_t, the means deviated from the UAC mean by about 0.4 ksi to 2.7 ksi, which is more significant than the deviation exhibited for q_u from $I_{s(50)}$. Variability was lowest for the results from Brazilian tension and highest for those from point-load. The results of correlating q_u with γ were beyond the upper bound of the confidence interval for each rock layer except the upper limestone layer for LS #1 – the difference between means ranging up to about 5 ksi. Mean q_u values from R_N were less than the lower bound of the confidence interval for each rock layer except the sandstone layer of LS #4. In addition, the correlation with R_N resulted in little variability between subsurface layers and between explorations. This lack of variation makes the results suspect, as results for all other correlations exhibited substantially more variability.

From the previous comparison it may be concluded that estimates of strength from correlation with $I_{s(50)}$ are relatively reliable in terms of estimating the actual strength of the rock samples tested. This conclusion is based on the assumption that UAC testing gives a reasonable estimate of the "true strength". However, these correlations should be calibrated on a case-by-case basis prior to use for engineering applications. The prediction based on σ_t was reliable for some layers in this case, but for the most part it overestimated q_u. The correlation with γ consistently overestimated q_u, and is considered unreliable for use on weak rock. The correlation with R_N resulted in consistently low estimates and exhibited little variability within and between rock layers. In most cases, the variability resulting from the index testing was less than that resulting from UAC testing.

7.3 Rock Mass Strength versus Intact Rock Strength

The discussion thus far has focused largely on the strength and deformation characteristics of intact rock, as these properties can be readily determined in the laboratory. However, the capacity of a rock foundation is not solely governed by the properties of the intact rock, but is largely dependent on the characteristics of the rock mass. The strength and deformability of the rock mass are highly influenced by natural discontinuities such as fractures, joints, and bedding planes that are typically present in rock masses. It is therefore necessary to determine equivalent rock mass properties that account for both the strength of the intact rock and the influence of the discontinuities (Zhang and Einstein 2004). Characterizing the strength properties in this way is typically done using methods that use rock mass rating (RMR) by Bieniawski (1976), or geological strength index (GSI) by Hoek et al. (1992). This section explores empirical models that use these characterization parameters to predict effective shear strength and deformation properties of the rock mass. These models are then evaluated by comparing the results to those obtained from the PMT data, which are deemed the most reliable of all available data.

The strength properties needed to characterize the rock mass include deformation modulus (E_{rm}) and the Mohr-Coulomb effective shear strength parameters ϕ' and c'. E_{rm} is the ratio of applied stress to corresponding strain, including both elastic and inelastic behavior. E_{rm} is dependent on rock mass quality and in-situ stress conditions, and generally increases with increasing levels of stress. Empirical correlations are available for shear strength parameters based on RMR and GSI. Hoek (1980) developed these relationships with RMR and later with GSI (Hoek et al. 1992), which is more applicable to weak rock masses. Nicholson and Bieniawski (1990) developed a relationship

between E_{rm} and RMR. Additional relationships directly between E_{rm} and RQD have been developed (e.g. Zhang and Einstein 2004). These relationships were utilized in this study for the purpose of evaluation, comparison, and providing a reasonable estimate of rock mass strength.

Prior to investigating the afore-mentioned relationships, both the RMR and GSI (Section 2.2) must be determined, which requires a closer look at the discontinuity characteristics. The RMR is based on q_u, RQD, fracture spacing, fracture condition, fracture orientation, and ground water conditions (Section 2.2.1). GSI is based on the 'blockiness' of rock pieces and the observed condition of discontinuities (Section 2.2.2). The weathered rock between 6 and 19 ft exhibited tightly spaced weathered discontinuities with random orientation. Natural fractures were present as very tight oblique fissures within portions of the upper limestone layer between 19 ft and 29 ft. One of these fractures is shown in Fig. 7-3, which indicates moderate weathering and a relatively smooth surface. This fracture was exposed only after testing the specimen in point-load, which is indicative of the tight nature of the fissure. In addition, portions of the upper limestone were mechanically fractured along bedding planes, particularly between 24 and 29 ft. Tight fractures were also found to be present within the sandstone layer between 29 ft and 42 ft. These fractures were relatively abundant, with an average spacing of about 1 ft and orientation ranging between 24 and 75 degrees. As indicated in Fig. 7-4, these fractures are relatively planar, with a moderately weathered, slightly rough, rustic surface. Natural fractures were not encountered in the limestone layer between 42 and 54 ft, although mechanical fracturing did occur along bedding planes.

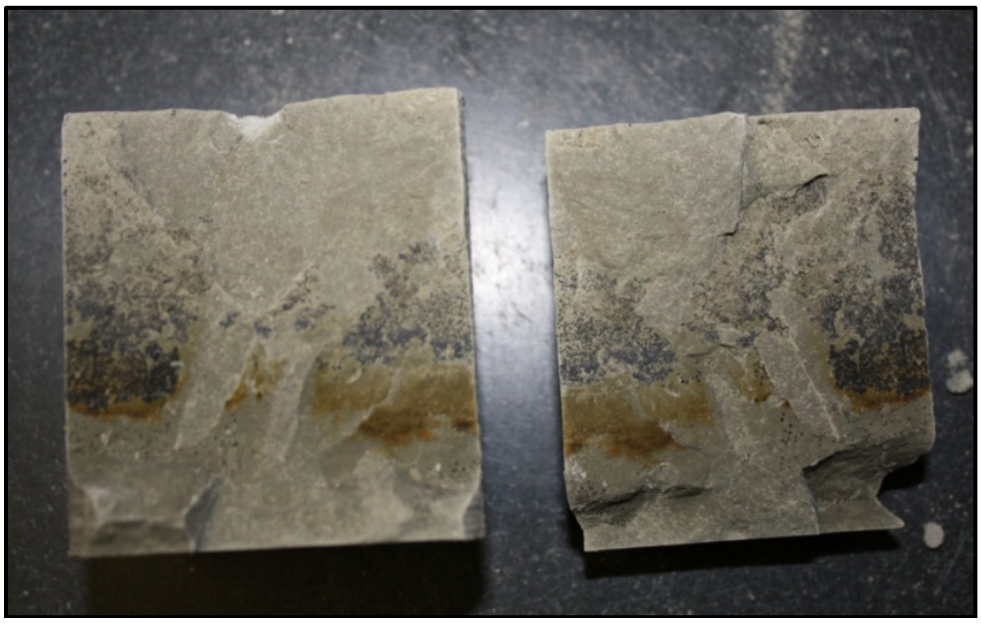

Fig. 7-3. Appearance of natural fissure in limestone between 20 and 24 ft

Fig. 7-4. Appearance of natural fracture in sandstone between 29 and 42 ft

The RMR for each subsurface layer is shown in Table 7-6, and is based on Bieniawski (1976) as discussed in Section 2.2.1. The GSI was determined in accordance with the method given by Marinos and Hoek (2005), as discussed in Section 2.2.2. Hoek-Brown failure criterion rock mass constants were determined from Hoek et al. (2002). These constants and the GSI are shown in Table 7-7. Ideally the rock mass should be characterized with properties and characteristics of the intact rock and discontinuities in all directions. However, it should be noted that only information in the vertical direction was known in this case. Consequently, the RMR and GSI are estimates based on minimal information, and in this study it is assumed that they are the same in all directions. This assumption is based on orientation of the natural fractures within the subsurface material, which was generally about 45° in most cases and is some indication that horizontal RQD would be the same as vertical. This assumption, however, may be conservative because the RQD was affected by weakness along the bedding planes, which would likely not affect RQD as much in the horizontal directions.

The effective strength properties were derived using two different methods, both of which were developed by Hoek. The first method was based on RMR using Hoek (1980) as reported by EPRI (2009), and the second method was based on GSI and the rock mass constants shown in Table 7-7 (Hoek 2002). Strength properties based on RMR were determined graphically using EPRI (2009). Those properties based on GSI were determined using Eqs. 2-1 through 2-9 provided in Section 2.2.2. These equations were applied using the recommended engineering properties for intact rock discussed in Section 7.4.1 and the Hoek-Brown rock mass parameters shown in Table 7-7. Intermediate values obtained in computing the rock mass shear strength parameters using

Table 7-6. Rock Mass Rating (RMR) for Subsurface Layers

Layer	RQD (%)	Strength Rating	RQD Rating	Discont. Spacing Rating	Discont. Condition Rating	GW Rating	RMR	Class.
CS	72*	0	3	10	12	7	32	IV - Poor
ULS	19	4	3	10	12	7	36	IV - Poor
SS	57	1	13	10	12	7	43	III - Fair
LLS	67	2	13	20	12	7	54	III - Fair
S	17	1	3	25	12	7	48	III - Fair

Table 7-7. GSI Range and Hoek-Brown Rock Mass Constants

Subsurface Layer	Depth Range (ft)	GSI Range	m_i	m_b	s	a
Claystone	6 - 19	30 - 35	4	0.33	0.0004	0.522
Upper Limestone	19 - 29	35 - 40	10	0.98	0.0007	0.516
Sandstone	29 - 42	50 - 55	17	2.85	0.0039	0.506
Lower Limestone	42 - 54	50 - 55	10	1.68	0.0039	0.506
Shale	54 - 59	45 - 50	6	0.84	0.0022	0.508

Hoek (2002) are shown in Table 7-8. As can be seen in Table 7-9, the effective friction angles (ϕ') derived using each method are comparable for the harder rock, but are significantly different for the weaker, weathered rock, with the method based on GSI producing lower values. In comparing the cohesion intercept (c'), the method using GSI consistently results in the highest estimates. In terms of selecting values for design, those properties determined using GSI (Hoek 2002) would be more appropriate because this method is more conducive to estimating strength for weak rock, as it is more directly associated with q_u. Unfortunately, the effective shear strength parameters of the rock mass could not be estimated from the pressuremeter data. Consequently, the methods used to obtain these parameters *c*ould not be compared with "true" strength parameters.

Table 7-8. Intermediate Values for Determining Rock Mass Strength Parameters

Subsurface Layer	Depth to Center of Layer, H (ft)	Average Unit Weight, γ_{ave} (pcf)	UAC Strength of Intact Rock, q_u (psi)	Rock Mass Strength, σ'_{cm} (psi)	Maximum Confining Stress, σ'_{3max} (psi)	σ'_{3n} (psi)
Weathered Claystone	14.0	101.9	263	18.1	7.53	0.42
Upper Limestone	24.0	119.5	5040	626	19.6	0.03
Sandstone	35.5	128.1	1483	334	28.1	0.08
Lower Limestone	48.0	132.2	3114	543	39.8	0.07
Shale	56.5	134.2	1060	130	41.1	0.32

Table 7-9. Rock Mass Effective Strength Properties using Two Methods

Subsurface Layer	Depth Range (ft)	Effective Friction Angle, ϕ' (deg).		Effective Cohesion, c' (psi)	
		Hoek (1980)	Hoek et al. (2002)	Hoek (1980)	Hoek et al. (2002)
Weathered Claystone	9 - 19	33.0	14.9	18.1	9.00
Upper Limestone	19 - 29	34.0	42.9	19.4	50.2
Sandstone	29 - 42	36.0	44.2	22.2	42.2
Lower Limestone	42 - 54	38.0	40.7	26.4	72.1
Shale	54 - 59	37.0	23.1	23.6	47.9

The deformation modulus of the rock mass was computed using three different methods – Nicholson and Bieniawski (1990), Zhang and Einstein (2004), and Hoek (2002) – using RMR, RQD, and GSI, respectively (as discussed in Section 2.3.2). The equations used for E_{rm} are shown in Table 7-10 (same as Table 2-4). The results for the rock mass modulus derived using these equations and those determined using the PMT data (Section 6.5.1) are shown in Table 7-11. Also shown in this table is the deformation modulus of the intact rock. The above results are also shown plotted versus depth in Fig. 7-5. It is common to compare the computed rock mass modulus to that of the intact rock

Table 7-10. Methods Used to Determined Rock Mass Deformation Modulus

Independent Variable	Equation	Authors
RMR	$E_{rm,RMR} = \frac{E_{t50}}{100}\left[0.0028(RMR)^2 + 0.9e^{\left(\frac{RMR}{22.82}\right)}\right]$	Nicholson & Bieniawski (1990)
RQD	$E_{rm,RQD} = E_{t50}10^{0.0186RQD-1.91}$	Zhang & Einstein (2004)
GSI	$E_{rm,GSI} = \sqrt{\frac{q_u}{100}}10^{((GSI-10)/40)}$	Hoek et al. (2002)

Table 7-11. Comparison of Methods for Determining E_{rm}

	Intact Rock Modulus, E_{t50}	Rock Mass Modulus, E_{rm} (ksi)			
Subsurface Layer	(ksi)	PMT (Sec. 5.5.1)	Zhang & Einstein (2004) (RQD)	Nicholson & Bieniawski (1990) (RMR)	Hoek et al. (2002) (GSI)
Weath. Claystone	14.6	4.73	3.92	0.95	58.1
Upper Limestone	679	106	18.9	54.2	365
Sandstone	164	177	23.2	18.3	470
Lower Limestone	345	243	74.9	61.3	681
Shale	75.1	32.9	1.91	10.4	298

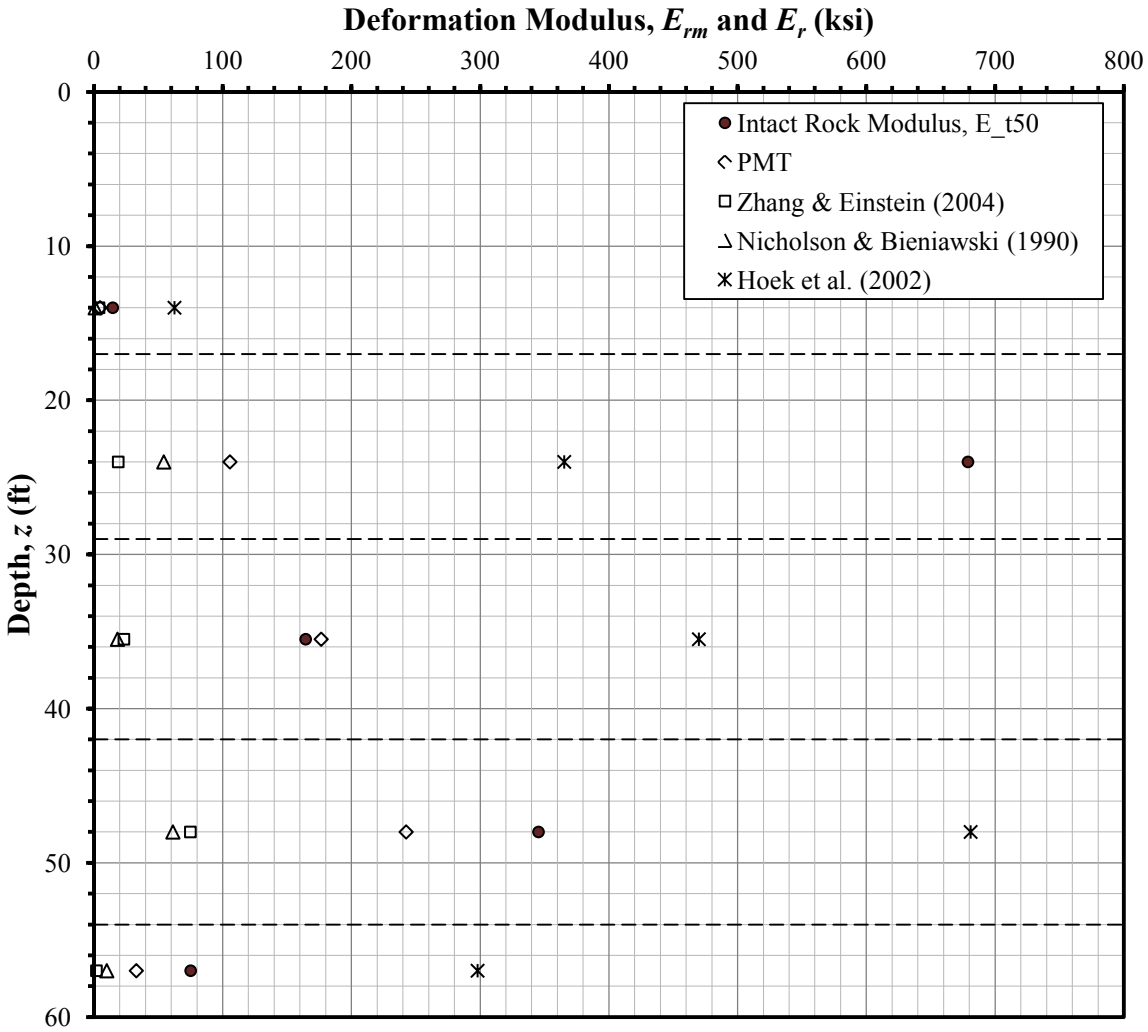

Fig. 7-5. Rock mass elastic modulus versus depth using various methods.

core by the ratio $\alpha_E = E_{rm}/E_{r.}$. This ratio was computed for each method described above and the results are shown in Table 7-12.

In terms of comparing the various methods used to predict the rock mass modulus, it is insightful to compare the modulus ratio (α_E) shown in Table 7-12. As indicated in this table, all the values for α_E reduced from the PMT data are all less than one (1) except for the sandstone layer. For the sandstone layer, α_E being greater than unity may indicate the influence of confining stresses is substantial. The values of α_E derived from the PMT data are assumed to be the most reliable estimates produced by all methods. Therefore, the values produced by all other methods will be compared to those from the PMT. The method using GSI results in the highest values of α_E, all of which are greater than one (1) except that for the upper limestone layer (this ratio is typically not taken greater than unity). It should be noted that this is the only method that does not directly relate E_{rm} to E_{t50} – it is more directly related to q_u. This method does, however, account for the effect of in-situ confining stresses. However, α_E determined using GSI far exceeds the values determined using the PMT data. It may therefore be concluded that this method does not accurately predict the deformation characteristics of the rock

Table 7-12. Comparison of Methods for Determining E_{rm} in Terms of Modulus Ratio

	Rock Mass to Intact Rock Modulus Ratio, $\alpha_E = E_{rm}/E_{t50}$			
Subsurface Layer	PMT (Sec. 5.5.1)	Zhang & Einstein (2004) (RQD)	Nicholson & Bieniawski (1990) (RMR)	Hoek et al. (2002) (GSI)
Weath. Claystone	0.32	0.27	0.066	3.98
Upper Limestone	0.16	0.028	0.080	0.538
Sandstone	1.1	0.14	0.11	2.86
Lower Limestone	0.70	0.22	0.18	1.97
Shale	0.44	0.025	0.14	3.97

mass in this case. The methods using RQD and RMR are comparable in terms of their relative magnitude, with the exception of the claystone layer. Of these two methods, that using RMR is likely more reliable because it incorporates the strength of the intact rock, q_u. However, neither of these two methods produces values of α_E that are in agreement with those derived from the PMT data. It may be concluded that using the methods based on RQD and RMR produces conservative estimates in this particular case.

7.4 Recommendation for Geotechnical Design Parameters

In terms of designing a drilled concrete shaft for the given site, it is first necessary to select representative geotechnical properties for the intact rock and the rock mass. These properties are dependent on the magnitude and variability of the strength and index data obtained in the field and laboratory. The strength of the rock mass was previously characterized using strength data from the laboratory with additional consideration regarding the joint properties (e.g. joint spacing, orientation, roughness, etc.). The determination of strength properties to be used for design, based on analysis of previous data, is discussed in this section.

7.4.1 Strength Parameters of Intact Rock

The strength properties of the intact rock were determined directly from the results of laboratory testing for samples from LS #4. Sections 6.4 and 7.2 detail the statistical analysis performed on the laboratory data, which will be used as the basis for assessing reasonable engineering properties and their potential variation. The properties necessary to characterize the strength of the intact rock include unit weight (γ), water

content (w), UAC strength (q_u), and elastic modulus (E_{t50}). For all engineering properties of the intact rock, the observed mean was taken as the best estimate for the recommended design values, as shown in Table 7-13. In terms of comparing foundation designs, it was concluded that this estimate would produce the most meaningful results. Note that the strength properties for the claystone layer between 6 and 12 ft were taken to be 50% of that for the layer between 12 and 19 ft. This was done on the basis that the PMT modulus determined at 5.5 ft was about 50% of the value determined at 16.5 ft.

In addition to providing best-estimate design parameters, it is important to give associated upper and lower bound values. The total variability of the strength estimates for design was calculated by pooling the variance of q_u determined from UAC testing and application of the various index correlations previously discussed (Section 7.4). This pooling was accomplished by determining the total variance for all the data, and computing a corresponding standard deviation. The results of pooling the variance are shown in Table 7-14.

Table 7-13. Recommended Engineering Properties of Intact Rock

Subsurface Layer	Top (ft)	Bottom (ft)	Unit Weight, γ_d (pcf)	Water Content, w (%)	UAC Strength, q_u (ksi)	Tangent Elastic Modulus, E_{t50} (ksi)
Sandy Clay	0	6	88.7	8.10	--	--
Weath. Claystone	6	12	103.8	6.50	0.131	8.63
Weath. Claystone	12	19	135.7	9.61	0.263	17.3
Upper Limestone	19	29	152.6	5.87	5.04	679
Sandstone	29	42	141.0	12.6	1.48	164
Lower Limestone	42	54	147.3	8.45	3.11	345
Shale	54	59	140.0	12.6	1.06	75.1

Table 7-14. Results of Pooling Data Variability for Upper and Lower Bound q_u Values

Subsurface Layer	Top (ft)	Bottom (ft)	Sample Size, n	Observed Mean UAC Strength, $\underline{q_u}$ (ksi)	CoV (%)
Claystone	9	19	4	0.263	36
Upper Limestone	19	29	18	5.04	44
Sandstone	29	42	36	1.48	44
Lower Limestone	42	54	35	3.11	28
Shale	54	59	5	1.06	36

A set of upper and lower bounds were determined using the Student's *t*-distribution, which adjusts the statistics for the uncertainty associated with the sample size. The bounds were determined based on 70% confidence interval, which approximate plus-and-minus one true standard deviations from the mean. The mean of the strength confidence interval was determined using the mean of the UAC data, as this value was considered to be the most reliable and unbiased estimate of the "true strength". It was previously shown (Section 6.4.4) that the variation in E_{t50} is similar to that of q_u, and that the two parameters have strong correlation. Consequently, the lower and upper bounds for intact rock deformation modulus were determined by assuming the CoV values and sample size for q_u could be applied to E_{t50} for the respective layers. This assessment was made by expressing the lower and upper bounds for q_u as ratios of the respective mean. These same ratios were subsequently applied to the mean E_{t50} value of each layer to determine the lower and upper bounds. Upper and lower bound values for q_u and E_{t50} are presented in Table 7-15.

Table 7-15. 70% True Mean Confidence Interval for q_u and E_{t50}

Subsurface Layer	Top (ft)	Bottom (ft)	Lower, q_{uL} (ksi)	Upper, q_{uU} (ksi)	Lower, E_{t50L} (ksi)	Upper, E_{t50U} (ksi)
Upper Claystone	6	12	0.102	0.161	6.70	10.5
Lower Claystone	12	19	0.204	0.322	13.4	21.1
Upper Limestone	19	29	3.97	6.11	535	823
Sandstone	29	42	1.24	1.73	137	192
Lower Limestone	42	54	2.71	3.52	300	390
Shale	54	59	0.74	1.38	52.3	98.0

7.4.2 Strength Parameters of the Rock Mass

The effective shear strength properties and deformation modulus of the rock mass have been estimated using several different methods in Section 7.3. The recommended design values for these parameters are shown in Table 7-16. The effective shear strength parameters selected were those determined using the method prescribed by Hoek et al. (2002) and are dependent on GSI. This method is more conducive to estimating strength of weaker rock than other methods. The average deformation modulus reduced from the PMT data was selected to best represent the behavior of the rock mass. These data were obtained in-situ, and were assumed to be the most reliable. The rock mass deformation

Table 7-16. Recommended Engineering Properties for Rock Mass

Subsurface Layer	Depth Range (ft)	Effective Friction Angle, ϕ' (deg)	Effective Cohesion, c' (psi)	Deformation Modulus, E_{rm} (ksi)
Weathered Claystone	9 - 19	15	9.00	4.73
Upper Limestone	19 - 29	43	50.2	106
Sandstone	29 - 42	44	42.2	164
Lower Limestone	42 - 54	41	72.1	243
Shale	54 - 59	23	47.9	32.9

modulus was taken to be equal to the value determined for intact rock core in the laboratory in these cases where the value for rock mass was greater than for intact rock (sandstone layer, Table 7-12 and Fig. 7-5).

7.5 Summary

In this chapter, the high quality data obtained in the field and laboratory were used to evaluate existing empirical correlations typically used to estimate strength of intact rock and rock masses. The UAC strength data were used to evaluate empirical correlations between strength and index properties of intact rock. This task was accomplished by applying various correlations available in the literature to the index property data, and assessing how the output compared to the estimated "true" values (UAC data). It was found that the correlation with the point-load index [$I_{s(50)}$] produced the best results in terms of estimating actual strength, as estimates were typically within the 70% confidence interval computed for the UAC data. Correlations with all other index properties produced results that were biased high or low. The results of applying the correlation with R_N exhibited little variability within and between layers, and it was therefore concluded these test data are not applicable in this case because all other tests indicated substantially more variability.

The in-situ PMT data were used to evaluate empirical correlations typically used to estimate deformation parameters of the rock mass. Three methods were applied to the available data, and it was found that none provided reasonable estimates of the rock mass deformation characteristics in terms of the available pressuremeter data.

8 EVALUATION OF ANALYTICAL METHODS

8.1 Overview

The present study is an extension of a research project conducted to demonstrate the benefit of conducting a detailed geotechnical investigation prior to final foundation design. This demonstration was accomplished by first obtaining detailed geotechnical information, and then conducting the design of a laterally loaded drilled shaft using several different models, methods, and sources of data – including data produced by a geotechnical consulting firm. The designs resulting from these analyses were then compared in terms of size to demonstrate the financial benefit of performing a detailed geotechnical investigation. The exact details and results of these analyses are not presented here in this study [see Lawton et al. (2011)]. Rather, pertinent technical issues are analyzed in more detail in this chapter. In particular, the method used by *LPILE* to develop *p-y* curves for weak rock (Reese 1997) is evaluated in detail. Furthermore, the results of analyzing a drilled shaft using this model are compared with the results assuming the shaft is an elastic beam in a homogeneous, isotropic, elastic continuum.

To execute the tasks outlined above, several analyses were conducted using *LPILE*. Prior to discussing these analyses, it is necessary to state overlying assumptions and to establish governing criteria. The objective of each analysis was to determine the required shaft diameter and embedment depth that would satisfy the given strength and

deflection criteria. Each analysis was performed assuming the same strength parameters for the shaft material:

- Compressive strength of the concrete, f'_c = 4,000 psi
- Yield stress of the reinforcing steel, f_y = 60,000 psi
- Stress-strain (Young's) modulus of the steel, E_{st} = 29,000,000 psi

The design load cases used for each analysis in this study are shown in Table 8-1 (see Fig. 8-1 for loading orientation). Load case 1 was used to check conformance with allowable geometrical deformations of the shaft. These allowable deformations are a maximum permanent ground-line (GL) deflection (y_{GL}) of 2.0 in., and a maximum permanent ground-line rotation (θ_{GL}) of 0.5 degrees. Permanent deformations were assumed to be 0.85 times the total deformation resulting from the applied service loads. This assumption results in an allowable ground-line deflection and rotation of 2.3 in. and 0.59 degrees, respectively.

Load case 2 was used to assure structural adequacy of the reinforced concrete shaft section, and therefore includes ultimate loads derived using overload capacity factors. Based on these loads, it was determined that an 11-ft diameter shaft with 84 #10 steel reinforcing bars would ensure structural adequacy ($\phi M_n \sim$ 27,700 kip-ft and $M_{u,max} \sim$ 27,000 kip-ft). This diameter was consequently used in each analysis described in this section. Deflection and rotation of the shaft were not considered for load case 2.

Resistance versus lateral deflection (*p*-*y*) curves were previously developed point-by-point directly from the PMT curves (Section 6.5.2). For this study, these curves are assumed to give the most accurate representation of the nonlinear deformation response of the subsurface material, given the available data and models used to develop *p*-*y*

Table 8-1. Design Loads for Serviceability and Ultimate States

Load Case	Axial, P_a (kips)	Lateral, V_L (kips)	Moment, M_u (kip-ft)
1 - Serviceability	58	201	19,354
2 - Ultimate	92	255	25,385

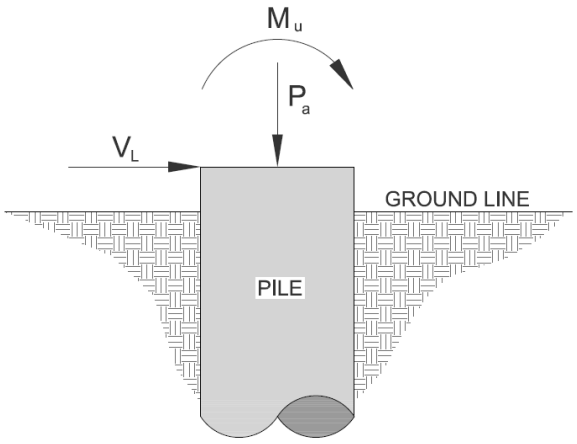

Fig. 8-1. Loading orientation at shaft head

curves. Accordingly, these curves will be used in this section to evaluate the method proposed by Reese (1997) to develop *p-y* curves for weak rock.

LPILE can be used to analyze a shaft in terms of geometric deformations using either internally generated *p-y* curves or manually input *p-y* curves that represent the nonlinear response of the rock. For internally generated *p-y* curves for weak rock, *LPILE* uses the interim method proposed by Reese (1997) described in Section 2.5.2. The *p-y* curves developed directly from the PMT data (Section 6.5.2) can be manually input into *LPILE*. It was previously determined that an 11-ft diameter shaft with 81 #10 bars provides sufficient structural capacity to resist the ultimate loads shown in Table 8-1. Accordingly, for comparison purposes, a shaft of 11 ft diameter was analyzed to determine the length required to limit the geometric deformations to those of the

governing criteria. The analysis was done with *LPILE* using two different methods – internal generation of *p-y* curves (Reese 1997) and manual input of the *p-y* curves developed using the PMT data. A comparison of the two methods was then conducted in terms of length of embedment required to satisfy the deformation criteria. In addition, the method proposed by Reese (1997) was evaluated in terms of the *p-y* curves generated and how they compare to those developed using the PMT data. Furthermore, the simple analytical method described in Section 2.5.1 was used to analyze a shaft of the same size as that determined using *LPILE* with the PMT data. The geometric deformation determined using this method was compared to those found using LPILE. All these analyses and comparisons will be discussed in this chapter.

8.2 *LPILE* Analysis using *p-y* curves from PMT data

An analysis was conducted using the *p-y* curves developed from the PMT data (6.5.2, Figs. 6-14 through 6-16). If properly conducted, a PMT provides results that should reliably represent the in-situ horizontal load-deflection characteristics of the rock mass, because the test replicates the direction and type of load application. This method is particularly beneficial at a rock site, where the rock mass exhibits a high degree of variability and uncertainty in strength and stiffness. As mentioned in previous sections, the strength of the rock mass is governed by the properties of the intact rock in conjunction with the properties of the discontinuities. While there are existing methods available to estimate the deformation characteristics of the rock mass based on these properties (as discussed in Section 7.3), these methods are based on generalized observations that are often inferred from information limited to the vertical direction.

These observations should be based on data collected for two or three directions. PMT data, on the other hand, give a direct indication of the lateral stiffness of the rock mass and requires no generalized observations. Therefore, of all the data obtained during the present study, the PMT data are considered to be the most representative of the actual horizontal stiffness of the rock mass. Consequently, analysis using these data is assumed to produce the most reliable results in terms of *p-y* curves, shaft size, and lateral deflection.

The analysis using p-y curves from PMT data was performed on a shaft with an 11-ft diameter and 81 #10 longitudinal bars, as this section was previously determined (Section 8.1) to provide sufficient capacity to withstand the ultimate loads shown in Table 8-1. The solution converged at a length of 29 ft, as indicated in Table 8-2. The design was governed by ground-line rotation, which was found to be 0.57 degrees; the ground-line deflection was 2.0 in. The results of this model, including shaft length, ground-line deflection, and *p-y* curves, was then used to evaluate the *weak rock* model (Reese 1997) used by *LPILE*.

8.3 *LPILE* Analysis using *weak rock* model (Reese 1997)

An analysis performed to evaluate the *weak rock* model available in *LPILE* (Reese 1997) is discussed in this section. First, the 11-ft diameter shaft (previously determined) was analyzed using best-estimate parameters of the intact rock shown in Table 8-3 and the deformation criteria given in Section 8.1.

Table 8-2. Results of Shaft Design using Different Methods of *p-y* Curve Generation

p-y Curve Model	Shaft Diameter, B_s (ft)	Shaft Depth, L_s (ft)	Shaft Head Deflection, δ_{sh} (in)	Shaft Head Rotation, θ_{sh} (deg)
PMT Data	11	29.0	2.0	0.57
LPILE -- *Weak Rock*	11	21.5	1.8	0.56

Table 8-3. *LPILE* Input Parameters for Intact Rock Developed in Present Study

LPILE Soil Model	Depth to Bottom of Layer, z_{bot} (ft)	Design Unit Weight, γ_d (pcf)	Elastic Modulus, E_{t50} / [k_h] (ksi) /[(pci)]	UAC Strength, q_u / [Effective Friction Angle, ϕ'] (psi) / [(deg)]	RQD (%)	Assumed k_{rm} ($*10^{-4}$)
Sand (Reese)	6	88.7	[21]	[44]	N/A	N/A
Weak Rock	12	103.8	8.65	132	72	5
Weak Rock	19	135.7	17.3	263	72	5
Weak Rock	29	152.6	133[a]	1000[a]	19	5
Weak Rock	42	141.0	94.9[a]	1000[a]	57	5
Weak Rock	54	147.3	111[a]	1000[a]	67	5
Weak Rock	59	140.0	79.1[a]	1000[a]	17	5

[a] Limited by *LPILE weak rock* model

For design of shafts in rock, *LPILE* includes two model options for internal generation of the *p-y* curves. The first option is the *weak rock* model, which is an interim empirical model for developing *p-y* curves based on Reese (1997). As discussed in Section 2.5.2, this model requires known values for UAC strength (q_u), rock elastic modulus (E_{t50}), rock unit weight (γ), RQD, and a rock mass stiffness parameter, k_{rm}. The *weak rock* model limits q_u to values ranging from 100 to 1,000 psi. The second *LPILE* option is a *strong rock* model, which is valid for q_u greater than 1,000 psi and requires input parameters for γ and q_u.

Ideally, both the *strong* and *weak rock* models should be utilized to represent the layers within the geological strata, as the reduced laboratory data indicate moderately

strong rock layers with q_u up to about 5,000 psi. However, the *strong rock* model does not account for RQD, and thus the effect of discontinuities on rock mass strength. It was therefore concluded that the *weak rock* model would be most appropriately used for each rock layer within the strata. With this conclusion, however, q_u for the stronger layers had to be limited between 100 psi and 1,000 psi, as limited by the *weak rock* model. Along with this reduction, E_{t50} was reduced in a proportional manner using the E_{t50}/q_u values shown in Table 6-5.

An *LPILE* analysis was conducted using the best-estimate strength parameters shown in Table 8-3. The value of k_{rm} was assumed to be 0.0005 for all layers, which is the upper bound recommended by Reese (1997) and results in the softest *p-y* curves. The solution for the analysis using these parameters converged at a depth of 21.5 ft, with a diameter of 11 ft and 81 #10 longitudinal bars, and a ground-line deflection and rotation of 1.8 in. and 0.57°, respectively. The results of the above analysis, in addition to those of the analyses conducted using *p-y* curves from the PMT data, are shown in Table 8-2 and Fig. 8-2.

8.4 Comparison of *p-y* Curves from PMT Data and *LPILE Weak Rock* Model

As indicated by the results shown in Table 8-2 and Fig. 8-2 for the above analyses, the two methods of generating *p-y* curves (PMT data and *LPILE weak rock* model) result in significantly different shaft lengths – a difference of 7.5 ft. It is assumed that the shaft size resulting from use of the PMT data is the most reliable in terms of satisfying the deformation criteria. With this difference in size, it is difficult to place confidence in the results produced from the *LPILE weak rock* model for this particular

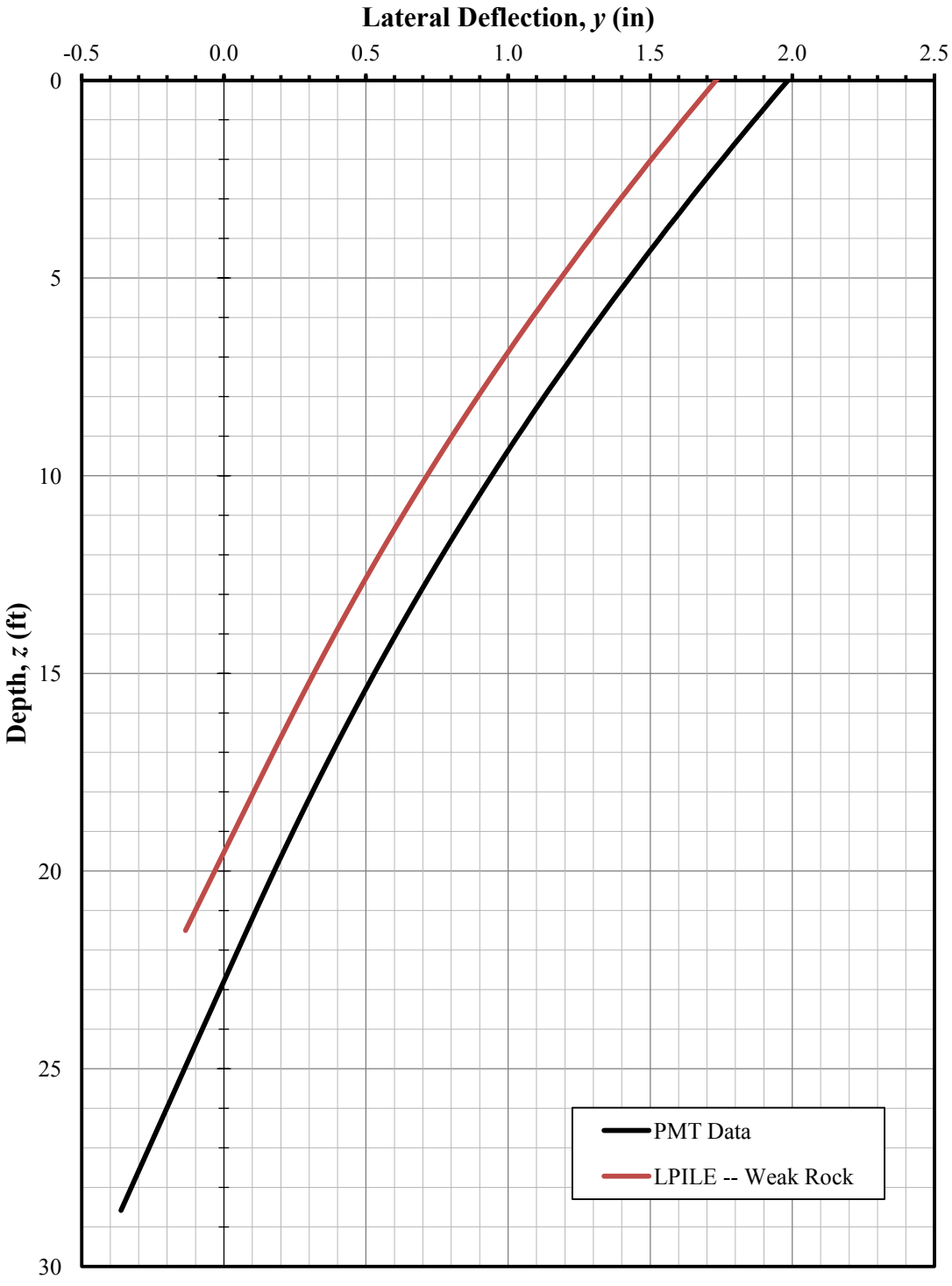

Fig. 8-2. Deflected shape of shaft from *LPILE* analysis using *p-y* curves generated from PMT data and Reese (1997) *weak rock* model.

case, as they indicate about a 26% reduction in size compared to the length of 29 ft determined using *p-y* curves developed from the PMT results.

The difference in size resulting from the two models is a direct indication of the difference in *p-y* curves generated at each depth. Therefore, it is insightful to compare these curves to assess the difference and perhaps provide a possible explanation. *P-y* curves corresponding to selected depths (6.0, 16.5, 32, 36 and 57 ft) generated using each of the two methods are shown graphically in Figs. 8-3 through 8-7. Depths were chosen based on locations where PMT data are available, and whether or not the corresponding rock layer exhibited strength within the bounds of the *weak rock LPILE* model (100 to 1000 psi). The average q_u values in the sandstone layer (29 to 42 ft) and the shale layer (z > 54 ft) were slightly above 1,000 psi, but it was assumed that bounding the strength at 1,000 psi would serve as a reasonable estimate. This assumption allowed for comparison of more curves. Because q_u for the two limestone layers is significantly higher than 1,000 psi, developing *p-y* curves based on the *weak rock* model would not provide meaningful insight.

As indicated by the *p-y* curves shown in Figs 8-3 through 8-7, there is a stark difference in slope and behavior, and therefore lateral stiffness of the rock material indicated by the two methods. The results of the *weak rock LPILE* model indicate that the rock is much stiffer than that indicated from the PMT data, especially at small lateral deflection. This higher stiffness is an explanation for the difference in shaft length determined using each model (Sections 8.2 and 8.3, Table 8-2).

An influential factor in developing *p-y* curves using the *weak rock* model is k_{rm}, which indicates the overall stiffness of the rock. As indicated in Figs 8-3 through 8-7,

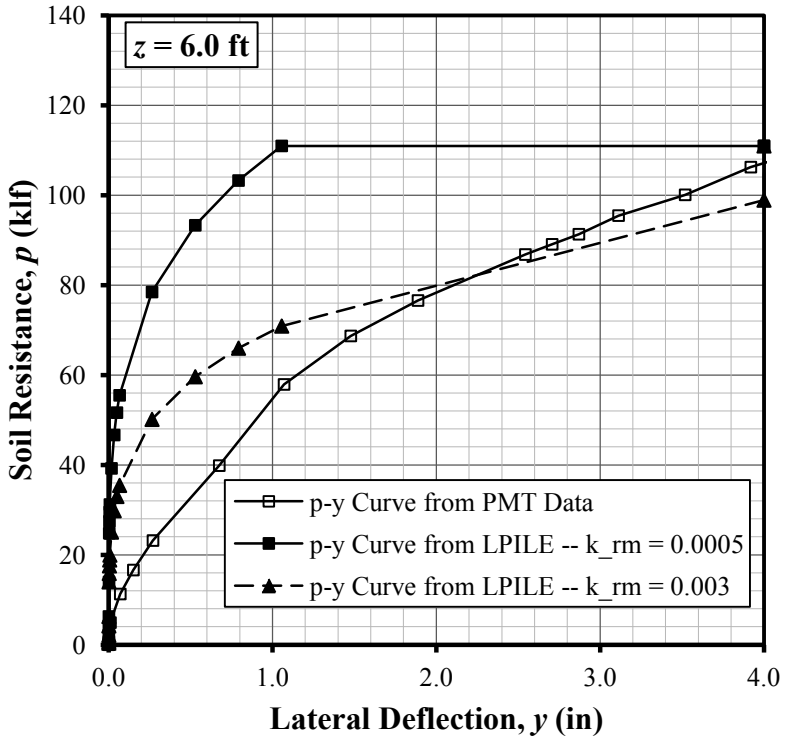

Fig. 8-3. *P-y* curves reduced from PMT data and *LPILE weak rock* model at z = 6.0 ft

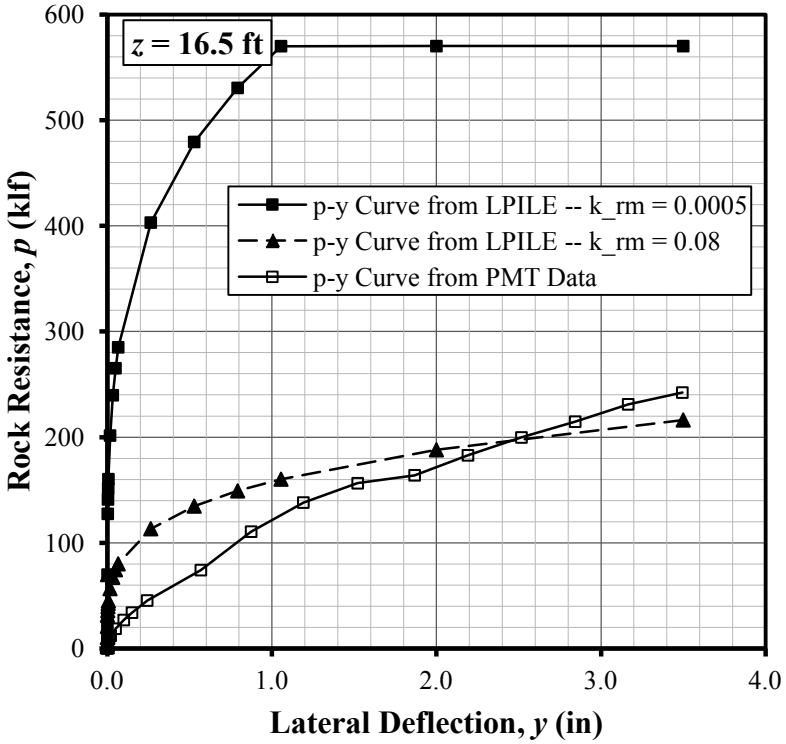

Fig. 8-4. *P-y* curves reduced from PMT data and *LPILE weak rock* model at z = 16.5 ft

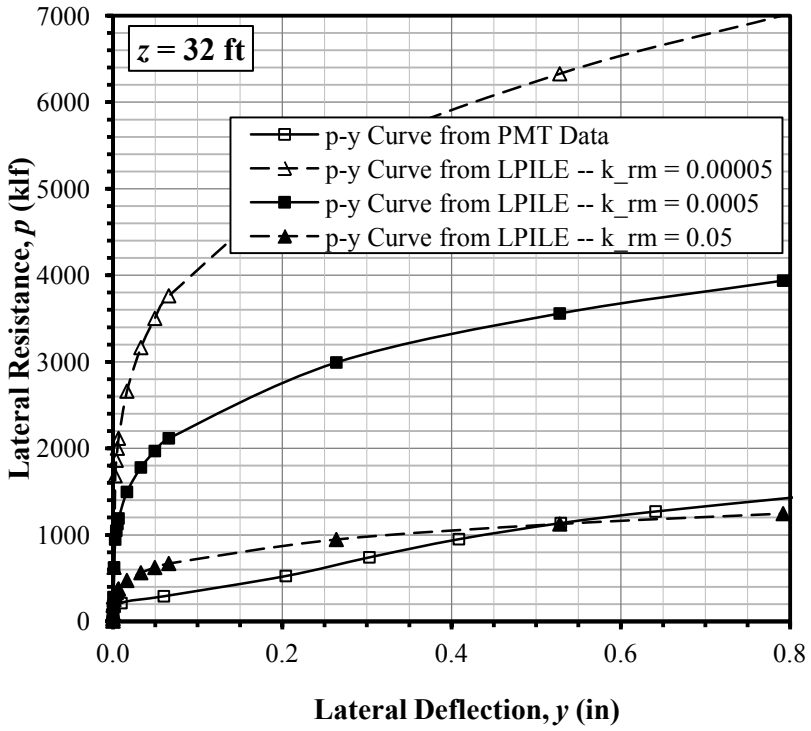

Fig. 8-5. *P-y* curves reduced from PMT data and *LPILE weak rock* model at z = 32 ft

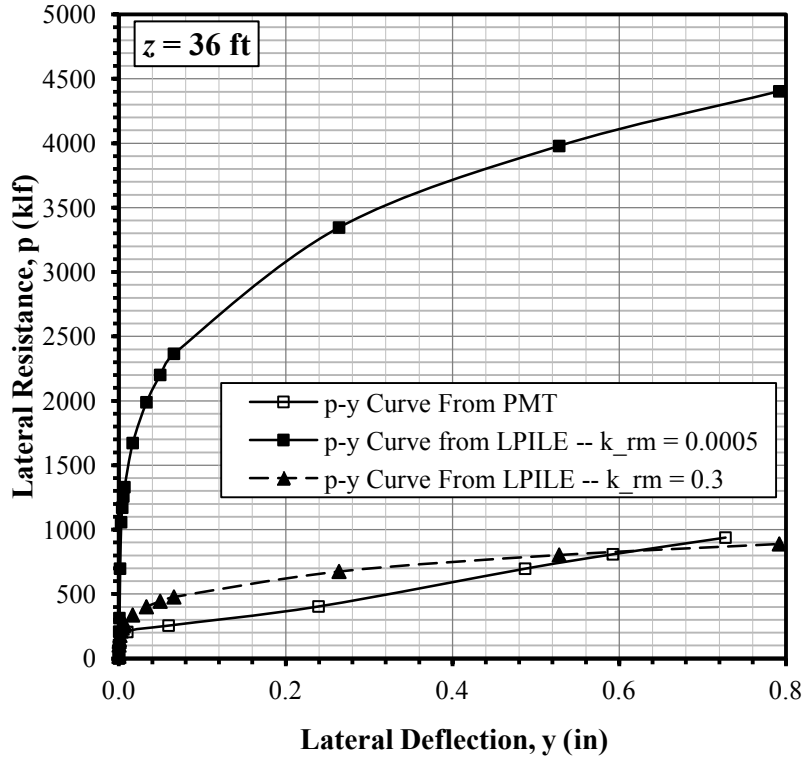

Fig. 8-6. *P-y* curves reduced from PMT data and *LPILE weak rock* model at z = 36 ft

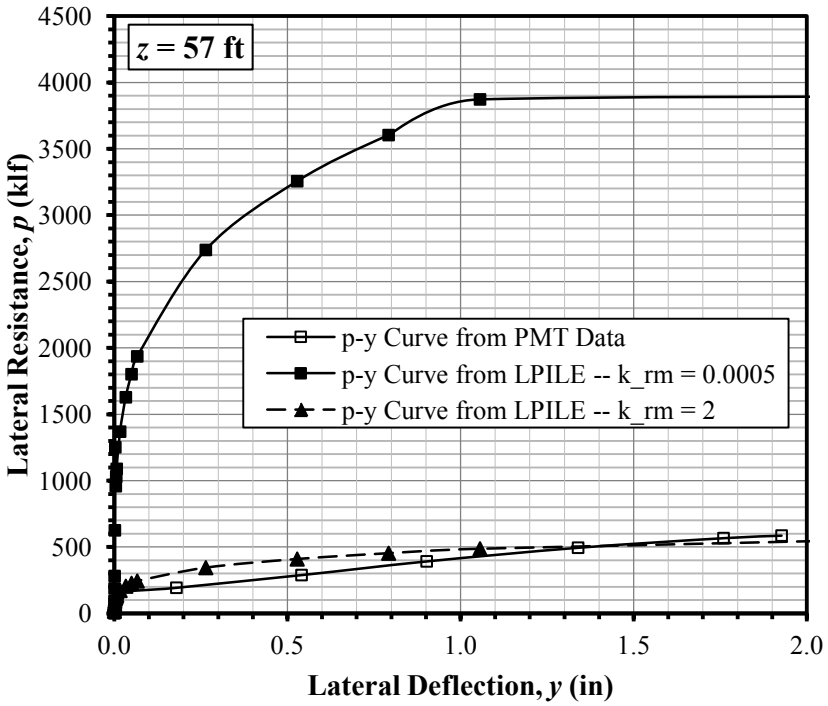

Fig. 8-7. *P-y* curves reduced from PMT data and *LPILE weak rock* model at z = 57 ft

this factor has a significant impact on the behavior of the *p-y* curve. Reese (1997) recommends that k_{rm} be taken between 0.0005 and 0.00005, which is the extent of the discussion given by Reese (1997) for this particular parameter. It can be seen from Fig. 4 of Reese (1997) and Eqs. 2-39 and 2-40 that the overall stiffness of the *p-y* curve increases as k_{rm} decreases, and vice versa. This characteristic is demonstrated in Fig 8-5 (z = 32 ft) where *p-y* curves for k_{rm} = 0.05, 0.0005, and 0.00005 are shown. Because the rock used for this study is relatively weak, k_{rm} was taken to be 0.0005 for each subsurface layer. However, as indicated by Figs. 8-3 through 8-7, it is clear that this value is too low to depict the stiffness of the rock accurately.

To demonstrate the influence of k_{rm}, this factor was varied for each of the *p-y* curves shown in Figs. 8-3 through 8-7 until there was reasonable agreement between the *p-y* curves developed using the two methods. As seen in these figures, k_{rm} ranging between 0.3 and 0.05 produced reasonable results. However, this range is orders of magnitude higher than that recommended, and therefore may not apply to the model as originally intended. In addition, significantly higher resistances are indicated at small deflections for each case that k_{rm} was adjusted, which is significant considering lateral deflections in the rock mass are typically small. An additional analysis was conducted using the k_{rm} values producing more reasonable *p-y* curves. This analysis resulted in a shaft length of 26 ft, a lateral deflection of 2.0, and shaft head rotation of 0.58, which is closer in size to that resulting from use of the PMT data (L_s = 29.0 ft).

A note should be made regarding the assumption that the PMT data are the most accurate representation of lateral stiffness of the subsurface material. This assumption was made on the basis that the PMT data were obtained in-situ, and that the expansion of the PMT probe mimics the behavior of a cylindrical shaft being pushed laterally. However, a significant extrapolation of the data is made in reducing *p-y* curves from the PMT results. In rock material, the data obtained from the PMT data represent the behavior of the material for a probe radial expansion ranging up to about 0.12 in. This information is extrapolated to produce a *p-y* curve that represents the behavior of the material over a deformation up to about 1.0 in. There is supporting data for both the *weak rock* and PMT *p-y* models (Reese 1997, Briaud 1992, and Yang et al. 2010), but in this case there is a stark difference in the results produced by each. It would be

interesting to perform a full-scale load test to evaluate the accuracy of each method in terms of predicting lateral deflections.

8.5 Analysis Assuming Elastic Beam in Elastic Rock Continuum

Sometimes in engineering practice emphasis is given to the use of complex models to analyze and design systems. These models often require substantial information and require intense numerical computations, and, without adequate information, the complex model may not be reliable for a given situation. In such a case, it can be beneficial to use a simple model that will take minimal time and provide a ball-park result. This approach can be applied for this case using the method described in Section 2.5.1, modeling the given shaft socket as an elastic beam in an elastic rock continuum. The results of this analysis will be described in this section.

The analysis was conducted on the 11-ft diameter x 29-ft long shaft (with a 10 ft socket into the harder limestone layer) designed using *LPILE* and the *p-y* curves generated from the PMT data (Section 8.2). The method proposed by Carter and Kulhawy (1992) (given in Section 2.5.1) outlines a way to account for the effect of soil overlying bedrock. In this case, the intermediate soil/weak, weathered rock between 6 and 19 ft was taken as overlying soil, and the rock socket was assumed to start at the surface of the stronger limestone layer (19 ft). Accounting for the effect of this soil is done by assuming that soil resistance is fully mobilized along the length of the shaft in the soil zone, and that this resistance can be treated as a distributed load along a cantilevered beam, as shown in Fig. 5 of Carter and Kulhawy (1992). Traditional beam theory may then be applied to determine deflections of the cantilevered beam within this

zone. However, it may be unconservative to assume full mobilization of soil resistance in the soil zone, especially near the hard rock surface where displacements are typically small. Carter and Kulhawy (1992) indicate the resistance of the overlying soil may be neglected as a conservative measure, because it is assumed that the rock socket provides the majority of the resistance. Therefore, for this analysis, the resistance of the overlying soil was neglected.

Neglecting the resistance of the overlying soil, the decomposition of the shaft with rock socket may be modeled as shown in Fig. 5 (b) of Carter and Kulhawy (1992). The loading condition shown in Table 8-1 was applied to this analysis. The lateral load at the rock surface was equal to the lateral load at the top of the shaft (V_L = 201 kips). The moment applied to the shaft at the rock surface is the sum of the moment applied at the top of the shaft and the product of the lateral load and a moment arm of 20 ft [shaft rises 1 ft above ground surface (M = 23,374 kip-ft)].

The geometric deformations of the shaft are determined using the principle of superposition – computing the deflections for the cantilever and rock socket separately, and adding them for the final result. The deflections of the cantilever portion of the beam were determined using traditional beam theory as follows:

$V_L := 201\text{kips}$	lateral load applied at shaft head V
$M_u := 19354\ \text{kip-ft}$	bending moment applied at shaft head
$EI_{s,e} = 1.089 \times 10^8\ \text{kip-ft}^2$	effective bending rigidity of shaft

$$y_{V,\,cant} := \frac{V_L \cdot L_{cant}^3}{3 \cdot EI_{s,\,e}} \cdot 12 = 0.059 \text{ in.}$$ lateral deflection due to lateral load

$$y_{M,\,cant} := \frac{M_u \cdot L_{cant}^2}{2 \cdot EI_{s,\,e}} \cdot 12 = 0.427 \text{ in.}$$ lateral deflection due to bending moment

$$\theta_{V,\,cant} := \frac{V_L \cdot L_{cant}^2}{2 \cdot EI_{s,\,e}} \cdot \frac{180}{\text{pi}} = 0.0212°$$ shaft head rotation due to lateral load

$$\theta_{M,\,cant} := \frac{M_u \cdot L_{cant}}{EI_{s,\,e}} \cdot \frac{180}{\text{pi}} = 0.204°$$ shaft head rotation due to bending moment

$y_{cant} := y_{V,\,cant} + y_{M,\,cant} = 0.486$ in. total shaft head deflection for cantilever

$\theta_{cant} := \theta_{V,\,cant} + \theta_{M,\,cant} = 0.225°$ total shaft head rotation for cantilever

The deflection of the shaft socket was determined using the method outlined in Section 2.5.1, as follows:

$E_{rm} = 15264$ ksf rock mass modulus (PMT limestone)

$v_{rm} = 0.22$ rock mass Poisson's ratio

$G_{rm} := \frac{E_{rm}}{2 \cdot (1 + v_{rm})} = 6256$ ksf rock mass shear modulus

$G^*_{rm} := G_{rm} \cdot \left(1 + \frac{3 \cdot v_{rm}}{4}\right) = 7288$ ksf rock mass equivalent shear modulus

$\frac{L_{sock}}{B_s} = 0.91$ depth to width ratio (assume to be 1)

$E_e := \frac{EI_{s,\,e}}{\frac{\text{pi} \cdot B_s^4}{64}} = 1.515$ x 105 shaft equivalent elastic modulus

$\frac{E_e}{E_{rm}}$ shaft to rock mass modulus ratio

$0.05 \cdot \left(\frac{E_e}{G^*_{rm}}\right)^{\frac{1}{2}} = 0.228$ rigid shaft boundary

$\left(\frac{E_e}{G^*_{rm}}\right)^{\frac{2}{7}} = 2.38$ flexible shaft boundary

$L_{sock}/B_s \sim 1$, which indicates the shaft is intermediate between rigid and flexible ($0.228 < L_{sock}/B_s \sim 1 < 2.38$). Therefore, as prescribed by Carter and Kulhawy (1992), the deflection will be determined for both the rigid and flexible case, and the largest value

will be multiplied by 1.25 to produce an estimate of the deflections. Applying the equations for the rigid and flexible case gives:

$L_{cant} = 20$ ft — socket length

$V_{L,r} := V_L = 201$ kips — lateral load at rock surface

$M_{u,r} := V_L \cdot L_{cant} + M_u = 23{,}374$ kip-ft — bending moment at rock surface

$e_L := \frac{M_{u,r}}{V_{L,r}} = 116$ — eccentricity at rock surface

Deflection of socket for rigid case:

$$y_{rig} = 0.4\left(\frac{H_r}{G_{rm} * B_s}\right)\left(\frac{2L_s}{B_s}\right)^{-1/3} + 0.3\left(\frac{M_r}{G_{rm} * B_s^{\,2}}\right)\left(\frac{2L_s}{B_s}\right)^{-7/8} = 0.0664 \text{ in.}$$

$$\theta_{rig} = 0.3\left(\frac{H_r}{G_{rm} * B_s^{\,2}}\right)\left(\frac{2L_s}{B_s}\right)^{-7/8} + 0.8\left(\frac{M_r}{G_{rm} * B_s^{\,3}}\right)\left(\frac{2L_s}{B_s}\right)^{-5/3} = 0.0153°$$

Deflection of socket for flexible case:

$$y_{flex} = 0.50\left(\frac{H_r}{G_{rm} * B_s}\right)\left(\frac{E_e}{G_{rm}*}\right)^{-1/7} + 1.08\left(\frac{M_r}{G_{rm} * B_s^{\,2}}\right)\left(\frac{E_e}{G_{rm}*}\right)^{-3/7} = 0.103 \text{ in.}$$

$$\theta_{flex} = 1.08\left(\frac{H_r}{G_{rm} * B_s^{\,2}}\right)\left(\frac{E_e}{G_{rm} *}\right)^{-3/7} + 6.40\left(\frac{M_r}{G_{rm} * B_s^{\,3}}\right)\left(\frac{E_e}{G_{rm} *}\right)^{-5/7} = 0.101°$$

The maximum deflection for the rock socket resulted from application of the flexible case (y_{flex} = 0.103 in. and θ_{flex} = 0.101°). Applying a factor of 1.25 to these figures gives:

$$y_{sock} = (1.25) \cdot (0.103) = 0.129 \text{ in.}$$

$$\theta_{sock} = (1.25) \cdot (0.101) = 0.125°$$

Adding the deflection of the socket to the deflection of the cantilever portion gives a total shaft deflection of:

$$y_{shaft} = 0.129 + 0.486 = 0.62 \text{ in.}$$

$$\theta_{sock} = 0.125° + 0.225° = 0.35°$$

The above values correspond well with the deflections determined for a shaft length of 29 ft using the *weak rock* model in *LPILE* (Fig 8-2), which were found to be: y_{sh} = 0.60 in. and θ_{sh} = 0.28°. The same values, however, are significantly less than those resulting from the *LPILE* analysis using *p-y* curves from the PMT data, which were determined to be: y_{sh} = 2.0 in. and θ_{sh} = 0.57°. It should be remembered that the

overlying soil resistance was neglected for this analysis, and that this is, therefore, a conservative estimate of geometric deformations obtained assuming an elastic beam in an elastic continuum.

8.6 Summary

In this chapter, an evaluation of a few analytical methods available for analyzing a laterally loaded shaft for deflection were presented. A brief overview of the two methods evaluated was given in Section 2.5 – one employing a simple approach, in which the shaft is modeled as an elastic beam within an elastic continuum; the other, the *p-y* method, employing nonlinear springs to model the response of the soil upon lateral loading.

The *p-y* method of analysis was employed using two methods to generate *p-y* curves. For the first method, *p-y* curves were developed directly from the PMT data, and were taken to be the most accurate representation of the nonlinear deformation response of the subsurface material. The second method utilized an empirical model developed for weak rock by Reese (1997) that employs the use of laboratory data. The results for these analyses are shown in Table 8-2. When using *p-y* curves from PMT data, the required shaft length was determined to be 29 ft, and when using the *weak rock* model (Reese 1997), the required shaft length was found to be 21.5 ft – a difference of 7.5 ft (-26%).

A direct comparison was made between the *p-y* curves developed using each method of generation. It was found that the weak rock model developed by Reese (1997) predicts a much stiffer response than that resulting from the PMT data, and consequently results in a significantly shorter shaft design length. It was also found that the value

selected for k_{rm} has a significant impact on the overall stiffness represented by the *p-y* curve.

Geometrical deformations were computed using the elastic beam within an elastic foundation approach. It was found that this model underestimates the lateral deflection compared to the analysis that used the *p-y* curves generated from the PMT data.

This study would have included a sensitivity / uncertainty analysis for the given drilled shaft foundation and LPILE weak rock model, but the limitation on the model included a q_u input of 100 psi to 1,000 psi. The strength for a large portion of the rock at this site was greater than the upper bound, so such an analysis would have been meaningless.

9 SUMMARY AND CONCLUSIONS

Details of a geotechnical case-study conducted for a site near Opal, Wyoming at Lima Substation were presented in the foregoing chapters. A summary of the tasks completed during this study is given in this chapter, including noteworthy conclusions drawn from the evaluation and analysis conducted in previous chapters. In addition, recommendations for future research are also given.

The primary objective of this study was to evaluate existing correlations and models used to estimate strength and deformation characteristics of intact rock and rock mass with respect to analyzing laterally loaded drilled shafts. Specific major objectives for this study were as follows:

- Assess the variability of strength and index properties of the subsurface material at the given site of investigation.
- Develop site-specific correlations between strength and index properties of the subsurface material at the site of investigation.
- Evaluate existing correlations typically used to estimate uniaxial compressive strength (q_u) of intact rock based on index properties.
- Evaluate existing correlations used to estimate strength and deformation characteristics of rock mass based on strength of intact rock and characterization parameters of the rock mass.

- Evaluate the *weak rock* model, used in the computer program *LPILE* (Reese 1997) to develop *p-y* curves, in terms of how well it applies to rock at the site of investigation.

The literature review conducted for this study is presented in Chapter 2. This review includes details concerning rock mass classification systems [rock mass rating (RMR) and geological strength index (GSI)], and existing methods commonly used to estimate strength and deformation characteristics of intact rock and rock mass. In addition, the details regarding methods of analysis used to design and estimate deflections of laterally loaded drilled shafts in rock are presented. The primary method investigated was the *p-y* method, which is used in the computer program *LPILE*. Specifically, the *weak rock* model (Reese 1997) used in *LPILE* for internal generation of *p-y* curves was investigated, as generating these curves is perhaps the most challenging aspect in using the method. Also investigated was a technique to generate *p-y* curves using results from the pressuremeter test (PMT).

Detailed geological and geotechnical investigations were conducted for the site. The data collection methods and procedures used in those investigations are presented in Chapters 3 through 5. The objective of the geological investigation (Chapter 3) was to attain a general understanding of the geologic history and subsurface strata based on existing maps and data. It was found that the subsurface material is predominantly rock overlain by a layer of clayey sand. The field investigation (Chapter 4) employed sampling methods such as rock coring to obtain specimens that could be tested in the laboratory. Furthermore, in-situ PMT testing was conducted during the field investigation to obtain accurate lateral load-deformation characteristics of the subsurface

material. The subsurface samples obtained during the field investigation were used for testing in a detailed laboratory investigation (Chapter 5) to determine strength and index properties. Uniaxial compression, point-load, Brazilian tension, rebound hardness, unit weight, and water content tests were conducted in the laboratory.

The field and laboratory data were reduced, evaluated, and presented in Chapter 6. The subsurface profile was shown to consist of alternating layers of claystone, limestone, and sandstone, overlain by a layer of clayey sand. The purpose of this chapter was to develop the basis for evaluating existing correlations and models. This was done by first assessing the variability associated with each strength and index property. As expected for rock material, it was found that each property exhibited relatively high variability, with the coefficient of variation ranging between about 10 and 70%. In addition, site-specific correlations were developed between q_u and the various index properties of the rock materials. Each of the correlations exhibited similar overall behavior compared to those existing in the literature, but in most cases varied in magnitude of prediction. This difference is likely due to differences in water content, rock fabric, bedding, and several other site-specific factors, and demonstrates why it is important to calibrate existing correlations or even develop site-specific correlations whenever possible. The basis for evaluating existing models and correlations included the high quality data obtained from PMT, from which reasonable estimates for *p*-*y* curves and other deformation properties were obtained. In addition, the results of uniaxial compression (UAC) tests were taken as the best estimate for q_u of intact rock core.

The predictive capability of existing correlations was examined in Chapter 7. Such correlations include those developed in the literature for the purpose of estimating

q_u based on index properties. Assuming the UAC data produce the most reliable results, it was found that the point-load index ($I_{s(50)}$) correlation provided the best estimate of q_u. Estimates of q_u using other index correlations were typically biased high or low. Additional correlations exist between the strength and deformation characteristics of rock mass, q_u for intact rock, and characteristics of discontinuities. These correlations were evaluated on the basis of the strength and deformation characteristics derived from the PMT data. It was found that neither of the methods explored (those using RMR and GSI) produced reasonable estimates of rock mass deformation characteristics for this case (assuming those derived from the PMT data to be most accurate). In addition, several methods for estimating effective shear strength parameters of rock mass were compared in terms of relative magnitude. It was concluded that the method using GSI produces the most reasonable estimate of effective shear strength because it factors in q_u. Finally, recommendations were made for strength, index, and deformation characteristics of the intact rock and rock mass.

The method used by the computer program *LPILE* to develop *p-y* curves for weak rock (Reese 1997) was evaluated in detail in Chapter 8. This model was examined in terms of how well the *p-y* curves developed compare with those developed using PMT data. It was found that the method proposed by Reese (1997) for developing *p-y* curves in weak rock significantly overestimates the stiffness of the rock mass for this particular site and that the value k_{rm} (a constant that represents the overall stiffness) highly influences the overall shape of the *p-y* curve. This overestimation is particularly evident at small lateral deflection, and can significantly affect the results of a drilled shaft design in rock. For example, a design for a laterally loaded drilled shaft foundation was

conducted using each of the two methods for generating *p-y* curves. It was found that a length of 29.0 ft is required when using *p-y* curves developed from PMT data, and that a length of 21.5 ft is required when using *p-y* curves developed using Reese (1997), a reduction of 26% in size. With this unconservative difference, an engineer may find it difficult to place confidence in the *LPILE weak rock* model for the site of investigation. This conclusion is based on the assumption that PMT data produce the most reliable *p-y* curves.

Several recommendations are made for further research that may be conducted to supplement and enhance the findings of this study: a) First and foremost would be to conduct a full-scale load test on a drilled shaft foundation embedded at the site of investigation. The results of this test could be used to more critically evaluate empirical methods for developing *p-y* curves in weak rock, including methods proposed by Reese (1997) and Gabr et al. (2002). The results from this test could be used to provide insight regarding how the Reese (1997) model might be changed to better represent the subject material, and possibly adjust it to include a wider range of strength (q_u) input than is currently permitted (a maximum of 1000 psi) . b) The data from this study could be used to evaluate the *p-y* model proposed by Gabr et al. (2002). This evaluation could be done in much the same way that the method proposed by Reese (1997) was investigated in this study – by comparing *p-y* curves generated using the prescribed method to those developed from PMT data, and conducting designs using each method. c) Finally, the data from the present study could be used to conduct an in-depth reliability or sensitivity / uncertainty analysis. This could be done by first using statistics to describe a probability distribution of each pertinent engineering property, and then using random selection to

produce multiple instances of property combinations. Using each of these combinations to conduct a design would produce a distribution of design results. These results could be used to compute the probability of failure associated with any particular design, or to explore the sensitivity of the design as a function of strength and several other parameters. Such an analysis, however, would require that a reliable input model be used for the design analyses.

APPENDIX

SYMBOLS AND NOTATION

a	=	Hoek-Brown rock mass constant
AASHTO	=	American Association of State Highway and Transportation Officials
ASTM	=	American Society for Testing and Materials
ave	=	average
BR-X	=	specimen number X tested in Brazilian tension
BST	=	borehole shear test
c'	=	effective cohesion
CoV	=	coefficient of variation
CS	=	claystone
d	=	specimen diameter
D_c	=	cavity diameter
D_e	=	equivalent specimen diameter for rectangular section
D_S	=	shaft diameter
deg	=	degrees
DS	=	direct shear
EI	=	pile rigidity – modulus of elasticity times moment of inertia
E_o	=	initial pressuremeter modulus
E_r	=	elastic modulus of intact rock
E_R	=	reload pressuremeter modulus
E_{rm}	=	deformation modulus of rock mass
E_s	=	elastic modulus of steel
E_{t50}	=	intact rock tangent elastic modulus at 50% failure
f'_c	=	compressive strength of concrete

f_y = yield strength of steel

ft = feet/foot

F = friction resistance

F-y = tangential shear load-displacement curve

G = shear modulus

GL = groundline

GSI = Geological Strength Index

H = depth to center of subsurface layer

I = moment of inertia

ID = inside diameter

in. = inch

I_s = point-load index

$I_{s(50)}$ = corrected point-load index

ISRM = International Society for Rock Mechanics

K_h = horizontal subgrade modulus

kip = 1000 pounds

K_0 = lateral stress coefficient

kPa = kilo-Pascal

k_{rm} = rock stiffness constant

ksf = kips per square foot

ksi = kips per square inch

l = specimen length

LL = Atterberg liquid limit

L_S = shaft length

LS = limestone

LS #X = borehole number X at Lima Substation

M = constrained modulus

m_b = Hoek-Brown rock mass constant

MFAD = Moment Foundation Analysis and Design

m_i = Hoek-Brown rock mass constant

min = minute

ϕM_n = factored nominal moment capacity

M_u = ultimate moment

$M_{u,max}$ = maximum ultimate moment

n = sample size

NQ = 1.87 in. diameter rock core

NX = 2.16 in. diameter rock core

OD = outside diameter

p = passive resistance per unit length in soil adjacent to a pile or a shaft

P_a = axial load

p_A = atmospheric pressure

P_L = limit pressure

P_L^* = net limit pressure

p_{PMT} = pressuremeter pressure

Δp_{PMT} = change in pressuremeter pressure

pcf = pounds per cubic foot

PI = plasticity index

PL = Atterberg plastic limit

P-L = point-load

PL-X = specimen number X tested in point-load compression

PMT = pressuremeter test

psf = pounds per square foot

psi = pounds per square inch

PSI = Professional Service Industries

PVC = polyvinyl chloride

PWP = porewater pressure

p-y = load-displacement curve

q_u = uniaxial compressive strength of intact rock

Q = front resistance

Q-y = normal resistance load-displacement curve

R = probe radius

R^2 = coefficient of determination

ΔR = change in radius of pressuremeter probe

R_c = cavity radius

ΔR_c = change in radius of cavity

RMR = rock mass rating

R_N = rebound hardness for N-type hammer

R_o = initial pressuremeter probe radius

R_{oc} = initial radius of cavity

RQD = rock quality designation

RR = relative rigidity factor

S = shale

s_u = undrained shear strength

SH-X = specimen number X tested with Schmidt rebound hardness hammer

SPT = standard penetration test

SS = sandstone

T = torque measurement from SPT-T

u_o = hydrostatic porewater pressure

UAC = uniaxial compression

USCS = Unified Soil Classification System

UC-X = specimen number X tested in uniaxial compression

ν = Poisson's ratio

V = volume

ΔV = change in volume

v_c = corrected volume

V_L = lateral load

V_o = initial volume of PMT probe

V_{oc} = volume of PMT probe at contact with cavity wall

V_{or} = volume of PMT probe at start of reload curve

w = water content

w/ = with

w/o = without

y = lateral displacement

y_{GL} = lateral deflection at ground-line

z = depth below ground surface

α = shaft reduction factor

α_E = ratio of rock mass deformation modulus to intact rock deformation modulus

β = shaft reduction factor

γ = total unit weight

γ' = effective unit weight

γ_d = design unit weight

σ = total normal stress

σ_{oh} = in-situ horizontal stress

σ' = effective normal stress

σ_{max} = maximum normal stress

σ_p' = preconsolidation stress

σ_t = Brazilian tensile strength

σ_v' = effective vertical stress

σ_v = total vertical stress

σ_{vo}' = effective vertical overburden stress

τ_{max} = maximum shear stress

θ_{GL} = rotation at ground-line

ϕ' = effective friction angle

REFERENCES

ASTM (1963). "Standard test method for particle-size analysis of soils." *D422 – 63*, West Conshohocken, PA.

ASTM (2005a). "Standard test method for determination of rock hardness by rebound hammer method." *D5873 – 05,* West Conshohocken, PA.

ASTM (2005b). "Standard test methods for liquid limit, plastic limit, and plasticity index of soils." *D4318 – 05*, West Conshohocken, PA.

ASTM (2006). "Standard Practice for Classification of Soils for Engineering Purposes (Unified Soil Classification System)." *D2487 – 06*, West Conshohocken, PA.

ASTM (2007). "Standard test method for compressive strength and elastic moduli of intact rock core specimens under varying states of stress and temperatures." *D7012 – 07*, West Conshohocken, PA.

ASTM (2008a). "Standard practices for preparing rock core as cylindrical test specimens and verifying conformance to dimensional and shape tolerances." *D4543 – 08*, West Conshohocken, PA.

ASTM (2008b). "Standard practices for preserving and transporting rock core samples." *D5079 – 08*, West Conshohocken, PA.

ASTM (2008c). "Standard test method for determination of the point load strength index and application to rock strength classifications." *D5731 – 08*, West Conshohocken, PA.

ASTM (2008d). "Standard test method for splitting tensile strength of intact rock core specimens." *D3967 – 08*, West Conshohocken, PA.

Aydin, A. and Basu, A. (2005). "The Schmidt hammer in rock material characterization." *Engineering Geology,* 81, 1 – 14.

Baguelin, F., Jezequel, J. F. and Shields, D. H. (1978). *The Pressuremeter and Foundation Engineering*, Trans Tech Publications, Clausthal-Zellerfeld, W. Germany.

Basu, A. and Aydin, A. (2004). "A method for normalization of Schmidt hammer rebound values." *International Journal of Rock Mechanics and Mining Sciences,* 41, 1211 – 1214.

Becker, D. E., Crooks, J. H., Been, K., and Jefferies, M. G. (1987). "Work as a criterion for determining in situ and yield stresses in clays." *Canada Geotechnical Journal*, 24(4), 549 – 564.

Bieniawski, Z. T. (1975). "The point-load test in geotechnical engineering." *Engineering Geology*, 9(1), 1 – 11.

Bieniawski, Z. T. (1976). "Rock mass classifications in rock engineering." *Proceedings of Symposium on Exploration for Rock Engineering*, Balkema, Rotterdam, 1, 97 – 106, as reported by Goodman (1980).

Bradley, W. H. (1964). "Geology of green river formation and associated Eocene rocks in southwestern Wyoming and adjacent parts of Colorado and Utah." *U.S. Geological Survey Professional Paper,* (496-A) A1 – A86.

Briaud, J. -L. (1992). *The Pressuremeter*. A. A. Balkema, Rotterdam, reprinted by Taylor and Francis, London, 2005.

Broch, E. and Franklin, J. A. (1972). "The point-load strength test." *International Journal of Rock Mechanics and Mining Sciences,* 9(6), 669 – 697.

Brown, E. T. (1981). *Rock Characterization Testing and Monitoring: ISRM Suggested Methods*. Pergamon Press, Oxford.

Case, J. S. (1986). "Earthquakes and related geologic hazards in Wyoming." *The Geological Survey of Wyoming Public Information Circular,* (26).

Case, J. C. (1997). "Earthquakes and active faults in Wyoming." *Wyoming State Geological Survey Preliminary Hazards Report*, (97-2), 1 – 44 .

Deere, D. V. (1968). "Chapter 1: Geological considerations." *Rock mechanics in engineering practice,* K. G. Stagg and O. C. Zienkiewicz, eds. John Wiley and Sons, Inc. New York, N.Y., 1 – 20, as reported by Reese (1997).

Dickey, D. D., and M'Gonigle, J. W. (1992). "Map showing swelling clays in the Kemmerer 30' x 60' quadrangle, Lincoln, Uinta, and Sweetwater counties, Wyoming." *U.S. Geological Survey Miscellaneous Investigations*, (Map I-2080), scale 1:100,000.

Ensoft (2004). *LPILE Plus 5.0 Users Manual.* Ensoft., Inc., Austin, TX.

EPRI (2009). *MFAD 5.0: User Guide for MFAD 5.0 (Moment Foundation Analysis and Design)*. Electric Power Research Institute, Palo Alto, CA and DiGioia, Gray and Associates, LLC, Product ID No. 1015909.

Gabr, M. A., Borden, R. H., Cho, K. H., Clark, S., and Nixon, J. B. (2002). "P-y Curves for laterally loaded drilled shafts embedded in weathered rock." North Carolina Department of Transportation Technical Report No. FHWA/NC/2000-008.

Gibbons, A. B. (1986). "Surficial materials map of the Kemmerer 30' x 60' quadrangle, Lincoln, Uinta, and Sweetwater counties, Wyoming." *U.S. Geological Survey Coal Investigations,* (Map C-102), scale 1:100,000.

Gill, D. E., Corthésy, R., and Leite, M. H. (2004). "A statistical approach for determining practical rock strength and deformability values from laboratory tests." *Engineering Geology*, 78, 53 – 67.

Goodman, R. E. (1980). *Introduction to Rock Mechanics*. John Wiley and Sons, New York.

Gunsallus, K. L., and Kulhawy, F. H. (1984). "A comparative evaluation of strength measures." *International Journal of Rock Mechanics and Mining Sciences*, 21(5), 233 – 248.

Hassani, F. P., Whittaker, B. N., and Scoble, M. J. (1979). "Strength characteristics of rocks associated with opencast coal mining in the U. K." *Proceedings of the 20th U. S. Symposium on Rock Mechanics*, Austin, TX. 347 – 355.

Hoek, E., and Brown, E. T. (1980). "Emperical strength criterion for rock masses." *Journal of Geotechnical Engineering Division, ASCE*, 106(GT9), 1013 – 1035, as reported by Hoek et al. (2002).

Hoek, E., Carranza-Torres, B., and Corkum, B. (2002). "Hoek-Brown failure criterion – 2002 edition." *5th North American Rock Mechanics Symposium and 17th Tunneling Association of Canada Conference: NARMS-TAC*, 267 – 271.

Hoek, E., Wood, D., and Shah, S. (1992). "A modified Hoek-Brown criterion for jointed rock masses." *Proceedings of Rock Characterization, Symposium of the International Society for Rock Mechanics: Eurock '92,* Ed. J. A. Hudson, London, British Geotechnical Society, 209 – 214, as reported by Hoek et al. (2002).

Horvath, R. G., and Kenney, T. C. (1979). "Shafts resistance of rock socketed drilled piers." *Proceedings of the Symposium on Deep Foundations, ASCE*, New York, N. Y. 182 – 184, as reported by Reese (1997).

In-Situ Soil Testing (2010). Report on pressuremeter testing at Lima Substation, WY, prepared by In-Situ Soil Testing, Inc., Lancaster, VA, November.

Katz, O., Reches, Z., and Roegiers, J. -C. (2000). "Evaluation of mechanical rock properties using a Schmidt Hammer." *International Journal of Rock Mechanics and Mining Sciences,* 37, 723 – 728.

Kulhawy, F. H. (1978). "Geomechanical model for rock foundation settlement." *Journal of the Geotechnical Engineering Division, Proceedings of the ASCE,* 104(GT2), 211 – 227.

Kulhawy, F. H. (1975). "Stress deformation properties of rock and rock discontinuities." *Engineering Geology*, 9, 327 – 350.

Lawton, Evert C., Bartlett, Steven F., McClellan, Zachary R., Timpson, Thomas C., and Wood, Kari L. (2011). "Geotechnical analysis and design of foundations for transmission line structures at three locations." University of Utah. Report No. UUCVEEN2011-011, prepared for Professional Service Industries, Inc., September 30.

Marinos, P., and Hoek, E. (2000). "GSI: A geologically friendly tool for rock mass strength estimation." *Proceedings of the GeoEng2000 Conference, Melbourne.*

Marinos, V., Marinos, P., and Hoek, E. (2005). "The geological strength index: applications and limitations." *Bulletin of Engineering Geology and the Environment,* 64, 55 – 65.

M'Gonigle, J. W., and Dover, J. H. (1992). "Geologic map of the Kemmerer 30' x 60' quadrangle, Lincoln, Uinta, and Sweetwater counties, Wyoming." *U.S. Geological Survey Miscellaneous Investigations,* (Map I-2079), scale 1:100,000.

Nicholson, G. A., and Bieniawski, Z. T. (1990). "A nonlinear deformation modulus based on rock mass classification." *International Journal of Mining and Geological Engineering*. 8(3), 181 – 202, as reported by Gill et al. (2004).

PacifiCorp (2008). "General – transmission structure foundation design criteria for towers and monopole structures." *TA 071*, PacifiCorp.

Pariseau, W. G. (2007). *Design Analysis in Rock Mechanics*. Taylor and Francis, London.

Peck, R. B. (1976). "Rock foundations for structures." *Proceedings of a Specialty Conference on Rock Engineering for Foundations and Slopes, ASCE*, New York, N. Y., as reported by Reese (1997).

PSI (2010). "Geotechnical engineering report: proposed Lima Substation near Opal, Wyoming." Professional Service Industries, Inc., Project No. 0595111-1, prepared for PacifiCorp, April 13.

Reese, L. C. (1977). "Laterally loaded piles: Program documentation." *Journal of the Geotechnical Engineering Division, ASCE*, 103(GT4), 287 – 305.

Reese, L. C. (1997). "Analysis of laterally loaded piles in weak rock." *Journal of Geotechnical and Geoenvironmental Engineering*, 123(11), 1010 – 1017.

Reese, L. C., Wang, S. T., Isenhower, W. M., Arregllago, J. A., and Hendrix, J. (2004a). *Computer Program LPILE Plus Version 5.0 User's Guide*, Ensoft, Inc., Austin, TX, July.

Reese, L. C., Wang, S. T., Isenhower, W. M., and Arregllago, J. A. (2004b). *Computer Program LPILE Plus Version 5.0 Technical Manual*, Ensoft, Inc., Austin, TX, July.

Salgado, R. (2008). *The Engineering of Foundations*. New York, New York, The McGraw Hill Companies.

Smith, T. D. (2010). *Pressuremeter testing report: PacifiCorp transmission structures – Honeyville and Tremonton, UT and Lima, WY*., Prepared for University of Utah/PSI by In-Situ Tech., Inc., Beaverton, OR, September.

Smorodinov, M. I., Motovilov, E. A., and Volkov, V. A. (1970). "Determination of correlation relationships between strength and some physical characteristics of rocks." *Proceedings of the 2nd Congress ISRM,* Belgrade, 2, 35 – 37, as reported by Gunsallus and Kulhawy (1984).

USGS (2010). *United States Geological Survey*. http://seamless.usgs.gov/

WSGS (2010). *Wyoming State Geological Survey*. www.wsgs.uwyo.edu/GIS/DigitalData/

Yang, K., Liang, R. Y., and Nusairat, J. (2010). "*P-y* curves for rock and intermediate geomaterials using pressuremeter tests." *The Art of Foundation Engineering Practice*, *ASCE,* 717 – 132.

Zhang, L., and Einstein H. H. (1998). "End bearing capacity of drilled shafts in rock." *Journal of Geotechnical and Geoenvironmental Engineering*, 124(7), 574 – 578.

Zhang, L., and Einstein, H. H. (2004). "Using RQD to estimate the deformation modulus of rock masses." *International Journal of Rock Mechanics and Mining Sciences,* 41, 337 – 341.